การสังเคราะห์และสมบัติในการตรวจวัดของไตรแคตไอออนิกอิมิดาโซเลียม
และกัวนิดิเนียมฟลูออโรฟอร์

นายศตวรรษ เดือนสว่าง

วิทยานิพนธ์นี้เป็นส่วนหนึ่งของการศึกษาตามหลักสูตรปริญญาวิทยาศาสตรมหาบัณฑิต
สาขาวิชาปิโตรเคมีและวิทยาศาสตร์พอลิเมอร์
คณะวิทยาศาสตร์ จุฬาลงกรณ์มหาวิทยาลัย
ปีการศึกษา 2558

SYNTHESIS AND SENSING PROPERTIES OF TRICATIONIC IMIDAZOLIUM AND GUANIDINIUM FLUOROPHORE

Mr. Sattawat Dueansawang

A Thesis Submitted in Partial Fulfillment of the Requirements
for the Degree of Master of Science Program in Petrochemistry and Polymer Science
Faculty of Science
Chulalongkorn University
Academic Year 2015

Thesis Title	SYNTHESIS AND SENSING PROPERTIES OF TRICATIONIC IMIDAZOLIUM AND GUANIDINIUM FLUOROPHORE
By	Mr. Sattawat Dueansawang
Field of Study	Petrochemistry and Polymer Science
Thesis Advisor	Associate Professor Paitoon Rashatasakhon, Ph.D.
Thesis Co-Advisor	Professor Mongkol Sukwattanasinitt, Ph.D.

Accepted by the Faculty of Science, Chulalongkorn University in Partial Fulfillment of the Requirements for the Master's Degree

.....Dean of the Faculty of Science
(Associate Professor Polkit Sangvanich, Ph.D.)

THESIS COMMITTEE

.....Chairman
(Assistant Professor Warinthorn Chavasiri, Ph.D.)

.....Thesis Advisor
(Associate Professor Paitoon Rashatasakhon, Ph.D.)

.....Thesis Co-Advisor
(Professor Mongkol Sukwattanasinitt, Ph.D.)

.....Examiner
(Associate Professor Chawalit Ngamcharussrivichai, Ph.D.)

.....External Examiner
(Nakorn Niamnont, Ph.D.)

ศตวรรษ เดือนสว่าง : การสังเคราะห์และสมบัติในการตรวจวัดของไตรแคตไอออนิกอิมิดาโซเลียมและกัวนิดิเนียมฟลูออโรฟอร์ (SYNTHESIS AND SENSING PROPERTIES OF TRICATIONIC IMIDAZOLIUM AND GUANIDINIUM FLUOROPHORE) อ.ที่ปรึกษาวิทยานิพนธ์หลัก: รศ. ดร.ไพฑูรย์ รัชตะสาคร, อ.ที่ปรึกษาวิทยานิพนธ์ร่วม: ศ. ดร.มงคล สุขวัฒนาสินิทธิ์, 77 หน้า.

สารประกอบเรืองแสงที่เป็นอนุพันธ์ของไตรฟีนิลเอมีนและมีหมู่รอบนอกเป็นหมู่อิมิดาโซเลียม กัวนิดีน และกัวนิดิเนียม ได้ถูกสังเคราะห์ขึ้นอย่างมีประสิทธิภาพโดยใช้ปฏิกิริยาควบคู่ที่มีพัลเลเดียมเป็นตัวเร่งปฏิกิริยา และพิสูจน์เอกลักษณ์ด้วยเทคนิคโปรตอนและคาร์บอนนิวเคลียร์แมกเนติกเรโซแนนซ์ แมสเปกโตรเมตรี ยูวีวิซิเบิล และฟลูออเรสเซนต์สเปกโตรโฟโตเมตรี ในการศึกษาสมบัติทางแสงของสารดังกล่าวในสารละลายบัฟเฟอร์เฮปเปส พีเอช 7.0 ความเข้มข้น 10 มิลลิโมลาร์ พบว่าสารทั้ง 4 ชนิดมีค่าความยาวคลื่นของของการดูดกลืนแสงสูงสุดอยู่ระหว่าง 319 ถึง 362 นาโนเมตร และคายพลังงานแสงสูงสุดที่ความยาวคลื่นในช่วง 428 ถึง 456 นาโนเมตร โดยมีร้อยละของประสิทธิภาพเชิงควอนตัมของสาร F1 – F4 เท่ากับ 17.97, 7.40, 3.16 และ 2.39 ตามลำดับ ผลการทดสอบสมบัติการเป็นเซ็นเซอร์พบว่าสัญญาณการเรืองแสงของสาร F1 ซึ่งมีหมู่อิมิดาโซเลียมสามารถถูกระงับได้อย่างจำเพาะเจาะจงกับไฮโดรเจนซัลไฟด์ไอออน โดยมีค่าคงที่ของการระงับสัญญาณเท่ากับ 4.91×10^{5} $(\text{โมลาร์})^{-1}$ และมีขอบเขตของการตรวจวัดเท่ากับ 0.093 ไมโครโมลาร์ ผลจากการศึกษาด้วยนิวเคลียร์แมกเนติกเรโซแนนซ์บ่งชี้ว่ากลไกการเปลี่ยนแปลงสัญญาณฟลูออเรสเซนต์อาจเกี่ยวข้องกับการจับกันระหว่างโปรตอนบนตำแหน่งที่ 2 ของวงอิมิดาโซเลียมกับไฮโดรเจนซัลไฟด์ ส่วนสาร F2 ที่มีหน่วยรับเป็นกัวนิดีนสามารถระงับสัญญาณอย่างจำเพาะเจาะจงกับไทโอซัลเฟตไอออน มีค่าคงที่ของการระงับสัญญาณเท่ากับ 1.06×10^{5} $(\text{โมลาร์})^{-1}$ และ มีขอบเขตของการตรวจวัดเท่ากับ 1.31 ไมโครโมลาร์

สาขาวิชา ปิโตรเคมีและวิทยาศาสตร์พอลิเมอร์ ลายมือชื่อนิสิต .....

ปีการศึกษา 2558 ลายมือชื่อ อ.ที่ปรึกษาหลัก .....

ลายมือชื่อ อ.ที่ปรึกษาร่วม .....

5672100923 : MAJOR PETROCHEMISTRY AND POLYMER SCIENCE
KEYWORDS: TRIPHENYLAMINE / IMIDAZOLIUM / GUANIDINE / GUANIDINIUM / HYDROGEN SULFIDE ION / THIOSULFATE ION

SATTAWAT DUEANSAWANG: SYNTHESIS AND SENSING PROPERTIES OF TRICATIONIC IMIDAZOLIUM AND GUANIDINIUM FLUOROPHORE. ADVISOR: ASSOC. PROF. PAITOON RASHATASAKHON, Ph.D., CO-ADVISOR: PROF. MONGKOL SUKWATTANASINITT, Ph.D., 77 pp.

Fluorescent derivatives of triphenylamine containing imidazolium, guanidine, and guanidinium peripheries are efficiently synthesized by Palladium-catalyzed coupling reactions. The target compounds are characterized by ^{1}H- and ^{13}C nuclear magnetic resonance, mass-spectrometry, UV-Vis and fluorescent spectrophotometry. The photophysical investigation of these compounds in 10 mM of HEPES buffer pH 7.0 reveals their maximum absorption wavelengths ranging between 319 to 362 nm, maximum emission wavelengths of around 428 to 456 nm, and quantum efficiencies of 17.97, 7.40, 3.16 and 2.39% for F1 - F4, respectively. A screening for sensing properties indicates that the emission signal of F1, which contains imidazolium groups, can be selectively quenched by hydrogen sulfide ion with a Stern-Volmer quenching constant of 4.91×10^{5} M^{-1} and a detection limit of 0.093 μM. Mechanistic examination by NMR suggests that the fluorescent signal changes may involve the binding between the proton at the 2-position of the imidazolium ring with hydrogen sulfide. For F2 which contains guanidine receptor, the fluorescent signal is selectively quenched by thiosulfate ion with a Stern-Volmer constant of 1.06×10^{5} M^{-1} and a detection limit of 1.31 μM.

Field of Study:	Petrochemistry and Polymer Science	Student's Signature .....
		Advisor's Signature .....
Academic Year:	2015	Co-Advisor's Signature .....

ACKNOWLEDGEMENTS

I would like to express my deep gratitude to my advisor, Associate Professor Dr. Paitoon Rashatasakhon, my co-advisor Professor Dr. Mongkol Sukwattanasinitt for their generous advice, invaluable guidance and encouragement throughout the course of this research.

I would like to gratefully acknowledge the committee, Assistant Professor Dr. Warinthorn Chavasiri, Associate Professor Dr. Chawalit Ngamcharussrivichai and Dr. Nakorn Niamnont for their comments, guidance and extending cooperation over my presentation. I would like to thank Assistant Professor Dr. Sumrit Wacharasindhu, Dr. Anawat Ajavakom and Dr. Sakulsuk Unarunotai for their attention and suggestions during our research group meeting.

I especially thank to express my gratitude to Material Advancement via Proficient Synthesis group (MAPS), Department of Chemistry, Faculty of Science, Chulalongkorn University for providing the chemicals and facilities throughout the course of study.

Finally, I would like to express my thankfulness to my beloved parent who always stand by me side during both of my pleasant and hard time.

CONTENTS

Page

Page

Page

Page

LIST OF TABLES

LIST OF FIGURES

LIST OF SCHEMES

LIST OF ABBREVIATIONS

Ar	aromatic
^{13}C NMR	carbon-13 nuclear magnetic resonance
$CDCl_3$	deuterated chloroform
CD_3OD	deuterated methanol
DMSO- d_6	deuterated dimethyl sulfoxide
DMSO	dimethylsulfoxide
d	doublet (NMR)
dd	doublet of doublet (NMR)
ESIMS	electrospray ionization mass spectrometry
equiv	equivalent (s)
g	gram (s)
^{1}H NMR	proton nuclear magnetic resonance
Hz	Hertz
HRMS	high resolution mass spectrum
h	hour (s)
J	coupling constant
K_a	Association constant
mg	milligram (s)
mL	milliliter (s)
mmol	millimole (s)
m/z	mass per charge
m	multiplet (NMR)

M.W.	molecular weight
M	molar
MHz	megaHerz
rt	room temperature
s	singlet (NMR)
TFA	Trifluoroacetic acid
THF	tetrahydrofuran
TLC	thin layer chromatography
UV	ultraviolet
δ	chemical shift
°C	degree Celsius
µL	microliter (s)
µM	micromolar (s)
Φ	quantum yield
% yield	percentage yield

CHAPTER I

INTRODUCTION

1.1 Fluorescent chemosensor

Nowadays, fluorescent chemosensors play an important role as analytical methods for detection of anions, metal ions, and biomolecules in chemical, biological, and environment research. Most of fluorescent sensors are composed of the following two main components: 1) a receptor unit for selective binding of the analytes, and 2) a fluorophore unit that provides the means of signaling upon the receptor-analyte binding, whether by fluorescence quenching, fluorescence enhancement, or emission wavelength shift (Figure 1.1) [1]. The mechanism which controls the response of a fluorophore to substrate binding, includes Internal charge transfer (ICT) [2-4], photo-induced electron transfer (PET) [2-5], fluorescence (FÖrster) resonance energy transfer (FRET) [6, 7], aggregation-caused quenching (ACQ) [8] and excimer/exciplex formation or extinction [2-4, 9].

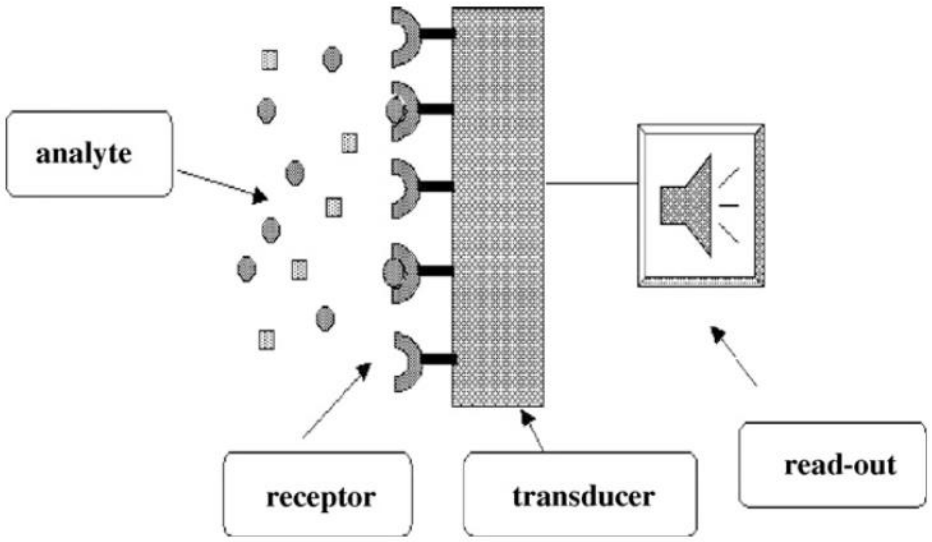

Figure 1.1 Basic principle of chemosensors.

1.2 Fluorescence

The fluorescence phenomenon is a light emission process of aromatic compounds or highly conjugated molecules. This process involves the absorption and

emission of light, and it usually can be described by the Jablonski diagram as shown in Figure 1.2 [10]. When a molecule at the electronic ground state (S_0) absorbs a sufficient amount of light energy, its electronic energy level will increase to a higher level called “excited state”. The molecule in excited state is unstable and it has to release energy in order to return to the S_0 state. For the excited fluorescence molecules, the first portion of energy is lost and the molecules will reside in the lowest excited electronic state (S_1) after geometrical relaxations by bond vibrations and molecular rotations. The transition from S_1 to S_0 is the release of the rest of energy in a form of light, which is called fluorescence.

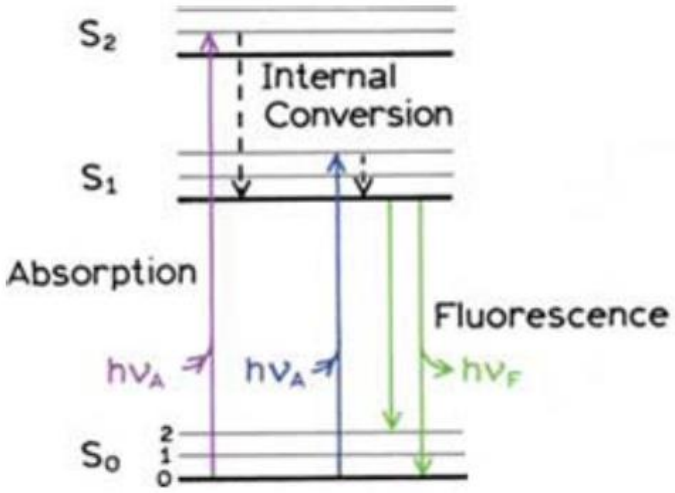

Figure 1.2 Jablonski Energy Diagram.

Two groups of fluorescent substances (fluorophores) can be classified by their structures; small molecules and conjugated polymers. The preparation and structural properties of these two classes of fluorophores are considered in the design of fluorescence sensors. Polymeric materials can be prepared with ease by polymerization of monomers [11], but their polydispersities can lead to uncontrollable photophysical properties of materials from different batches. For the small molecules, the synthesis could be more tedious and time-consuming, however, their monodispersities can assure the emission properties in every batch of materials. In addition, the well-defined structures of small molecules can lead to the assertive understanding in the interaction between fluorescent sensors and analytes. From these

reasons, small-molecule fluorophores have been widely used in fluorescent sensors in the past several decades. Some of the small-molecule fluorophores are shown in Figure 1.3. The structures of these compounds have been designed in order to occupy specific range in the fluorescent excitation or emission spectra.

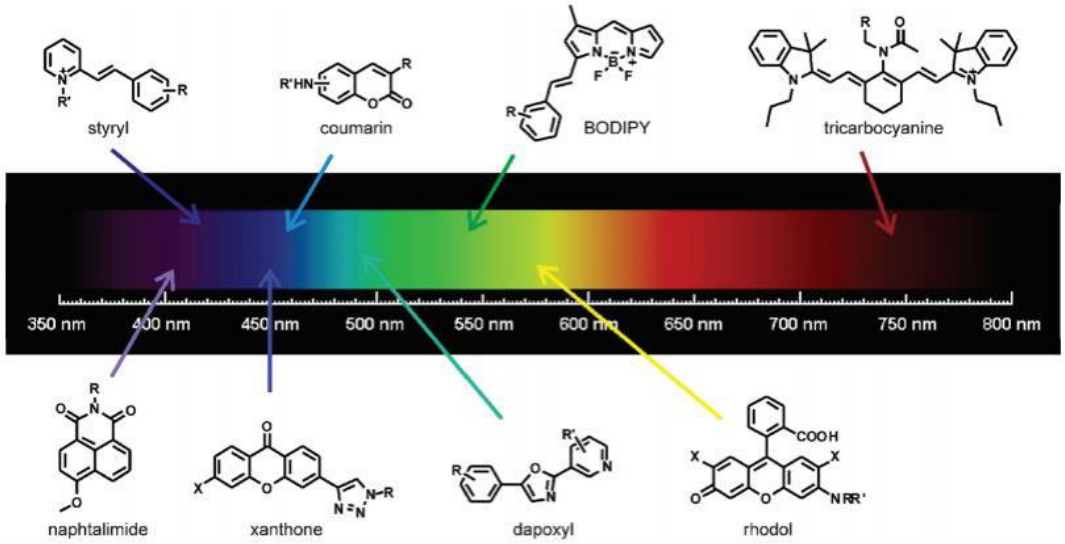

Figure 1.3 Molecule structure of some common **π**-conjugate molecules and their emission range in the visible region.

1.3 Fluorescent quenching

Fluorescent quenching is a process decreasing the intensity of the fluorescent emission. There have many processes involving fluorescent quenching such as excited state reactions, molecular rearrangements, ground state complex formation, and energy transfer. Generally, there are two mechanisms of quenching process involving dynamic (collisional) and static quenching. Both of the mechanisms require an interaction between the fluorophore and quencher. In the case of dynamic quenching, the quencher must diffuse to the fluorophore during the lifetime of the excited state upon contact the fluorophore then returns to the ground state without emission of a photon. In the case of static quenching, a non-fluorescent complex is formed between the fluorophore and the quencher. The formation of this complex does not rely upon population of the exited state. Moreover, the advantage of quenching experiments can be used as determine the accessibility of quencher to a fluorophore, monitor conformational changes, or monitored association reactions of the fluorescence of one

of the reactants change upon binding with the quencher. The fluorescent quenching is usually characterized by Stern–Volmer following equation.

$$\frac{I_0}{I} = 1 + k_q \tau_0 [Q] = 1 + K_{sv}[Q]$$

In this equation I_0 is the fluorescent intensity in the absence of quencher, I is the fluorescent intensities in the presence of quencher, kq is the bimolecular quenching constant, τ_0 is the lifetime of the fluorophore in the absence of quencher, and [Q] is the concentration of quencher. The Stern-Volmer quenching constant is given by K_D = kq τ_0. If the quenching is known to be dynamic, the Stern-Volmer constant will be represented by K_D. Otherwise, this constant will be described as K_{SV}. Quenching data are usually presented as plots of I_0/I versus [Q]. This is because I_0/I is expected to be linearly dependent upon the concentration of quencher. A plot of I_0/I versus [Q] yields an intercept of one on the y-axis and a slope equal to K_{SV}.

1.3.1 Photo-induced electron transfer (PET)

Photo-induced electron transfer (PET) often results in signal changing. The phenomenon of PET has been widely used in fluorescent sensor development [2-5]. The PET-based sensors can be categorized into two modes such as fluorescent 'turn-off' and 'turn-on' mode. For the turn-off mode, the receptor takes part only indirectly in the photophysical process. If the HOMO or LUMO state of receptor is between HOMO and LUMO gab of the energy levels of fluorophore shown in Figure 1.4 resulting in low or undetectable fluorescent emission.

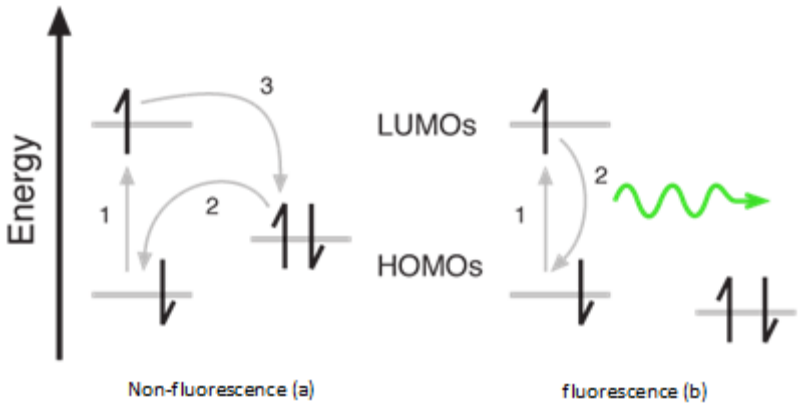

Figure 1.4 Orbital energy diagrams for fluorescent 'turn-off' PET sensors before and after binding with anion and (b) fluorescence emission; (b) forward electron transfer.

There are two possible mechanisms for fluorescent quenching by PET as depicted in Figure 1.5. If the HOMO level of the donor lies between the HOMO-LUMO gab of the fluorophore, an electron from the donor presumably transfer to the HOMO state of the excited fluorophore which acts as the electron acceptor (Figure 1.5, left). In another case where the empty LUMO state of the receptor lies between the HOMO-LUMO gab of the fluorophore. In this case, the excited fluorophore acts like the electron donor to the LUMO state of the acceptor before transferring back to the half-filled HOMO state of the fluorophore (Figure 1.5, right). The electron transfer processes are the non-radiative processes resulting in quenching of the fluorescent signal of the fluorophore.

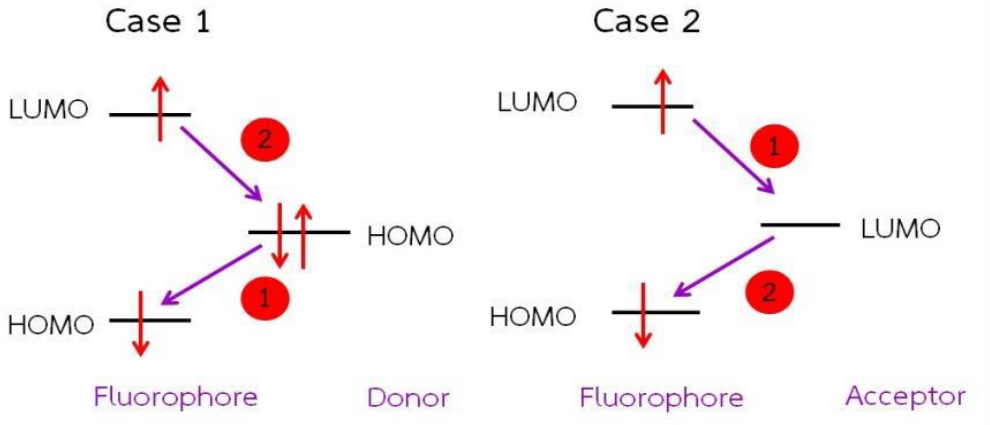

Figure 1.5 Photo-induced electron transfer mechanism.

1.3.2 Aggregation-caused quenching (ACQ)

Aggregation-caused quenching (ACQ) is a general property for organic luminescent materials which have strong emission in diluted organic solution. However, it is a common phenomenon that luminescence is often weakened or quenched at high concentrations or in solid forms. This high concentration is called "concentration quenching" that mainly caused by the "formation of aggregates". ACQ is usually arisen from the intermolecular **π–π** stacking interactions of **π**-conjugated plane molecules, because **π–π** interactions will facilitate the formation of excimers, which lead to emission quenching [8].

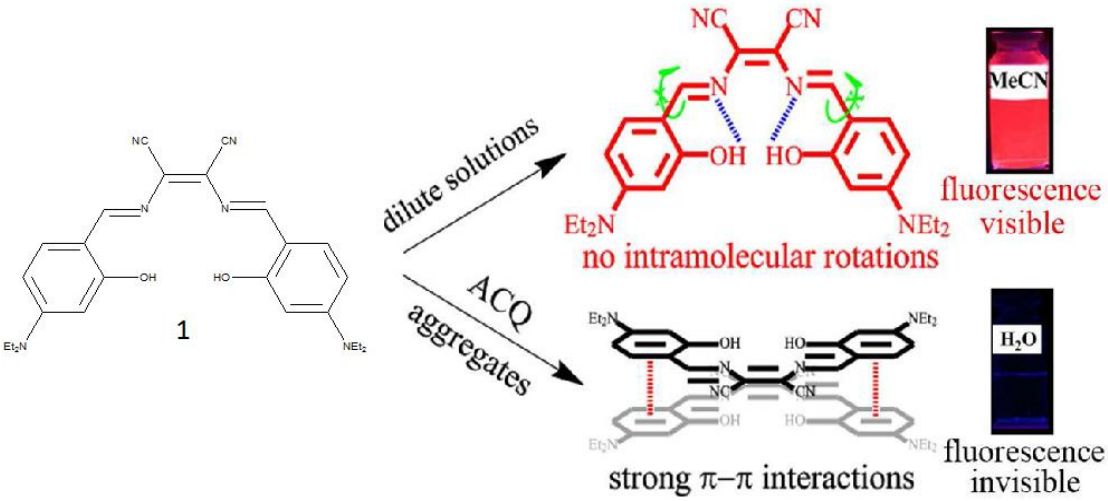

Scheme 1.1 Fluorescent mechanism for **1**.

1.3.3 Excited-state proton transfer

Excited state proton transfer (ESPT) effect of organic molecule is a fundamental reaction of photochemistry, and it exists widely in many chemical and biological processes. Some organic molecules can be excited to the excited state by the excitation of light. In the excited state, a hydroxyl proton of the molecule can transfer to the vicinity site of a nitrogen, oxygen, or sulfur atom within the molecule through the intermolecular hydrogen bond, and then the organic molecule changes into its isomer. This process is referred to as the ESPT effect. 7- hydroxyquinoline (**7-HQ**) is a kind of organic molecules which exhibits the ESPT effect. In normal conditions, **7-HQ** is present in the enol form. When **7-HQ** is excited by an UV light, it transits to the

excited state from the ground state of the enol form and quickly transfers to the excited state of the keto form via the intermolecular.

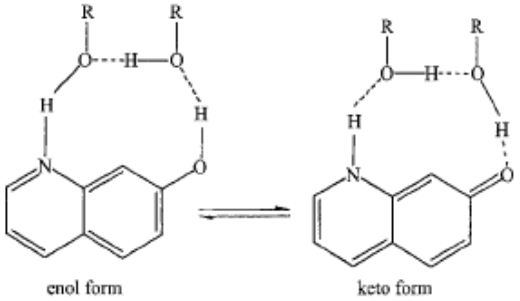

Figure 1.6 Scheme of ESPT effect of **7-HQ**.

1.4 Literature review on fluorescent chemosensors

Examples of literatures related to fluorescent sensors for anions during the past 7 years are as follows last 7 years are as follows:

1.4.1 Literature review on imidazolium-based fluorescent sensor

In 2012, Shirinfar et al. [12] synthesized probe **1** having naphthalene as a fluorophore and having imidazolium as a receptor group to generate turn-on mode for RNA (Figure 1.7). Probe **1** exhibited high selectivity to RNA in solution of phosphate buffer pH 7.4. Probe **1**. It binds RNA through the interaction of the imidazolium protons with the oxygen atoms of RNA with binding constant of 4.9×10^{6} M^{-1}. Additionally, it was utilized as RNA fluorescent imaging probe in onion cells and Hela cells.

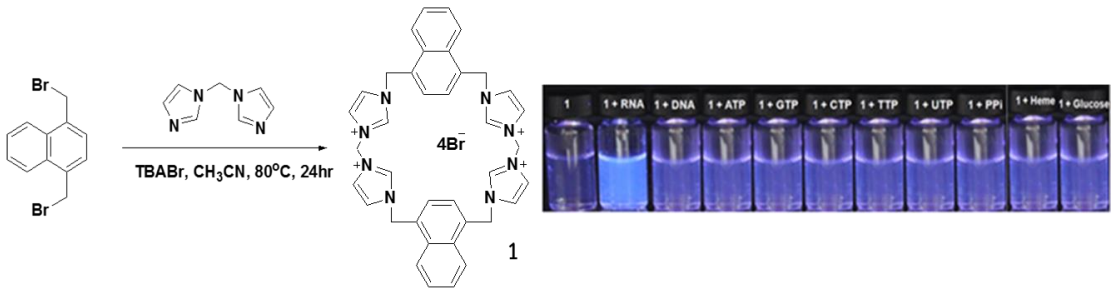

Figure 1.7 General methods for the preparation of **1** (left) and **1** solutions with various amino acid under black light (right).

In 2011, Ahmed and et al. [13] Synthesized **2** having anthracene and imidazolium as fluorophore and receptor group. This compound served as a turn-off

sensor for GTP and I^- in aqueous solution shown in Figure 1.8. The detection limits were estimated by the titration between solution of sensor molecule and analytes showing around $4.8x10^{-7}$ M and $8x10^{-5}$ M for GTP and I^-, respectively.

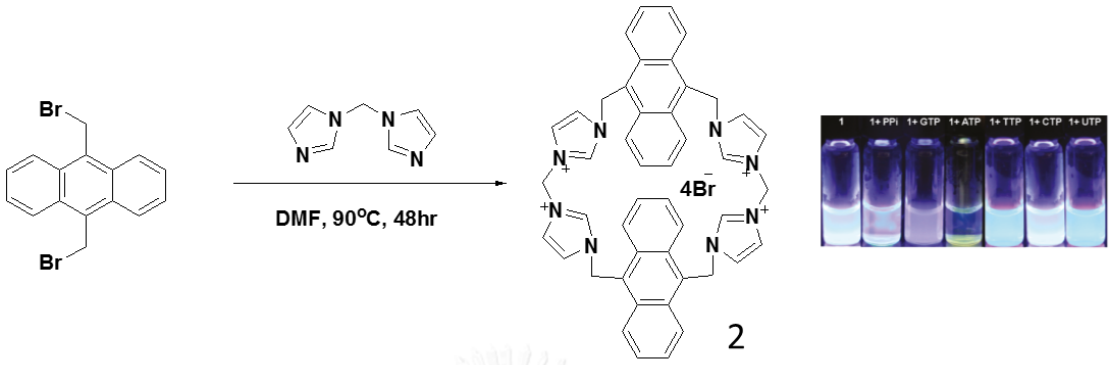

Figure 1.8 General methods for the preparation of **2** (left) and **2** solutions with various amino acid under black light (right).

In 2010, Kim and et al. [14] synthesized imidazolium anthracene derivative **3** (Figure 1.9). It exhibited selectivity fluorescent quenching effect by calf thymus DNA (CT DNA) in 10 mM of sodium phosphate buffer/CH_3CN (95:5 v/v) at pH 7.0 with an association constant is 8.9×10^6 M^{-1}. The quenching mechanism was proposed as a blinding between phosphate oxygens and imidazolium groups of **3**.

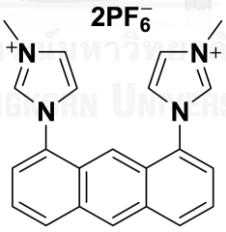

Figure 1.9 Chemical structure of **3**.

1.4.2 Literature review on guanidinium-based fluorescent sensor

In 2009, Sun and et al. [15] synthesized a new FRET-based ratiometric fluorescent chemodosimeter **4** for sulfite, in which guanidiniocarbonyl pyrrole moiety is covalently attached to 9-(aminomethyl)anthracene (Figure 1.10). It was discovered that guanidinium group responded to SO_3^{2-} and the limit of detection to 7.8×10^{-4} M.

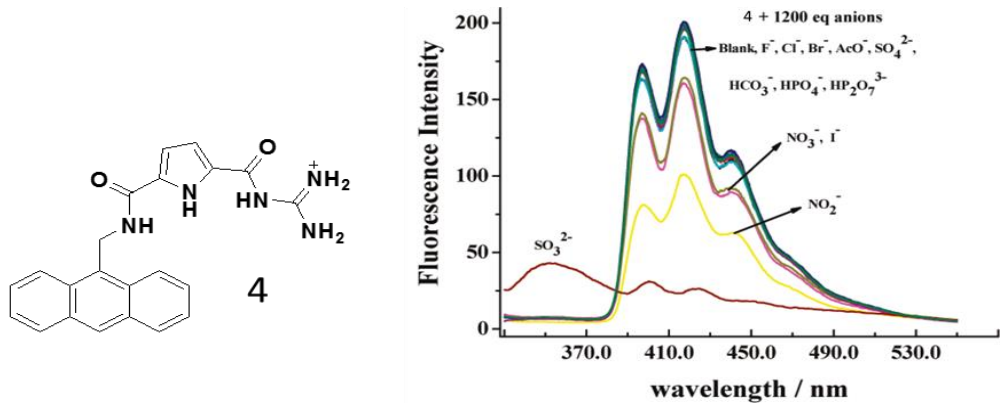

Figure 1.10 Chemical structure of **4** and Fluorescence spectra of **4** in 90% water/DMSO solution in the presence of other anions.

In 2012, Nogushi and et al. [16] Syntensized **TPE** having tetraphenylethene and guanidinium as fluorophore and receptor group, respectively. This sensor showed a selective turn-on signal for ATP, which was postulated to occur by ion-pairing complexation of **TPE** and ATP followed by aggregation-induced emission effect (AIE) (Figure 1.11).

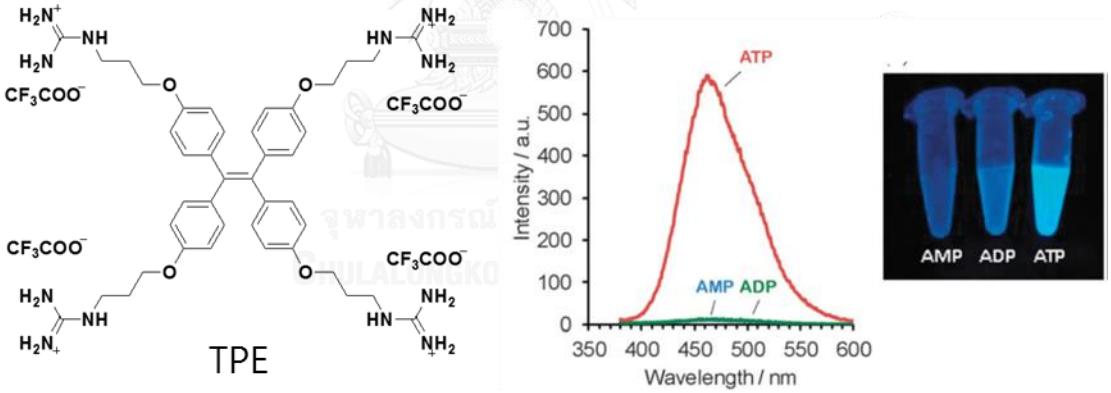

Figure 1.11 Chemical structure of **TPE** and Fluorescence spectra of **TPE** in HEPES buffer pH 7.4 in the presence of AMP, ADP and ATP.

1.4.3 Literature review on triethynyltriphenylamine fluorescent sensor

In 2009, Niamnont and et al. [17] reported the synthesis and sensing properties of water soluble fluorescent dendritic compound **A**. This dendritic compound composed of phenylene-ethynylene repeating units and anionic carboxylate peripheries. Without a surfactant, compound **A** exhibited a low fluorescent quantum yield, but a good selectivity toward Hg^{2+}. After adding Triton X-100, the quantum yield

was drastically increased and the sensitivity for the detection of Hg^{2+} was also improved. (Figure 1.12)

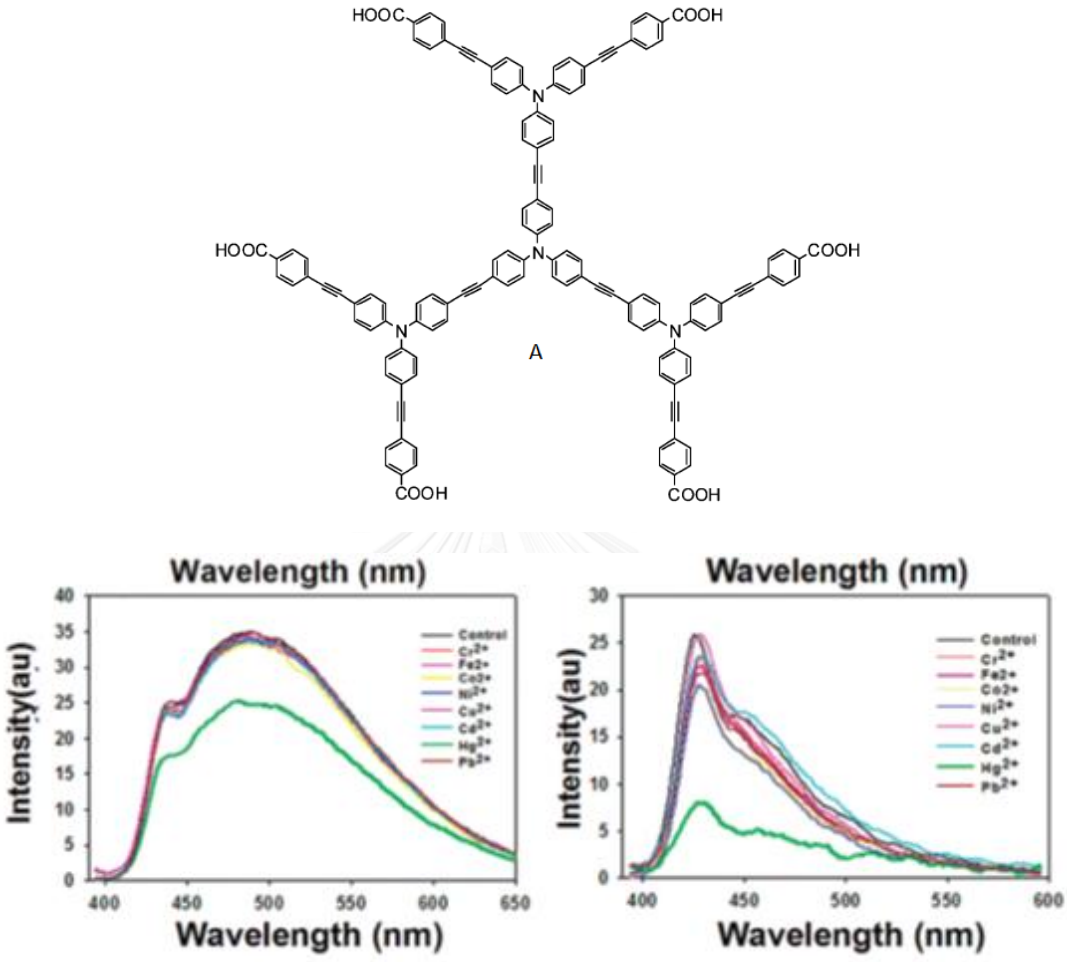

Figure 1.12 Structure of **A** and selectivity toward Hg^{2+} ion before (left) and after the surfactant added (right).

In 2013, Kimpitak and et al. [18] synthesized new molecule in which triethynyltriphenylamine core and salicylic acid as receptor group. When it was tested with various types of metal ions, the selectivity with Cu^{2+} had been discovered with 5.79×10^{6} M^{-1} of K_{sv} value. In addition, it was utilized as detector on paper in order to detect Cu^{2+} by naked-eyes.

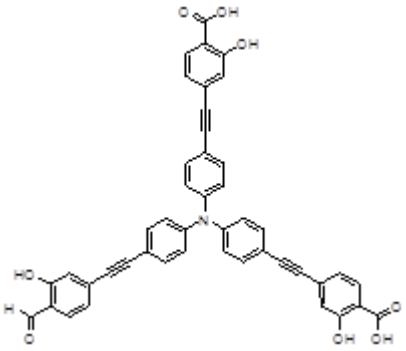

Figure 1.13 Structure of triethynyltriphenylamine core and salicylic acid as receptor group.

1.4.4 Literature review on fluorescent sensors for hydrogen sulfide

1.4.4.1 Replacement of copper complexes

In 2011, Cao and et al. [19] used tricabocyanine fluorophore containing 8-aminoquinoline coordinating with Cu^{2+} to generate a turn on mode in near-infrared range for sulfide ion in HEPES buffer/ethanol (6:4 v/v) pH 7.0. This sensor showed a detection limit of 280 nM. The enhancement mechanism was based on the displacement of sulfide ion to Cu^{2+} as shown in Figure 1.14.

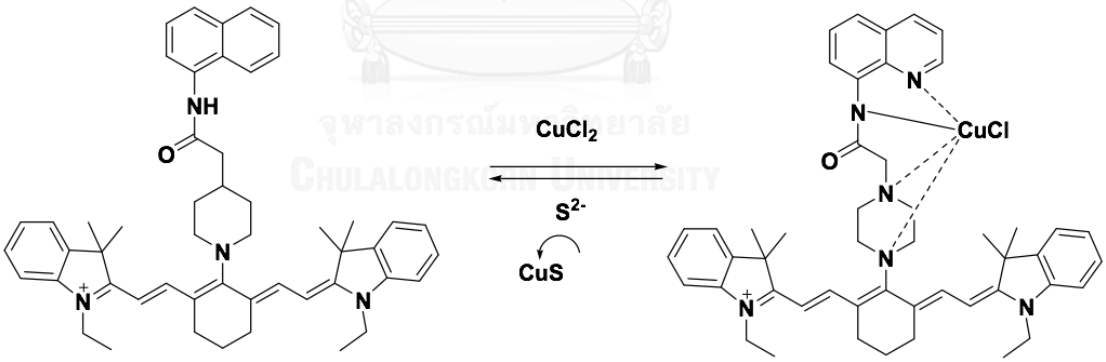

Figure 1.14 Mechanism for Sensing of Sulfide Anions.

In 2012, Qi and et al. [20] synthesized a new compound **R-1** for sensing application in water. They found that **R-1** had selectivity towards Cu^{2+} in fluorescent quenching mode (quenching efficiency of 86%). The signal could be restored selectively by sulfide ions with a detection limit of $4x10^{-6}$ M and a binding constant around $3x10^{2}$. (Figure 1.15).

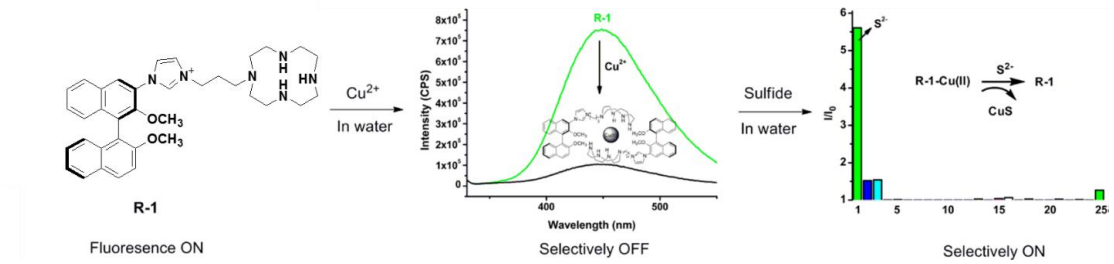

Figure 1.15 Structure of **R-1**, complex with Cu^{2+} and addition of sulfide anion.

1.4.4.2 Cleavage of the alcoxyl (R-O) bond

In 2015, Zhang and et al. [21] reported novel tetraphenylethene-base fluorescent probe for H_2S, which exhibited high selectivity and sensitivity. This compound can function as a fluorescent turn-on sensor as well as a colorimetric sensor. The detection of H_2S in living cells was also demonstrated in this work. (Figure 1.16)

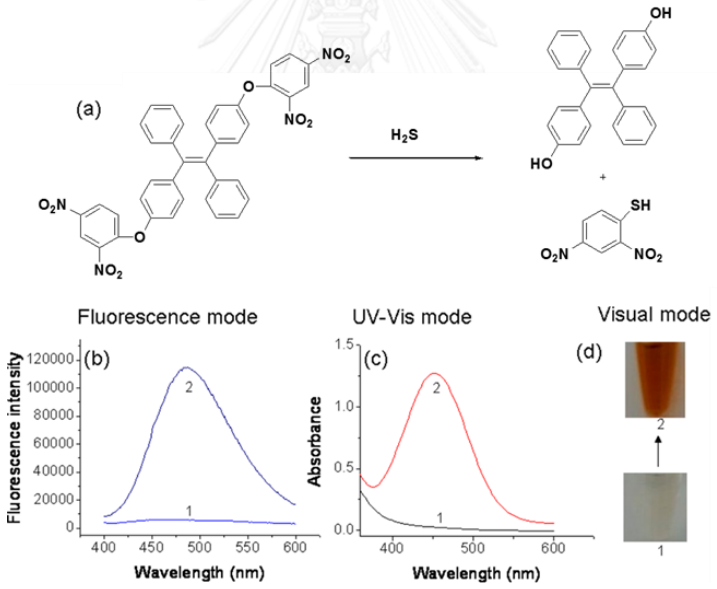

Figure 1.16 (a) Structures of sensor and products. (b) Fluorescence and (c) adsorption spectra of (1) sensor and (2) products. (d) Color changes of solutions of (1) sensor and (2) products.

In 2014, Liu and Feng [22] reported a probe based on the excited state intramolecular proton transfer (ESIPT) in 3-hydroxyflavone. This compound was originally light yellow and not fluorescent when dissolved in 20 mM PBS buffer pH 7.4 with 20% DMSO and 3 mM CTAB. The addition of SH^- led to emission at 538 nm with

a color change to deep yellow. The detection limit for SH^- of this probe was $0.13x10^{-6}$ M base on the signal to noise ratio (S/N) = 3. (Figure 1.17)

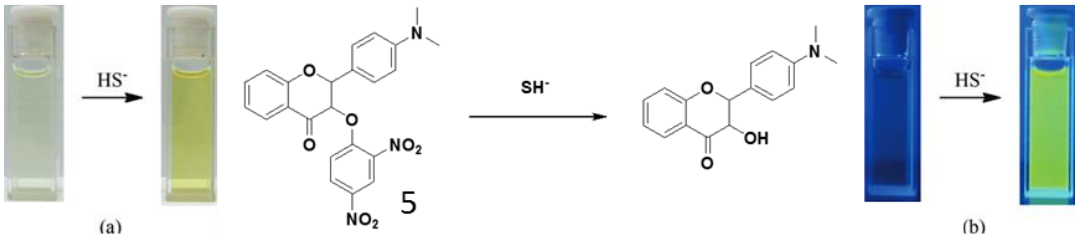

Figure 1.17 Reaction of probe **5** with SH^-. Color changes of probe **5** (20 mM) solution after the addition of NaHS (200 mM) (a) under room light and (b) under black light.

1.4.4.3 Reduction of azides

In 2011, Lippert et al [23] reported two azide-caged rodamine analogues as fluorescent probes **6** and **7** for detection of H_2S (Figure 1.18). The fluorescence properties of two probes were tested in 20 mM HEPES buffered pH 7.4. In addition of SH^-, the probes showed new absorption bands in the visible region and there was a significant enhancement in the fluorescence intensities. The change in fluorescence was due to the products of the reactions between **6** and **7** with SH^-, the corresponding rhodamine dye structures were confirmed by ^{1}H-NMR and liquid chromatography-mass spectrometry analyses.

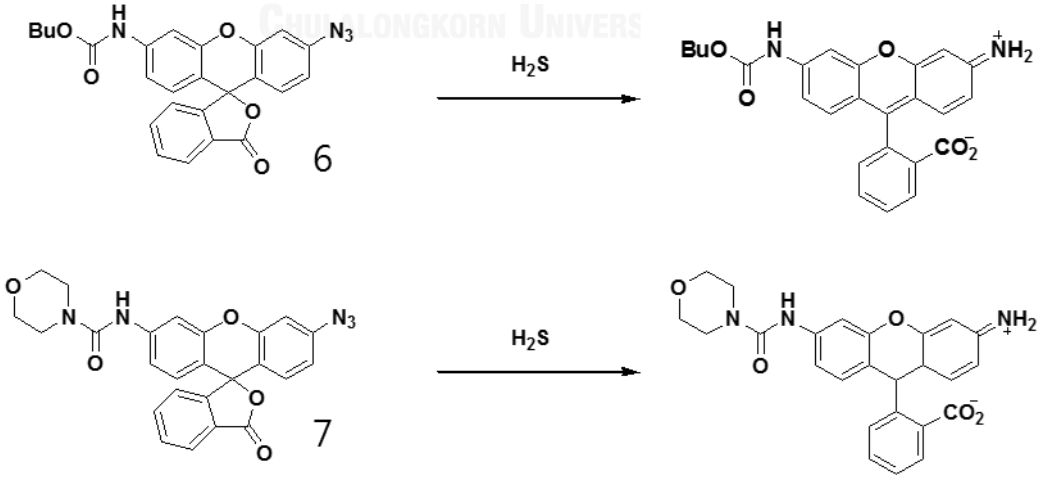

Figure 1.18 Fluorescent probes **6** and **7** for H_2S Detection.

In 2015, Zhang and et al [24] reported **8** based on iminocoumarin benzothiazole scaffold for detection H_2S in 50 mM Tris buffer pH 8.0: 50% DMF. The

probe **8** utilizes H_2S-induced cascade reaction consisting of three consecutive steps: reduction, elimination and cyclization (Figure 1.19). The fluorescence was measured after 60 min of incubation and the detection limit of **8** was determined to be $0.15x10^{-6}$ M.

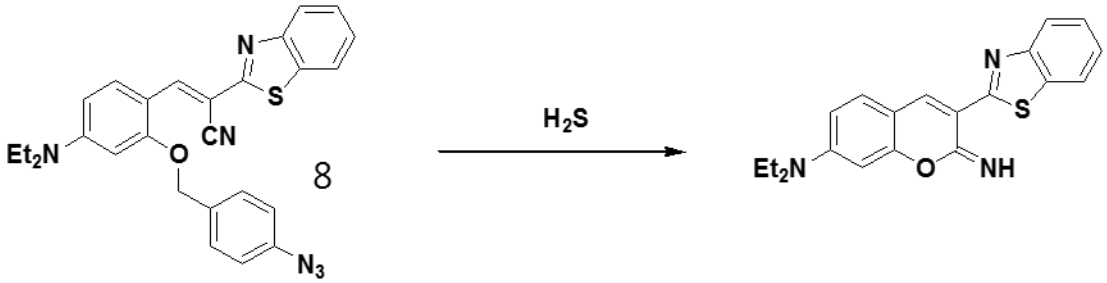

Figure 1.19 Fluorescent probe **8** for H_2S detection.

1.5 Objectives of this research

This research involved the design, synthesis and characterization of novel fluorophores from triphenylamine derivatives with imidazolium group or guanidinium group as receptor groups (Figure 1.20). The photophysical properties, applications for anion detection in aqueous media, and sensing mechanism were investigated.

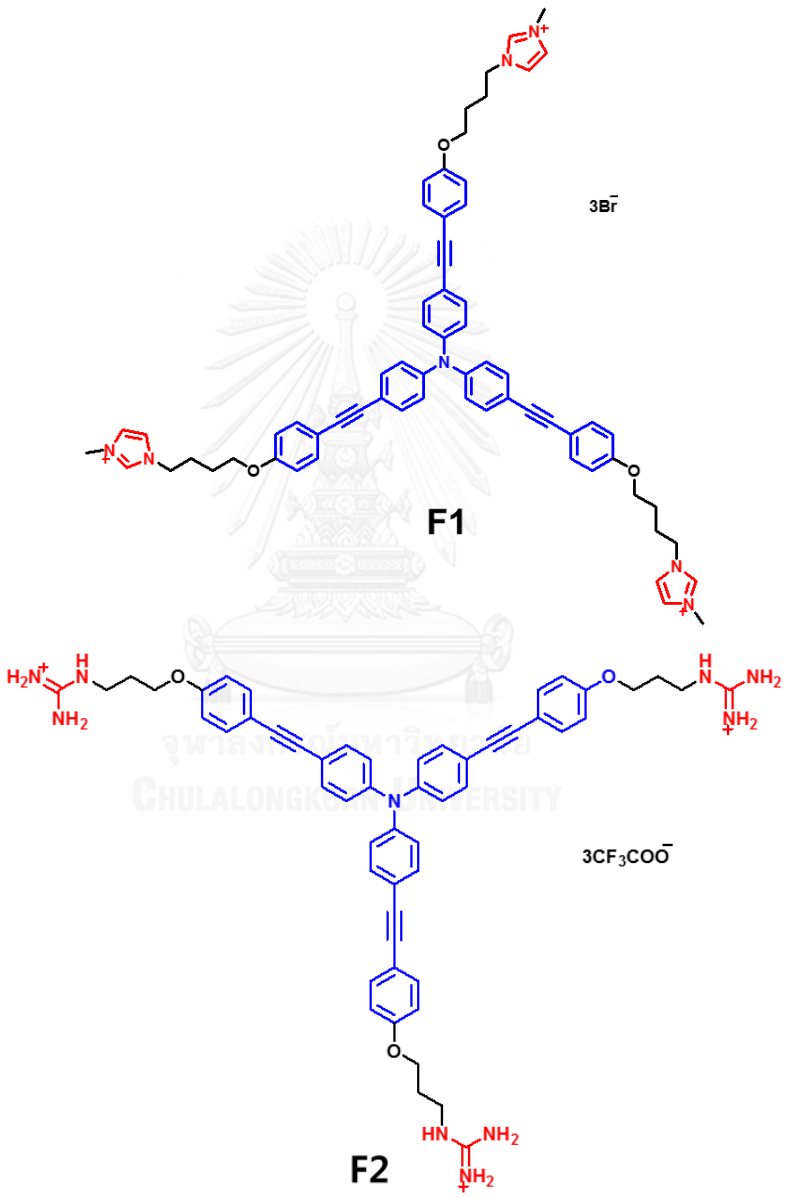

Figure 1.20 Target molecules.

CHAPTER II

EXPERIMENTAL

2.1 Chemicals and materials

Tetrakis(triphenylphosphine)palladium (0) $Pd(PPh_3)_4$, trimethylsilylacetylene, bis(triphenylphosphine)palladium (II) dichloride ($PdCl_2(PPh_3)_2$) and triphenylamine were purchased from Fluka. 4-iodophenol, methylimidazole, 3-bromopropylamine. hydrobromide, Di-tert-butyl dicarbonate, N-bromosuccinimide, 4-(Diphenylamino)phenylboronic acid and *N,N'*-di-boc-1H-pyrazole-1-carboxamidine were purchased from Sigma-Aldrich. All other reagents were non-selectively purchased from Fluka, Sigma-Aldrich or Merck. For most reactions, solvents such as ethanol (EtOH) and dichloromethane (CH_2Cl_2) were reagent grade stored over molecular sieves. For anhydrous reactions, solvents such as acetonitrile (CH_3CN) and tetrahydrofuran (THF) were dried before use according to the standard procedures. All of the column chromatography were operated using Merck® silica gel 60 (70-230 mesh). Thin layer chromatography (TLC) was performed on silica gel plates (Merck F245). Solvents used for extraction and chromatography such as dichloromethane, hexanes and ethyl acetate were commercial grade. Some reactions were carried out under positive pressure of N_2 filled in rubber balloons.

2.2 Analytical Instruments

The ^1H- and ^{13}C-NMR spectra were obtained on a Varian Mercury NMR spectrometer, which operated at 400 MHz for ^1H and 100 MHz for ^{13}C nuclei (Varian Company, CA, USA). The HRMS spectra were measured on an electrospray ionization mass spectrometer (microTOF, Bruker Daltonics). Absorption spectra were measured by a Varian Cary 50 UV-Vis spectrophotometer. Fluorescence spectra were obtained from a Varian Cary Eclipse spectrofluorometer.

2.3 Synthesis of F1, F2, F3 and F4

2.3.1 4, 4', 4''-Triiodotriphenylamine (1)

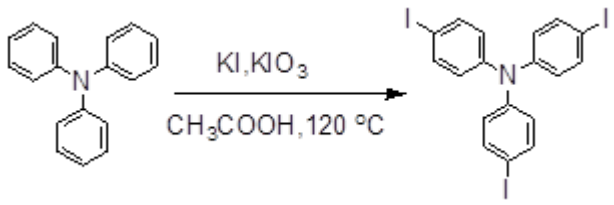

Triphenylamine (3.0 g, 12.2 mmol) was mixed with potassium iodide (6.53 g, 36 mmol) and potassium iodate (7.85 g, 36 mmol) in a 50-mL round-bottom flask under N_2 atmosphere. After that acetic acid (20 mL) was added to the flask and stirred at 120 ^{o}C for 48 hr. After the reaction was completed, the reaction was extracted 3 times with water and dichloromethane. The organic layer was dried over anhydrous sodium sulfate, followed by removing of solvent under reduced pressure. The organic residue was purified by column chromatography on silica gel eluting by hexane to afford **1** as white solid in 90% yield. ^{1}H NMR (400 MHz, $CDCl_3$) δ 7.54 (d, *J* = 8.8 Hz, 6H), 6.81 (d, *J* = 8.8 Hz, 6H). ^{13}C NMR (100 MHz, $CDCl_3$) δ 146.7, 138.4, 126.2, 86.8. [17]

2.3.2 1-(4-Bromobutoxy)-4-iodobenzene (2)

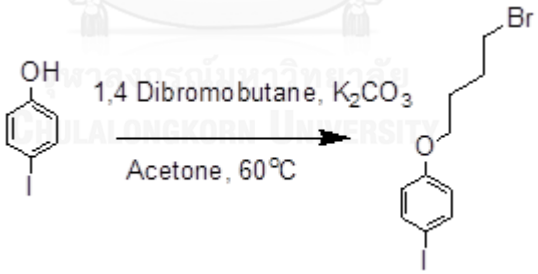

4-Iodophenol (1 g, 4.5 mmol) was mixed with 1,4-dibromobutane (1.07 ml, 9 mmol) and potassium carbonate (1.24 g, 9 mmol) in a 50-mL round-bottom flask under N_2 atmosphere. The mixture was diluted with acetone (10 mL) then stirred at 60 ^{o}C overnight. After the reaction was completed, the crude reaction was extracted 3 times with water and dichloromethane. The combined organic layer was dried over anhydrous sodium sulfate followed by removing of solvent under reduced pressure. The residue was purified by column chromatography on silica gel eluting with hexane to provide **2** as pale yellow oil in 90% yield. ^{1}H NMR (400 MHz, $CDCl_3$) δ 7.54 (d, *J* =

9.0 Hz, 2H), 6.66 (d, *J* = 9.0 Hz, 2H), 3.93 (t, *J* = 6.1 Hz, 2H), 3.47 (t, *J* = 6.6 Hz, 2H), 2.09 – 1.98 (m, 2H), 1.98 – 1.85 (m, 2H). ^{13}C NMR (100 MHz, $CDCl_3$) δ 158.6, 138.1, 116.8, 82.7, 66.9, 33.2, 29.3, 27.7. [25]

2.3.3 (2-(4-(4-Bromobutoxy)phenyl)ethynyl)trimethylsilane (3)

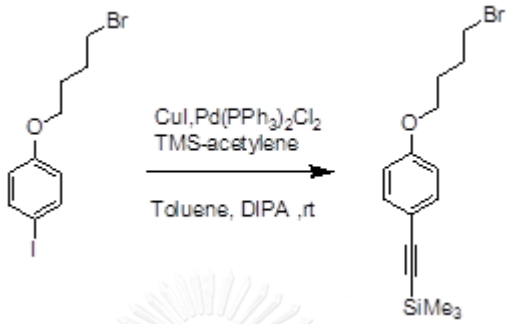

Iodobenzene **2** (0.3 g, 0.84 mmol) was mixed with $Pd(PPh_3)_2Cl_2$ (11 mg, 0.01 mmol), CuI (6.4 mg, 0.03 mmol) in a 50-mL round-bottom flask under N_2 atmosphere. The mixture was dissolved in toluene (10 mL) and then diisopropylamine (3 mL) was added, followed by TMS-acetylene (0.25 mL, 1.69 mmol). The mixture was stirred at room temperature overnight. After the reaction was completed, the solvent was evaporated and the crude was purified by column chromatography on silica gel using 10% ethyl acetate in hexane as eluting to afford **3** as yellow solid in 96% yield. The ^{1}H NMR spectrum of this product is in good agreement with the literature report. [26]

2.3.4 1-(4-Bromobutoxy)-4-ethynylbenzene (4)

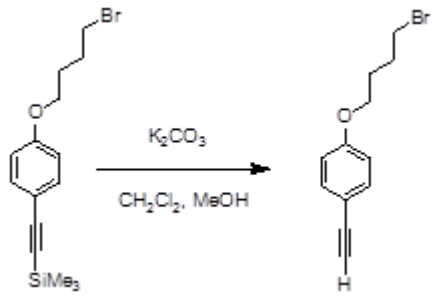

3 (0.3 g, 0.92 mmol) was mixed with potassium carbonate (0.38 g, 2.76 mmol) a in 50-mL round-bottom flask under N_2 atmosphere. The mixture was dissolved with dichloromethane (8 mL) and methanol (2 mL) and stirred at room temperature for 4 hr. After the reaction was completed, the reaction crude was extracted 3 times with water and dichloromethane. The organic layer was dried over anhydrous sodium

sulfate followed by removing of solvent under reduced pressure. The organic residue was purified by column chromatography on silica gel eluting with 10% ethyl acetate in hexane to provide **4** as white solid in 93% yield. ^{1}H NMR (400 MHz, $CDCl_3$) δ 7.42 (d, *J* = 8.6 Hz, 2H), 6.82 (d, *J* = 8.6 Hz, 2H), 3.98 (t, *J* = 5.9 Hz, 2H), 3.48 (t, *J* = 6.5 Hz, 2H), 3.01 (s, 1H), 2.11 – 2.00 (m, 2H), 2.00 – 1.89 (m, 2H). ^{13}C NMR (100 MHz, $CDCl_3$) δ 159.4, 133.7, 114.6, 83.8, 75.9, 67.0, 33.4, 29.5, 27.9.

2.3.5 Tribromo (5)

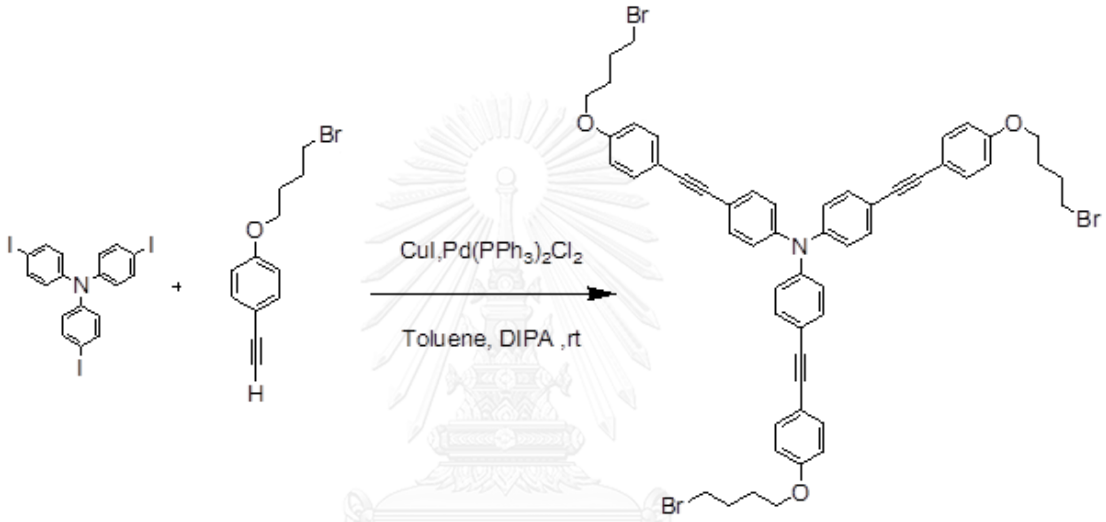

Compound **1** (0.1 g, 0.16 mmol) was mixed with $Pd(PPh_3)_2Cl_2$ (4.5 mg, 0.006 mmol) and CuI (1.2 mg, 0.006 mmol) in a 50-mL round-bottom flask under N_2 atmosphere. The mixture dissolved with toluene (7 mL) and diisopropylamine (3 mL). Then **4** (0.16 g, 0.64 mmol) was added into the mixture solution slowly. After that stirred at room temperature for 48 hr, evaporated of solvent. The organic crude was purified by column chromatography on silica gel using 20% ethyl acetate in hexane as eluting providing **5** as brown solid in 48% yield. ^{1}H NMR (400 MHz, $CDCl_3$) δ 7.43 (d, *J* = 15.0 Hz, 6H), 7.41 (d, *J* = 14.9 Hz, 6H), 7.05 (d, *J* = 8.4 Hz, 6H), 6.86 (d, *J* = 8.5 Hz, 6H), 4.01 (t, *J* = 5.9 Hz, 6H), 3.49 (t, *J* = 6.5 Hz, 6H), 2.14 – 2.02 (m, 1H), 2.02 – 1.89 (m, 6H).^{13}C NMR (101 MHz, CDCl3) δ 159.0, 146.7, 133.1, 132.8, 124.2, 118.4, 115.8, 114.7, 89.4, 88.1, 67.1, 33.4, 29.6, 28.0.

2.3.6 Synthesis of F1

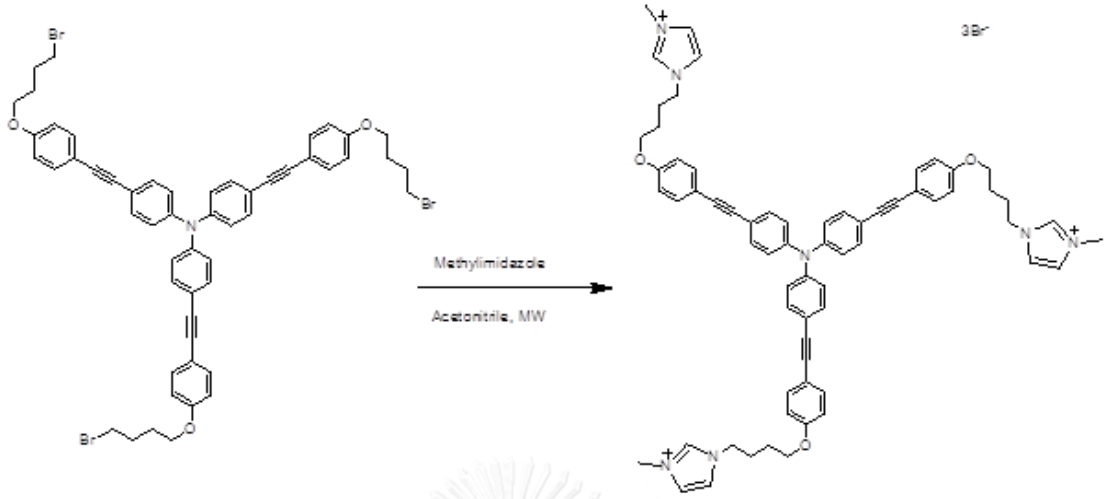

Compound **5** (0.05 g, 0.05 mmol) was mixed with 1-methylimidazole (0.016 mL, 0.2 mmol) in microwave tube. The mixture dissolved with acetonitrile (3 mL). The reaction was carried out under microwave irradiation at 120 W at 100 °C for 3 hr. After that the reaction was evapolated, washed with diethyl ether and dichloromethane, respectively. Finally, the residue was removed solvent by evaporation and vacuum dry providing **F1** product in 82% yield. ^{1}H NMR (400 MHz, CD_3OD) δ 9.00 – 8.94 (m, 3H), 7.68 (s, 3H), 7.59 (s, 3H), 7.42 (d, *J* = 8.7 Hz, 12H), 7.06 (d, *J* = 8.6 Hz, 6H), 6.92 (d, *J* = 8.8 Hz, 6H), 4.31 (t, *J* = 7.1 Hz, 6H), 4.07 (t, *J* = 5.5 Hz, 6H), 3.92 (s, 9H), 2.15 – 2.04 (m, 6H), 1.91 – 1.79 (m, 6H). ^{13}C NMR (75 MHz, CD_3OD) δ 160.3, 147.8, 134.0, 133.7, 125.0, 123.6, 119.6, 116.8, 115.8, 90.9, 89.0, 68.3, 36.6, 28.1, 27.0.

2.3.7 N-(tert-Butoxycarbonyl)-3-bromopropylamine (6)

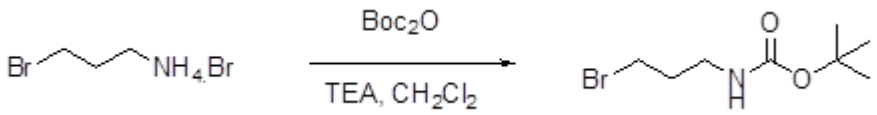

3-Bromopropylamine hydrobromide (2.00 g, 9.10 mmol) in dichloromethane (50 mL) were added Boc_2O (2.39 g, 10.10 mmol) and triethylamine (2.5 mL, 18.27 mmol). The mixture was stirred at room temperature for 18 h. After the reaction was completed, the crude reaction mixture was extracted with dichloromethane /1 N HCl, water, and brine. The combined organic layer was dried over anhydrous sodium sulfate followed by removing of solvent under reduced pressure. The residue was purified by

column chromatography on silica gel using 20% ethyl acetate in hexane to provide 6 as colorless oil in 80% yield. The ^{1}H NMR spectrum of this product is in good agreement with the literature report. [16]

2.3.8 Synthesis of 7

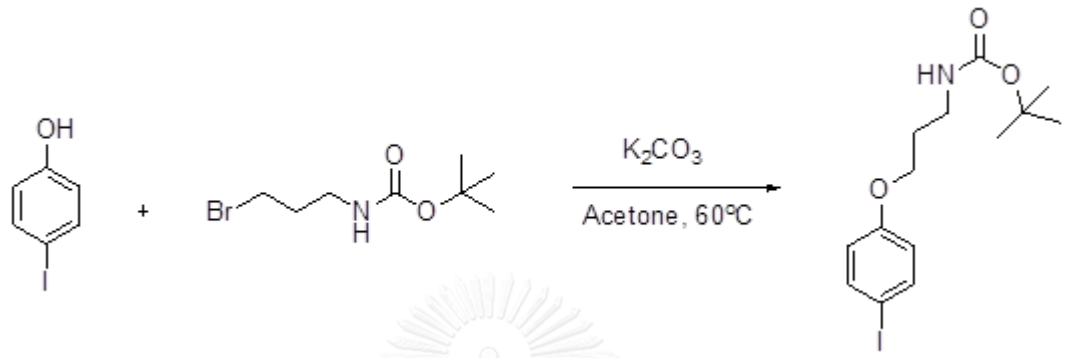

4-Iodophenol (1 g, 4.5 mmol) was mixed with *N*-(tert-Butoxycarbonyl)-3-bromopropylamine (1.30 g, 5.45 mmol) and potassium carbonate (1.24 g, 9 mmol) in a 50-mL round-bottom flask under N_2 atmosphere. The mixture was diluted with acetone 10 mL then stirred at 60 °C overnight. After the reaction was completed, the crude reaction mixture was extracted 3 times with water and dichloromethane. The combined organic layer was dried over anhydrous sodium sulfate followed by removing of solvent under reduced pressure. The residue was purified by column chromatography on silica gel using 20% ethyl acetate in hexane to provide **7** as pale white solid in 94% yield. The ^{1}H NMR spectrum of this product is in good agreement with the literature report. [27]

2.3.9 Synthesis of 8

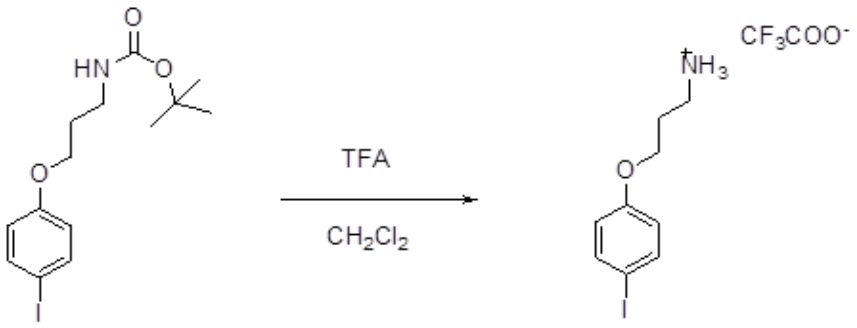

Compound **7** (0.5 g, 1.32 mmol) dissolved with dichloromethane (5 mL) was added TFA (3 mL, 39.0 mmol) in a 50-mL round-bottom flask under N_2 atmosphere,

after that stirred at room temperature overnight. The crude reaction mixture was poured into diethyl ether to precipitate **8** as a white solid, collected by filtration and washed with diethyl ether and dried in vacuum (42% yield). ^{1}H NMR (400 MHz, CD_3OD) δ 7.59 (d, *J* = 8.9 Hz, 2H), 6.78 (d, *J* = 2 Hz, 2H), 4.10 (t, *J* = 5.8 Hz, 2H), 3.15 (t, *J* = 2 Hz, 2H), 2.20 – 2.06 (m, 2H).

2.3.10 Synthesis of 9

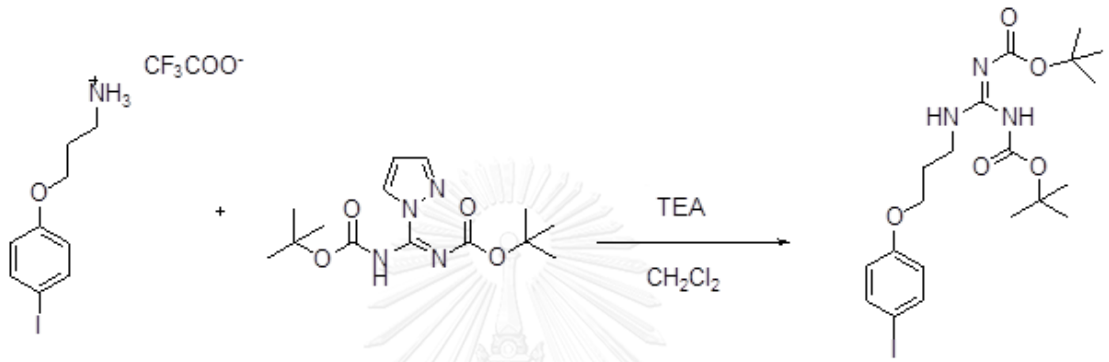

Compound **8** (0.3 g, 0.76 mmol) was mixed with 1-*H*-pyrazole-1-(*N*,*N*'-bis(*tert*-butyloxycarbonyl))carboxamidine (0.238 g, 0.76 mmol) in 50-mL round-bottom flask under N_2 atmosphere. The mixture was dissolved with dichloromethane (8 mL) and triethylamine (0.318 mL, 2.28 mmol) then stirred at room temperature for 48 hr. After the reaction was completed, the reaction crude was extracted 3 times with water and dichloromethane. The organic layer was dried by anhydrous sodium sulfate followed by removing of solvent under reduced pressure. The organic residue was purified by column chromatography on silica gel eluting with dichloromethane to provide **9** as white solid in 72% yield. ^{1}H NMR (400 MHz, $CDCl_3$) δ 11.49 (s, *J* = 49.7 Hz, 1H), 8.63 (s, 1H), 7.52 (d, *J* = 8.8 Hz, 2H), 6.72 (d, *J* = 8.9 Hz, 2H), 4.00 (t, *J* = 5.7 Hz, 2H), 3.62 (dd, *J* = 11.9, 6.1 Hz, 2H), 2.15 – 1.92 (m, 2H), 1.49 (s, *J* = 6.0 Hz, 18H). ^{13}C NMR (101 MHz, $CDCl_3$) δ 163.35, 158.38, 155.92, 152.94, 137.90, 116.68, 82.81, 82.69, 79.02, 66.31, 38.75, 28.32, 28.09, 27.88.

2.3.11 Synthesis of 10

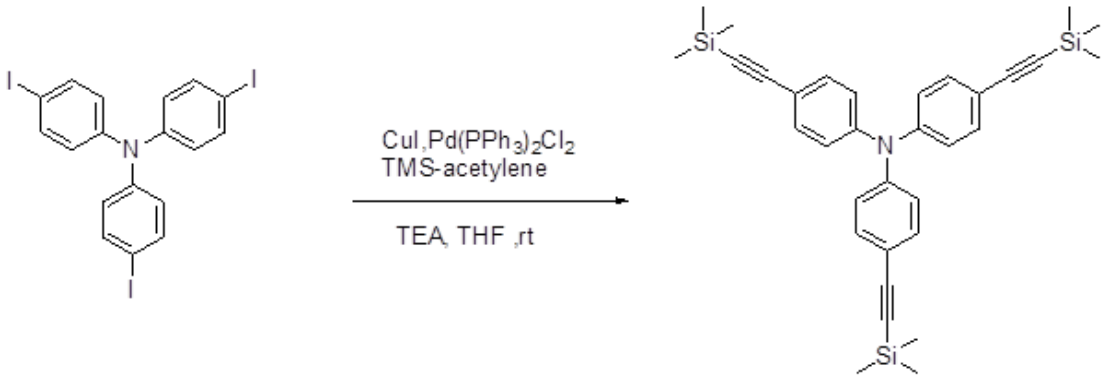

4, 4', 4''-triiodotriphenylamine (1.0 g, 1.60 mmol) was mixed with $Pd(PPh_3)_2Cl_2$ (18 mg, 0.0032 mmol) and CuI (6 mg, 0.0064 mmol) in a 50-mL round-bottom flask under N_2 atmosphere. The mixture was dissolved in THF (10 mL) and then triethylamine (4 mL) was added, followed by TMS-acetylene (0.94 mL, 6.41 mmol). The mixture was stirred at room temperature overnight. After the reaction was completed, the solvent was evaporated and the crude reaction was purified by column chromatography on silica gel using 10% dichloromethane in hexane as eluting to afford **10** as yellow solid in 96% yield. The ^{1}H NMR spectrum of this product is in good agreement with the literature report. [28]

2.3.12 Synthesis of 11

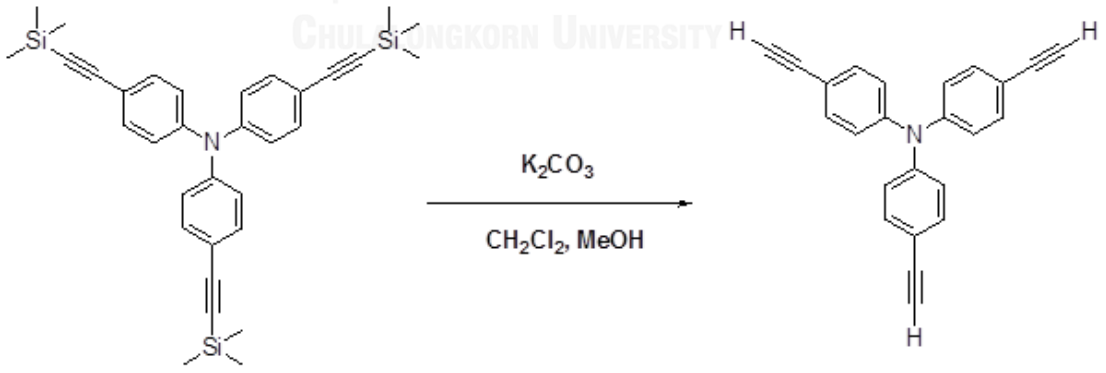

Compound **10** (2.0 g, 3.75 mmol) was mixed with potassium carbonate (2.07 g, 15.00 mmol) in a 50-mL round-bottom flask under N_2 atmosphere. The mixture was dissolved with dichloromethane (10 mL) and methanol (5 mL) and stirred at room temperature for 4 hr. After the reaction was completed, the reaction crude was extracted 3 times with water and dichloromethane. The organic layer was dried by

anhydrous sodium sulfate followed by removing of solvent under reduced pressure. The organic residue was purified by column chromatography on silica gel eluting with 20% dichloromethane in hexane to provide **11** as yellow solid in 93% yield. The ^{1}H NMR spectrum of this product is in good agreement with the literature report. [28]

2.3.13 Synthesis of F2

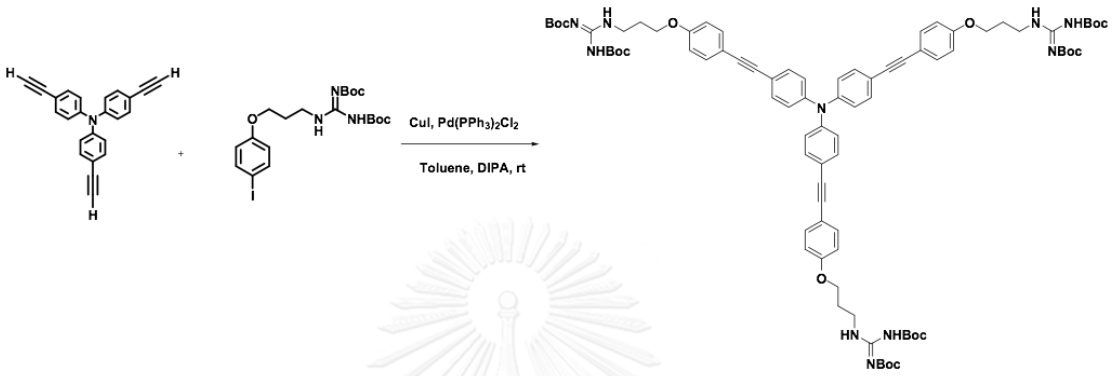

Compound **9** (0.25 g, 0.481 mmol) was mixed with $Pd(PPh_3)_2Cl_2$ (1.36 mg, 0.0019 mmol) and CuI (0.74 mg, 0.004 mmol) in 50-mL round-bottom flask under N_2 atmosphere. The mixture dissolved with toluene (7 mL) and diisopropylamine (3 mL). Then 11 (0.03 g, 0.097 mmol) was added into the mixture solution slowly. After that stirred at room temperature for 48 hr, evaporated of solvent. The organic crude was purified by column chromatography on silica gel using 20% ethyl acetate in hexane as eluting providing **F2** as yellow solid in 38% yield. ^{1}H NMR (400 MHz, $CDCl_3$) δ 11.51 (s, 3H), 8.68 (s, 3H), 7.42 (dd, *J* = 14.6, 8.8 Hz, 12H), 7.05 (d, *J* = 8.7 Hz, 6H), 6.93 (d, *J* = 8.9 Hz, 6H), 4.07 (t, *J* = 5.8 Hz, 6H), 3.65 (dd, *J* = 11.9, 6.0 Hz, 6H), 2.12 – 2.02 (m, 6H), 1.51 (d, *J* = 1.7 Hz, 54H).

2.3.14 Synthesis of 12

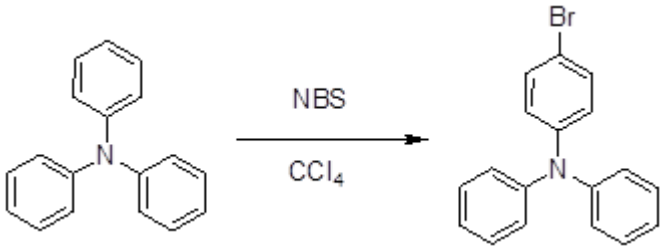

Triphenylamine (2 g, 8.15 mmol) was mixed with NBS (1.45 g, 8.15 mol) in sealed tube. The mixture dissolved with carbon tetrachloride (10 mL). The solution was

refluxed for 5 h. The precipitated succinimide was filtered, evaporated of solvent and recrystallized from ethanol providing **12** as white solid in 90% yield. The ^{1}H NMR spectrum of this product is in good agreement with the literature report. [29]

2.3.15 Synthesis of 13

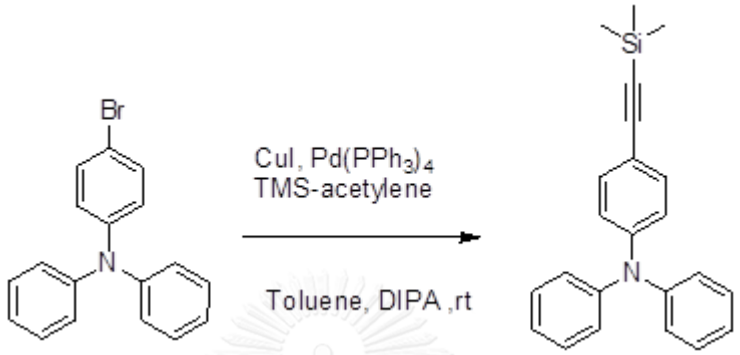

Compound **12** (0.5 g, 1.54 mmol) was mixed with $Pd(PPh_3)_4$ (88.9 mg, 0.08 mmol), CuI (14 mg, 0.08 mmol) in a 50-mL round-bottom flask under N_2 atmosphere. The mixture was dissolved in toluene (10 mL) and then diisopropylamine (3 mL) was added, followed by TMS-acetylene (0.22 mL, 1.54 mmol). The mixture was stirred at 80°C overnight. After the reaction was completed, the solvent was evaporated and the crude mixture was purified by column chromatography on silica gel using 10% ethyl acetate in hexane as eluting to afford **13** as yellow solid in 96% yield. The ^{1}H NMR spectrum of this product is in good agreement with the literature report. [30]

2.3.16 Synthesis of 14

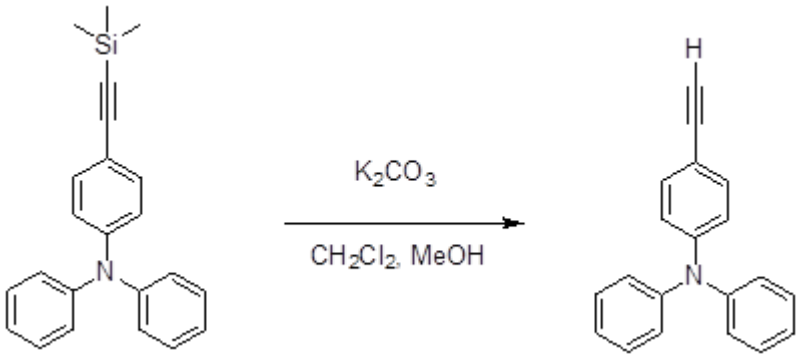

Compound **13** (0.27 g, 0.79 mmol) was mixed with potassium carbonate (0.16 g, 1.18 mmol) in 50-mL round-bottom flask under N_2 atmosphere. The mixture was dissolved with dichloromethane (5 mL) and methanol (2 mL) and stirred at room

temperature for 4 hr. After the reaction was completed, the reaction crude was extracted 3 times with water and dichloromethane. The organic layer was dried by anhydrous sodium sulfate followed by removing of solvent under reduced pressure. The organic residue was purified by column chromatography on silica gel eluting with 10% ethyl acetate in hexane to provide **14** as yellow solid in 93% yield. The ^{1}H NMR spectrum of this product is in good agreement with the literature report. [31]

2.3.17 Synthesis of 15

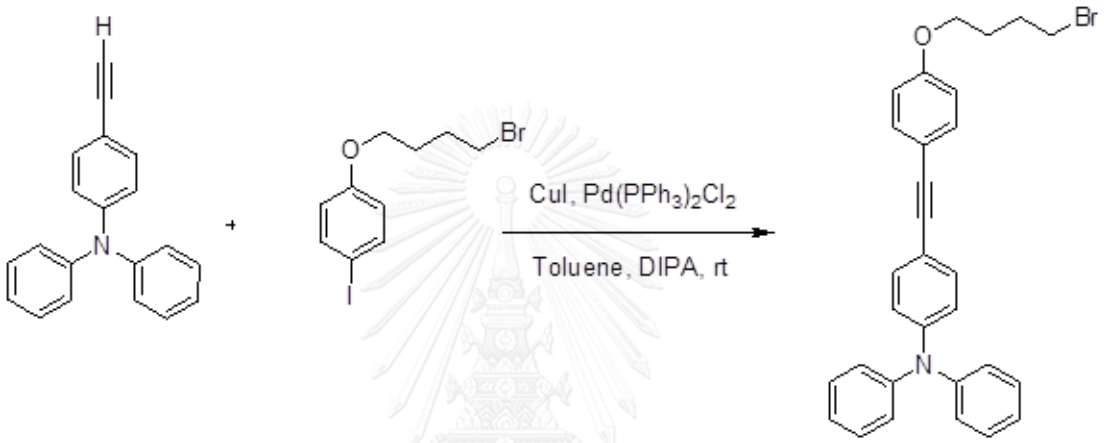

Compound **14** (0.3 g, 0.84 mmol) was mixed with $Pd(PPh_3)_2Cl_2$ (11.8 mg, 0.016 mmol) and CuI (6.4 mg, 0.033 mmol) in a 50-mL round-bottom flask under N_2 atmosphere. The mixture dissolved with toluene (7 mL) and diisopropylamine (3 mL). Then **2** (0.22 g, 0.84 mmol) was added into the mixture solution slowly. After that stirred at room temperature overnight, evaporation of solvent. The organic crude was purified by column chromatography on silica gel using 20% ethyl acetate in hexane as eluting providing **15** as brown solid in 72% yield. ^{1}H NMR (400 MHz, $CDCl_3$) δ 7.47 (d, *J* = 8.7 Hz, 2H), 7.39 (d, *J* = 8.6 Hz, 2H), 7.34 – 7.27 (m, 4H), 7.14 (d, *J* = 7.7 Hz, 4H), 7.09 (t, *J* = 7.3 Hz, 2H), 7.04 (d, *J* = 8.6 Hz, 2H), 6.88 (d, *J* = 8.7 Hz, 2H), 4.04 (t, *J* = 6.0 Hz, 2H), 3.52 (t, *J* = 6.5 Hz, 2H), 2.18 – 2.05 (m, 2H), 1.98 (dt, *J* = 12.3, 6.0 Hz, 2H).

2.3.18 Synthesis of F3

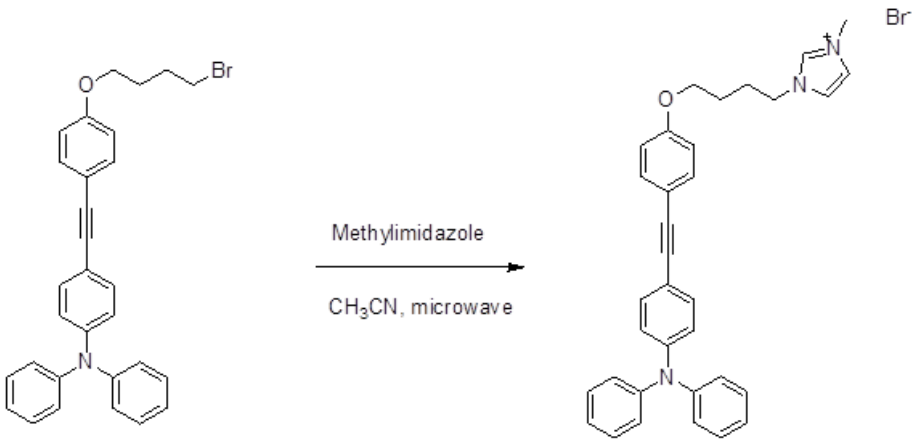

Compound **15** (0.1 g, 0.2 mmol) was mixed with 1-methylimidazole (0.08 mL, 1.0 mmol) in microwave tube. The mixture dissolved with acetonitrile (3 mL). The reaction was carried out under microwave irradiation at 120 W at 100 °C for 3 hr. After that the reaction was evapolated and washed with diethyl ether. Finally, the residue was removed solvent by evaporation and vacuum dry providing **F3** product in 86% yield. ^{1}H NMR (400 MHz, $CDCl_3$) δ 10.21 (s, *J* = 65.9 Hz, 1H), 7.47 (d, *J* = 11.5 Hz, 2H), 7.37 (d, *J* = 8.7 Hz,2H), 7.31 (d, *J* = 8.7 Hz, 2H), 7.24 (dd, *J* = 13.4, 5.0 Hz, 4H), 7.07 (d, *J* = 7.5 Hz, 4H), 7.05 – 6.99 (m, 2H), 6.96 (d, *J* = 8.7 Hz, 2H), 6.81 (d, *J* = 8.8 Hz, 2H), 4.43 (t, *J* = 7.3 Hz, 2H), 4.05 (s, *J* = 7.4 Hz, 2H), 4.02 – 3.96 (m, 2H), 2.12 (dt, *J* = 14.6, 7.5 Hz, 2H), 1.92 – 1.77 (m, 2H).

2.3.19 Synthesis of 16

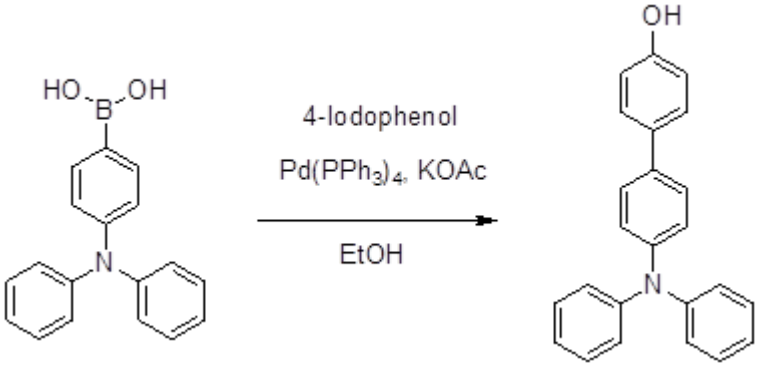

4-(Diphenylamino)phenylboronic acid (0.30 g, 1.03 mmol) was mixed with 4-Iodophenol (0.22 g, 1.03 mmol), $Pd(PPh_3)_4$ (59 mg, 0.05 mmol) and potassium acetate (0.29 g, 2.05 mmol) in a 50-mL round-bottom flask under N_2 atmosphere. The mixture

dissolved with ethanol (8 mL) then reflux overnight. After the reaction was completed, the solvent was evaporated and the crude mixture was purified by column chromatography on silica gel using 20% ethyl acetate in hexane as eluting to afford **16** as pale yellow solid in 52% yield. The ^{1}H NMR spectrum of this product is in good agreement with the literature report. [32]

2.3.20 Synthesis of 17

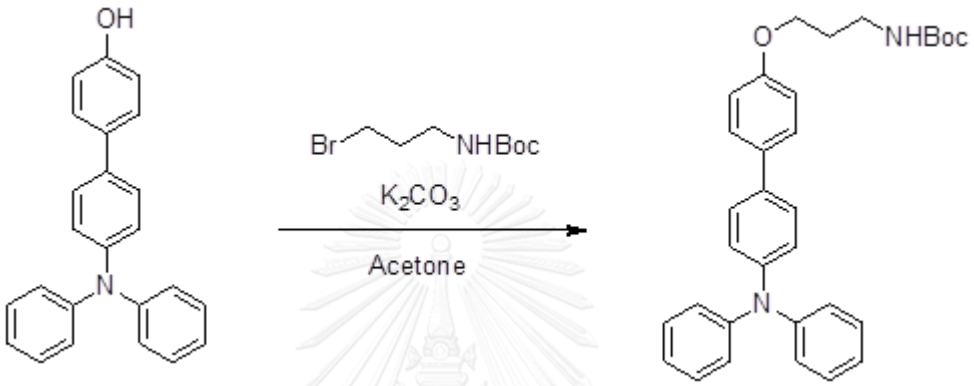

Compound **16** (0.14 g, 0.42 mmol) was mixed with N-(tert-Butoxycarbonyl)-3-bromopropylamine (0.10 g, 0.42 mmol) and potassium carbonate (0.11 g, 0.84 mmol) in a 50-mL round-bottom flask under N_2 atmosphere. The mixture was diluted with acetone (10 mL) then stirred at 60 °C overnight. After the reaction was completed, the crude reaction mixture was extracted 3 times with water and dichloromethane. The combined organic layer was dried over anhydrous sodium sulfate followed by removing of solvent under reduced pressure. The residue was purified by column chromatography on silica gel using 20% ethyl acetate in hexane to provide **17** as pale yellow solid in 76% yield. ^{1}H NMR (400 MHz, $CDCl_3$) δ 7.52 (d, *J* = 8.6 Hz, 2H), 7.45 (d, *J* = 8.4 Hz, 2H), 7.28 (dd, *J* = 14.1, 6.6 Hz, 4H), 7.16 (d, *J* = 7.5 Hz, 6H), 7.09 – 7.00 (m, 2H), 6.97 (d, *J* = 8.5 Hz, 2H), 4.90 (s, 1H), 4.07 (t, *J* = 5.9 Hz, 2H), 3.38 (s, *J* = 31.2 Hz, 2H), 2.12 – 1.88 (m, 2H), 1.50 (s, *J* = 25.5 Hz, 9H).

2.3.21 Synthesis of 18

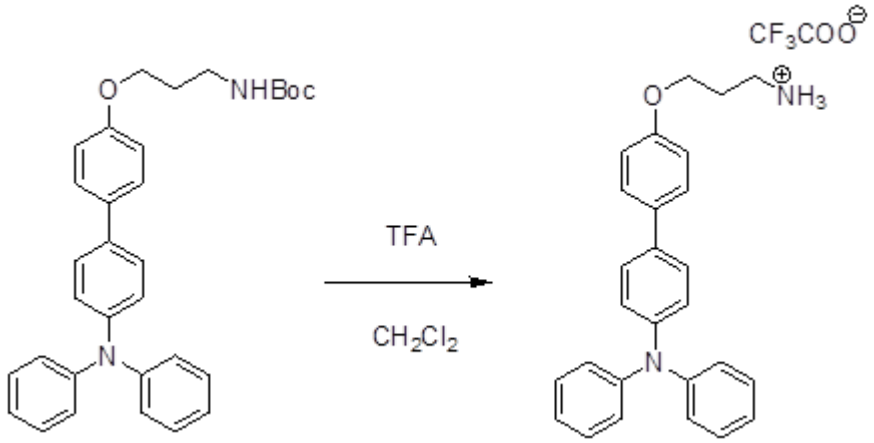

Compound **17** (0.4 g, 0.8 mmol) dissolved with dichloromethane (5 mL) was added TFA (3 mL, 39.0 mmol) in a 50-mL round-bottom flask under N_2 atmosphere, after that stirred at room temperature overnight. The crude reaction mixture was poured into hexane to precipitate **18** as a white solid, collected by filtration and washed with hexane and dried in vacuum (62% yield). ^{1}H NMR (400 MHz, CH_3OD) δ 7.53 (d, *J* = 8.6 Hz, 2H), 7.46 (d, *J* = 8.5 Hz, 2H), 7.26 (t, *J* = 7.8 Hz, 4H), 7.05 (d, *J* = 8.3 Hz, 6H), 7.01 (d, *J* = 8.5 Hz, 4H), 4.16 (t, *J* = 5.7 Hz, 2H), 3.19 (t, *J* = 7.3 Hz, 2H), 2.24 – 2.11 (m, 2H).

2.3.22 Synthesis of 19

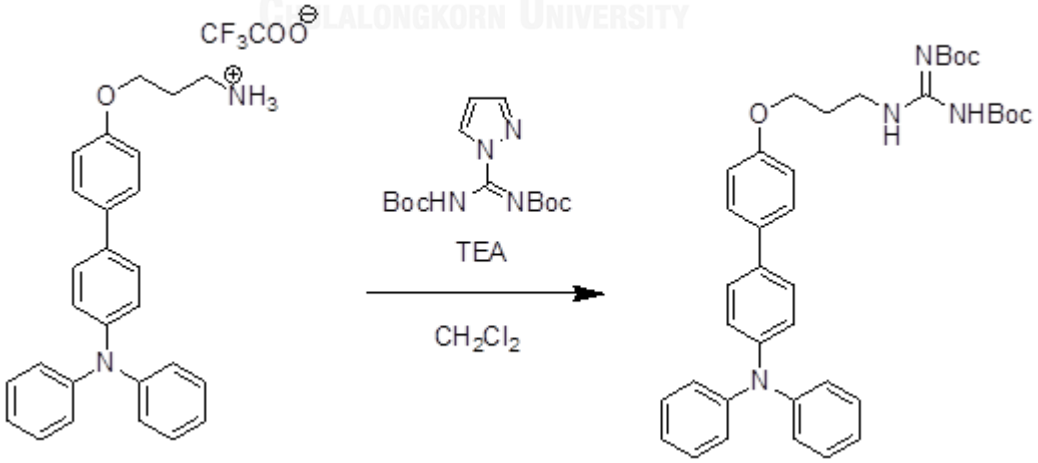

Compound **18** (40 mg, 0.10 mmol) was mixed with 1-*H*-pyrazole-1-(*N*,*N*'-bis(*tert*-butyloxycarbonyl))carboxamidine (31 mg, 0.10 mmol) in 25-mL round-bottom flask under N_2 atmosphere. The mixture was dissolved with dichloromethane (5 mL) and

TEA (0.042 mL, 0.3 mmol) then stirred at room temperature for 48 hr. After the reaction was completed, the reaction crude was extracted 3 times with water and dichloromethane. The organic layer was dried by anhydrous sodium sulfate followed by removing of solvent under reduced pressure. The organic residue was purified by column chromatography on silica gel eluting with dichloromethane to provide **19** as white solid in 46% yield. ^{1}H NMR (400 MHz, $CDCl_3$) δ 11.52 (s, 1H), 8.77 (s, 1H), 7.48 (d, *J* = 8.7 Hz, 2H), 7.42 (d, *J* = 8.6 Hz, 2H), 7.26 (t, *J* = 7.8 Hz, 4H), 7.12 (d, *J* = 7.5 Hz, 6H), 7.02 (t, *J* = 7.2 Hz, 4H), 4.10 (t, *J* = 5.4 Hz, 2H), 3.69 (d, *J* = 5.6 Hz, 2H), 2.28 – 1.89 (m, 2H), 1.51 (d, *J* = 1.3 Hz, 18H).

2.3.23 Synthesis of F4

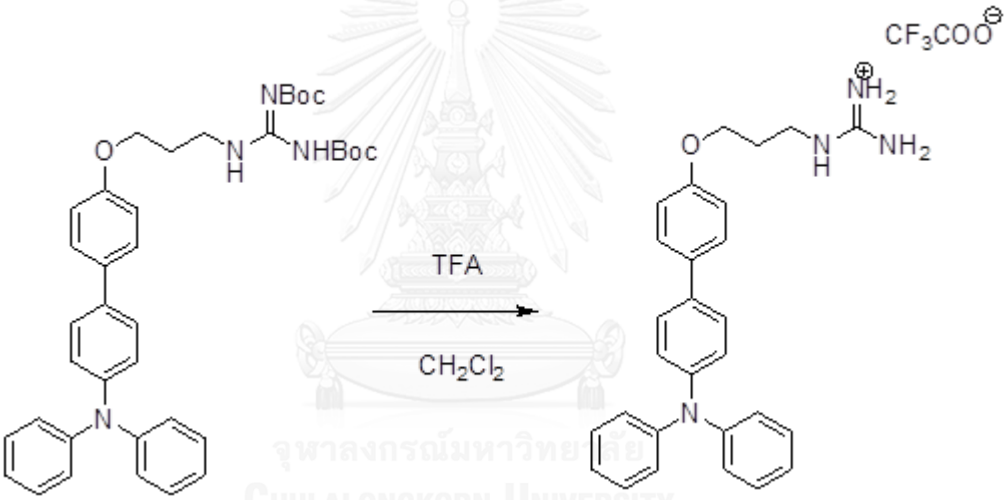

Compound **19** (0.2 g, 0.31 mmol) dissolved with dichloromethane (5 mL) was added TFA (3 mL, 39 mmol) in 50-mL round-bottom flask under N_2 atmosphere, after that stirred at room temperature overnight. The crude reaction mixture was poured into hexane to precipitate **F4** as a white solid, collected by filtration and washed with hexane and dried in vacuum (47% yield). ^{1}H NMR (400 MHz, CD_3OD) δ 7.44 (d, *J* = 6.7 Hz, 2H), 7.39 (d, *J* = 7.6 Hz, 2H), 7.19 (t, *J* = 7.6 Hz, 4H), 6.98 (d, *J* = 7.5 Hz, 6H), 6.93 (d, *J* = 8.0 Hz, 4H), 4.02 (d, *J* = 6.1 Hz, 2H), 3.59 (s, 2H), 3.34 (d, *J* = 6.0 Hz, 2H), 2.11 – 1.85 (m, 2H).

2.3.24 Synthesis of 1-butyl-3-methylimidazolium bromide (20)

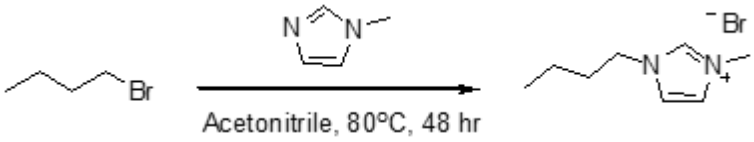

1-bromobutane (5.29 ml, 0.04 mol) mixed with 1-methylimidazole (3 mL, 0.03 mol) in 50-mL round-bottom flask. The mixture dissolved with acetonitrile (20 mL) then stirred at 80 °C for 48 hr. Finally, the residue was removed solvent by evaporation and vacuum dry providing 20 in 82% yield. The ^{1}H NMR spectrum of this product is in good agreement with the literature report. [33]

2.4 Photophysical property study

2.4.1 UV-Visible spectroscopy

The stock solutions of **F1** (0.3 mM) in Milli-Q water was dilute to 5 μM in HEPES buffer 10 mM, pH 7.0 and **F2**-**F4** (0.3 mM) in DMSO were dilute to 5 μM in 0.017% DMSO/HEPES buffer 10 mM, pH 7.0. The UV-Visible absorption spectra of all fluorophores were recorded from 250 nm to 700 nm at ambient temperature.

2.4.2 Fluorescence spectroscopy

The stock solutions of **F1** was dilute to 5 μM in 10 mM HEPES buffer pH 7.0 and **F2**-**F4** were dilute to 5 μM in 0.017% DMSO/10 mM HEPES buffer pH 7.0. The emission spectra of fluorophores were recorded from 360 to 700 nm at ambient temperature using an excitation wavelength at 350 to 362 nm.

2.4.3 Fluorescence quantum yield

The fluorescence quantum yields of **F1** was performed in HEPES buffer 10 mM, pH 7.0, while **F2**-**F4** were performed in 0.017% DMSO/10 mM HEPES buffer pH 7.0 using quinine sulfate (Φ_{ST} = 0.54) in 0.1 M H_2SO_4 as a reference [34] The maximum absorbance of all samples should not exceed 0.1. The fluorescence emission spectra of the same solution using appropriate excitation wavelengths selected were recorded based on the absorption maximum wavelength (λ_{max}) of each compound. Graphs of integrated fluorescence intensities were plotted against the absorbance at the

respective excitation wavelengths. Each plot should be a straight line with 0 interception and gradient *m*.

In addition, the fluorescence quantum yield (Φ_x) was obtained from a plot integrated fluorescence intensity and absorbance as represented into the following equation:

$$\Phi_X = \Phi_{ST}\left(\frac{Grad_X}{Grad_{ST}}\right)\left(\frac{\eta_X^2}{\eta_{ST}^2}\right)$$

The subscripts Φ_{ST} denote the fluorescence quantum yield of a standard reference which used quinine sulfate in 0.1 M H_2SO_4 (Φ_F = 0.546) and Φ_X is the fluorescence quantum yield of sample and η is the refractive index of the solvent.

2.5 Fluorescent sensor study

2.5.1 Anion sensor

2.5.1.1 Selectivity study

The stock solution 0.3 mM of the fluorophore **F1** was prepared in Milli-Q water and **F2**-**F4** were prepared in dimethyl sulfoxide (DMSO). All anion solutions were prepared in Milli-Q water and adjusted to 10 mM. The final volumes of the mixture were adjusted to 300 µL to afford final concentration of 5 µM for the fluorophore and 250 µM for anion, recored after mixing for 10 minutes using λ_{ex} = 362 nm (sensor **F1**), 350 nm (sensor **F2**), 349 nm (sensor **F3**) and 319 nm (sensor **F4**).

2.5.1.2 Competition with other anion

The mixture of **F1**/SH^-/other anion in concentration with ratio 1/10/50 used for investigating the interference of other anion to SH^- binding with sensors.

CHAPTER III

RESULTS AND DISCUSSION

3.1 Fluorescent sensors F1 and F2

3.1.1 Synthesis and characterization of F1 and F2

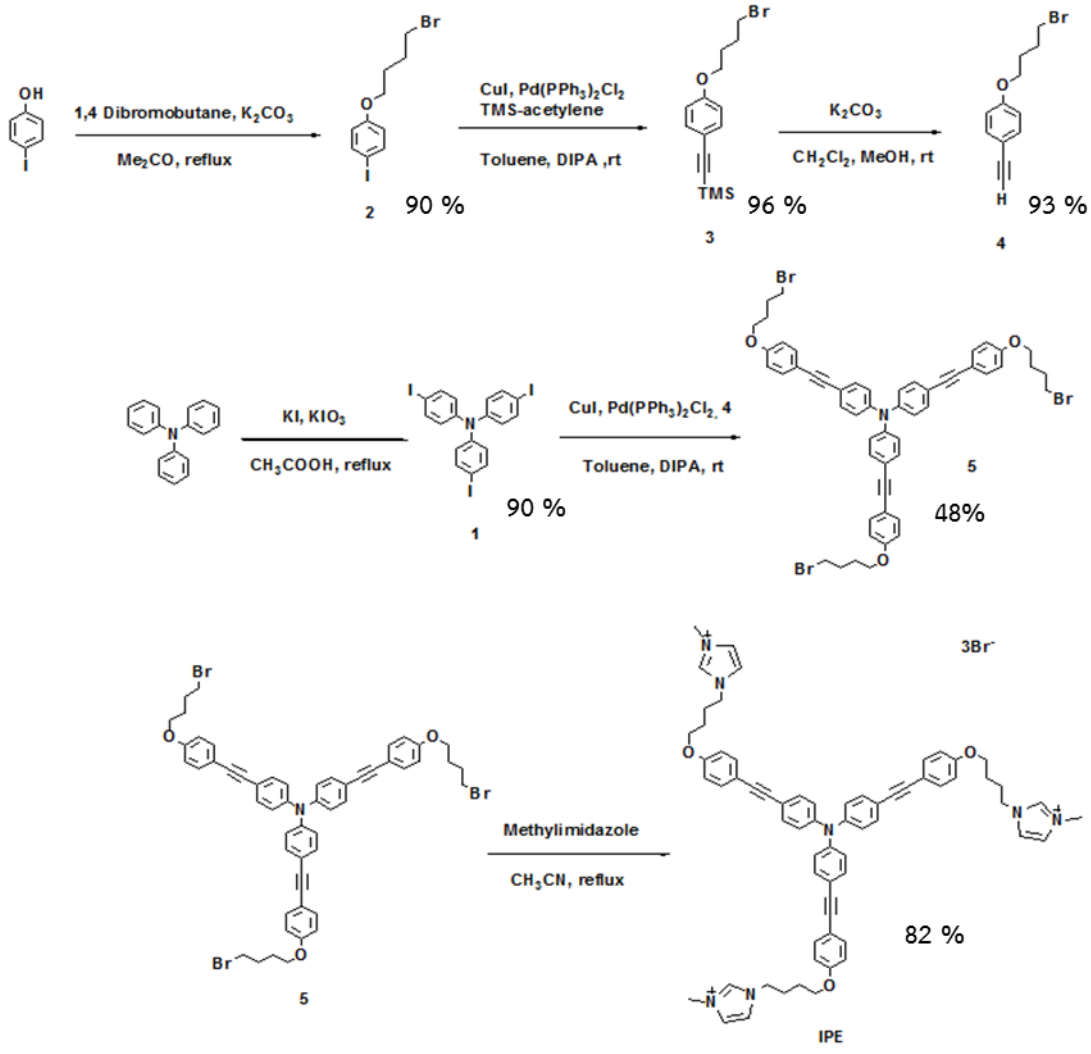

Scheme 3.1 Synthesis of **F1**.

The synthesis of **F1** began with the alkylation of 4-iodophenol using 1,4-dibromobutane, followed by a Sonogashira coupling on the iodo group with the commercially available trimethylsilyl acetylene. The desilylation afforded acetylenylarene **4** in excellent yield. After the iodination of triphenylamine core, the

Sonogashira coupling between triiodo core **1** and excess alkyne **4** provided the tribromo **5** in moderate yield of 48%. The final step involving the nucleophilic substitution of the bromo groups on **5** with N-methylimidazole to afforded **F1** in 82% yield.

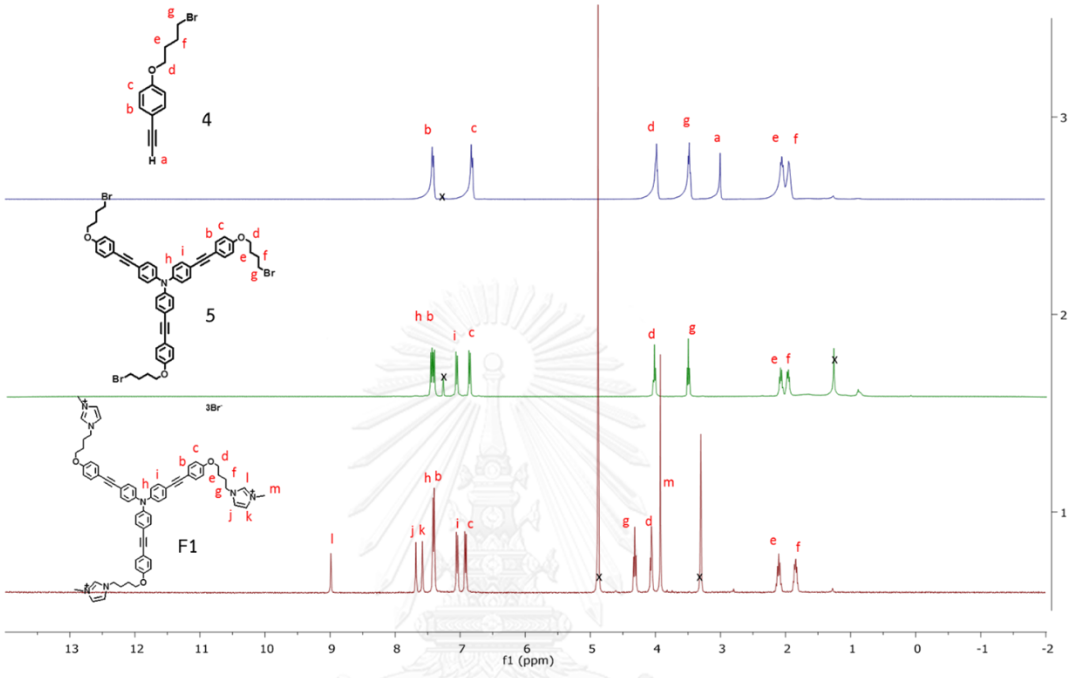

Figure 3.1 ^{1}H-NMR (400 MHz) of **4**, **5** in $CDCl_3$ and **F1** in CD_3OD.

The ^{1}H-NMR spectra of **4** and **5** in $CDCl_3$ and **F1** in CD_3OD are shown in Figure 3.1. In the spectra of **4**, there are two doublet signals at 7.42 and 6.82 ppm, and one singlet signal at 3.01 ppm corresponding to the aromatic and terminal alkyne groups, respectively. The signal methylene protons in **4** can be found around 1.89-3.98 ppm. After the Sonogashira coupling between **1** and **4**, the product **5** was formed and the signal for terminal alkyne proton disappeared. After the alkylation of **5** with N-methylimidazole, the methylene proton at the g-position moved downfield from 3.49 to 4.31 ppm which indicated a successful substitution with imidazole. In addition, the singlet peak at 3.92 ppm (m-position) belonging to the methyl on imidazole ring also confirmed the high purity of the substitution product. The analysis by mass spectrometry confirmed the chemical formular of **F1** whose calculated exact mass of 1165.3572 was found at m/z of 1165.0827.

The synthesis of **F2** began with protection of 3-bromopropylamine hydrobromide by Boc_2O, followed by alkylation of 4-iodophenol and deprotection of the Boc group using TFA to afford **8** in moderate yield. Compound **8** was then reacted with 1-*H*-pyrazole-1-(*N*,*N*'-bis(*tert*-butyloxycarbonyl))carboxamidine to provide **9** in 72% yield. Finally, compound **9** was coupled with **11** via the Sonogashira coupling to afford **F2** in moderate yield of 38%.

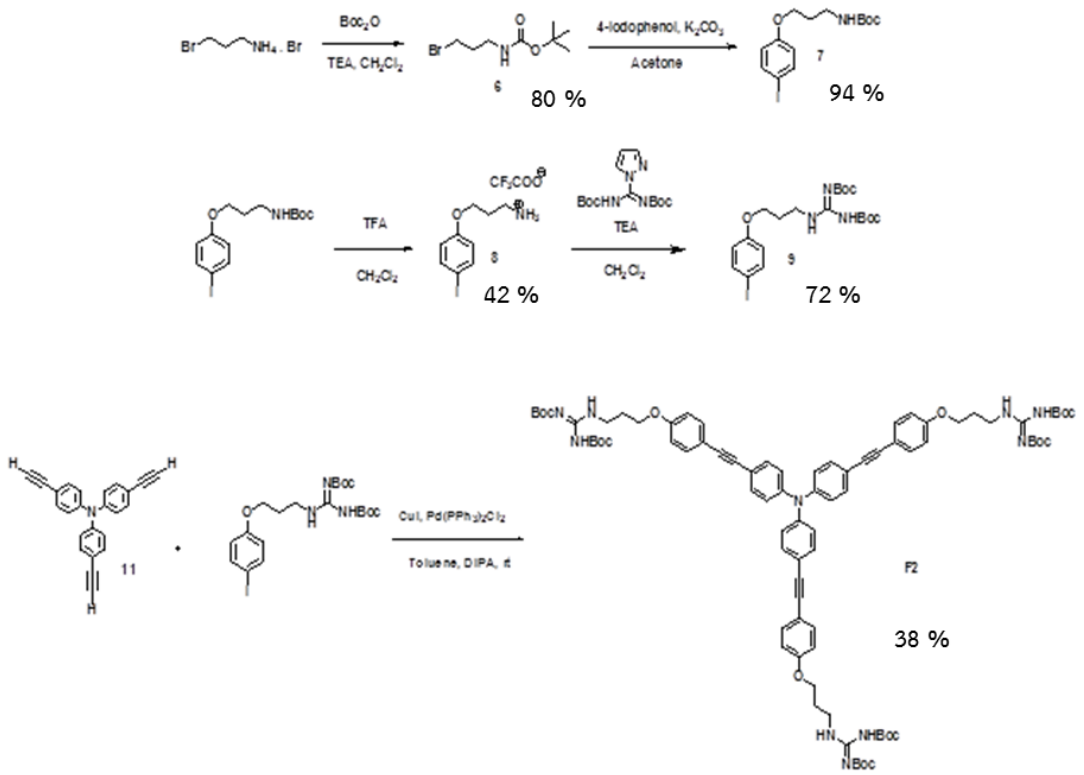

Scheme 3.2 Synthesis of **F2**.

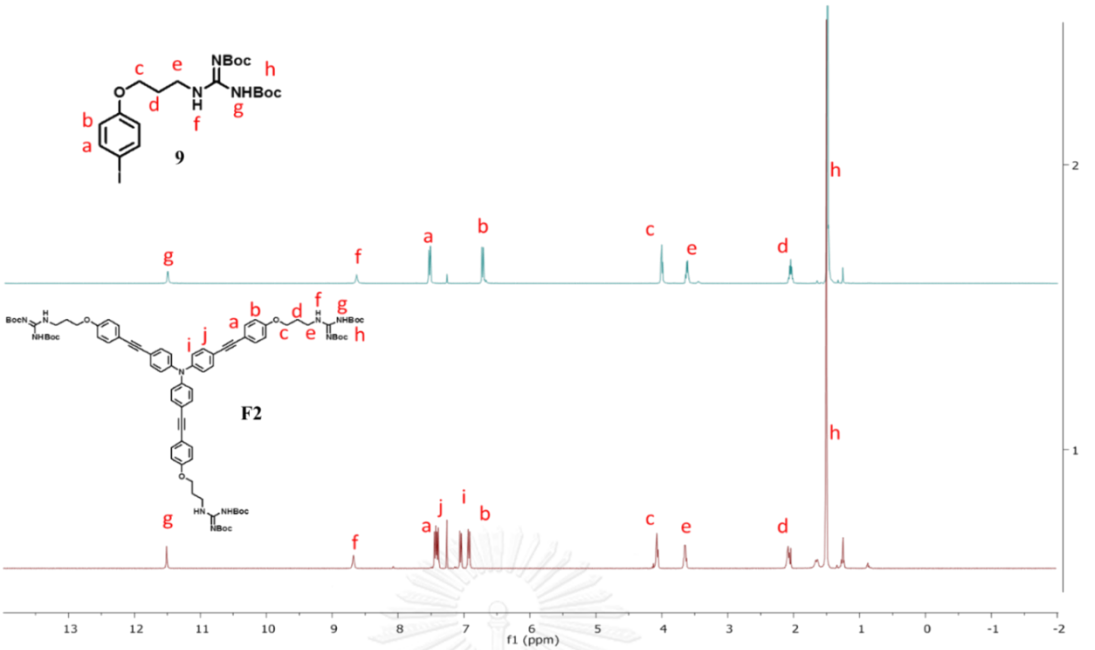

Figure 3.2 ^{1}H-NMR (400 MHz) of **9** and **F2** in $CDCl_3$.

The ^{1}H-NMR spectra of **9** and **F2** in $CDCl_3$ are shown in Figure 3.2. The spectrum of **9** shows two doublet signals at 7.52 and 6.72 ppm belong to the aromatic protons, three singlet signals at 11.49, 8.63 and 1.49 ppm corresponding to the guanidine group. The alkyl protons in **9** can be found around 2.04-4.00 ppm. After the Sonogashira coupling to yield **F2**, the signals for aromatic protons of triphenylamine core at the i- and j-positions appeared, which is a good indication of a successful coupling between the two building blocks. The analysis by mass spectrometry confirmed the molecular formular **F2** as a mass of 1491.7666 was found for this compound with a calculated exact mass of 1491.7600.

3.1.2 Photophysical properties of F1 and F2

The absorption and emission properties of **F1** were studied in 10 mM HEPES buffer, pH 7.0, while the less polar **F2** was studied in 0.017% DMSO/10 mM HEPES buffer, pH 7.0. From the normalized absorption and emission spectra (Figure 3.3) and data summarized in Table 3.1, **F1** and **F2** exhibited the absorption maxima at 362 and 350 nm, respectively. In the emission spectra, the emission maxima were observed at 450 nm for **F1** and 456 nm for **F2**. The absorption maxima of **F1** and **F2** and their molar extinction coefficients are in the same range since these compounds possess similar

conjugated systems of phenylene ethynylene [35]. The slightly longer absorption maxima for **F1** may be due to the solvent effect. The polar aqueous media could facilitate the solubility of **F1**, while it forces the more hydrophobic **F2** to aggregate via **π-π** stacking. This aggregation may lower the degree of conjugation between the triphenylamine core and ethynyl arene peripheries.

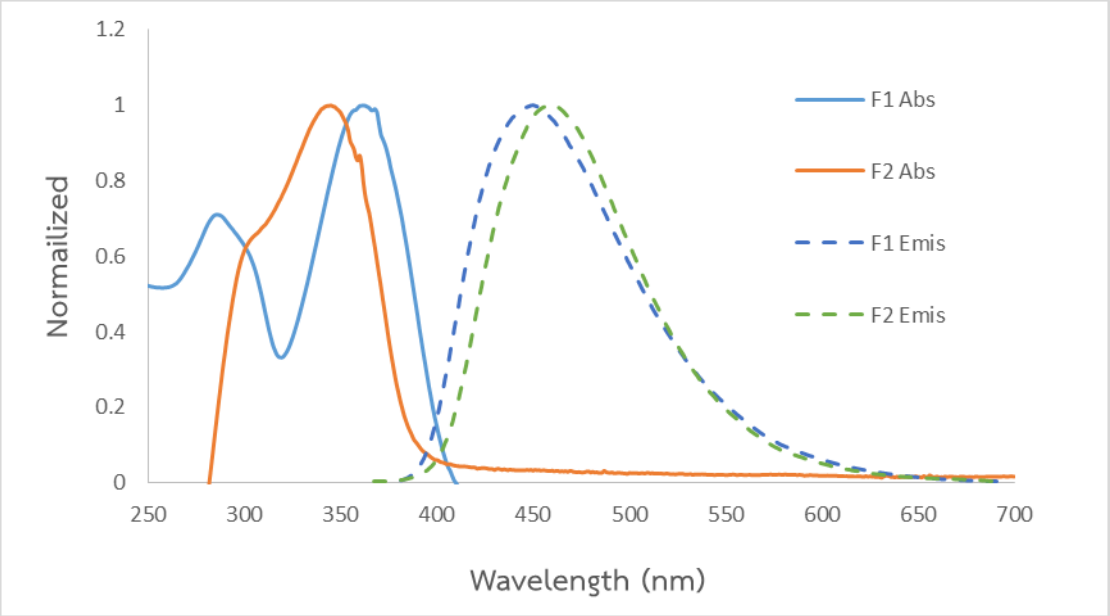

Figure 3.3 Normalized absorption and emission spectra of **F1** in 10 mM HEPES buffer pH 7.0 and **F2** in 0.017% DMSO/10 mM HEPES buffer, pH 7.0.

The quantum efficiencies of both fluorophores were determined using quinine sulfate 0.1 M H_2SO_4 (Φ = 54%) as standard. The quantum yield of **F1** was determined to be 17.97%, while that of **F2** was at 7.40%. The lower emission efficiency for **F2** may also result from the self-quenching as the compound has less solubility in aqueous media.

Table 3.1 Photophysical properties of sensor **F1**-**F2** in aqueous solution.

Sensor	Absorption		Emission	
	λab (nm)	Epsilon	λem (nm)	Φ (%)[a]
F1	362	42,200	450	17.97
F2	353	43,600	456	7.40

[a]Quinine sulfate in 0.1 M H2SO4 (Φ = 54%) was used as the standard.

3.2 Sensing property of F1

In this section, we screened the sensing ability of **F1** in 10 mM HEPES buffer pH 7.0. The fluorophore **F1** was tested with sixteen different anions such as N_3^-, AcO^-, HPO_4^{2-}, NO_3^-, NO_2^-, SO_3^{2-}, SO_4^{2-}, HCO_3^-, Cl^-, Br^-, I^-, F^-, CN^-, $S_2O_3^{2-}$, SCN^- and SH^- at 250 μM (50 equiv.), and the results were summarized in Figure 3.4. From these results, fluorescent signals of **F1** was significantly quenched by addition of SH^- and slightly quenched by addition of $S_2O_3^{2-}$ and SCN^- while it remained unchanged in the presence of 13 other anions.

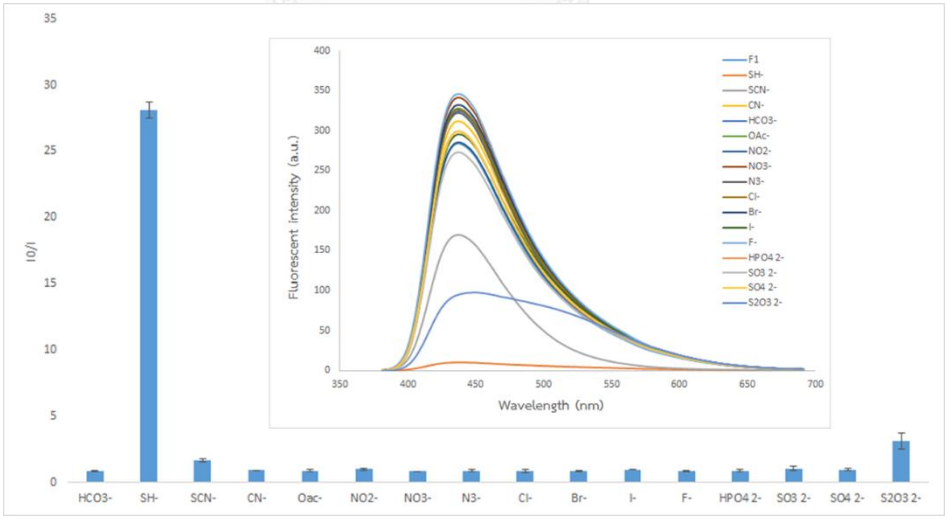

Figure 3.4 Fluorescence quenching of **F1** (5 μM) by various anions (250 μM) in 10 mM HEPES buffer pH 7.0. Inset: Fluorescence spectra of **F1** (5 μM) in the presence of 16 anion (250 μM) in 10 mM HEPES buffer pH 7.0.

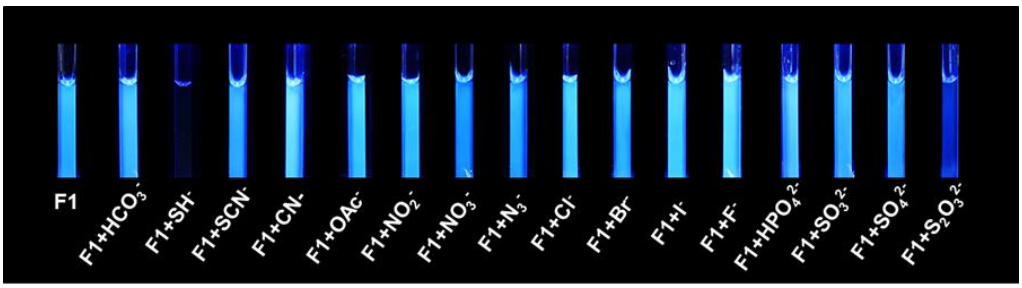

Figure 3.5 The photographed image of solutions of **F1** (5 μM) in the presence of various anions (20 eqiv) in 10 mM HEPES buffer pH 7.0 under irradiation by UV black light.

3.2.1 Effect of pH

From the selectivity screening for **F1** in the previous section, we opted to further investigate the optimal conditions to use **F1** as a SH^- fluorescent sensor. We first began to study the effect of pH in order to improve sensitivity of **F1** for the detection of SH^-. HEPES buffers of various pH in the range of 6-8 (pH 6, 6.5, 7.0, 7.4, and 8) were used as the media for SH^- sensing by **F1** as shown in Figure 3.6. From this data, it was apparent that the fluorescent intensity of **F1** was relatively unchanged at the pH range from 7.0 to 8.0. However, fluorescent quenching ratio was found in the highest at pH 7.0. We thus chose to study other parameters at pH 7.0 because it is close to the physiological conditions.

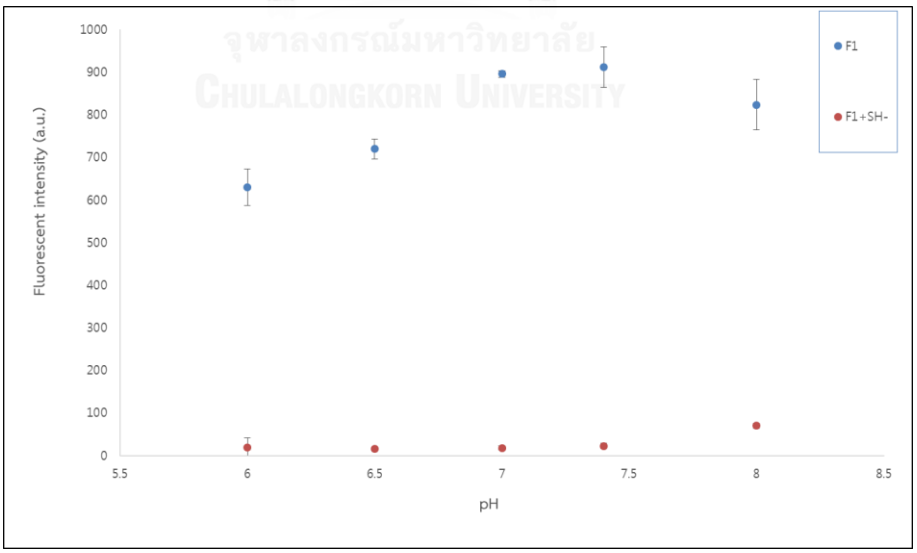

Figure 3.6 Effects of pH on fluorogenic response of **F1** with SH^- in HEPES buffer pH 7.0.

3.2.2 Time dependence study

In order to examine the fluorescent signal changes over time after the addition of hydrogen sulfide, thiocyanate and thiosulfate to **F1**, the fluorescent intensities were measured one minute after the addition of those analyses, and repeatedly after every minutes. Figure 3.7 indicated that the fluorescence intensity sharply decreased during the first minute and remained constantly throughout the entire experiment (5 minutes after). This result highlighted the spontaneous fluorescent quenching of **F1** by these three sulfur-containing anions.

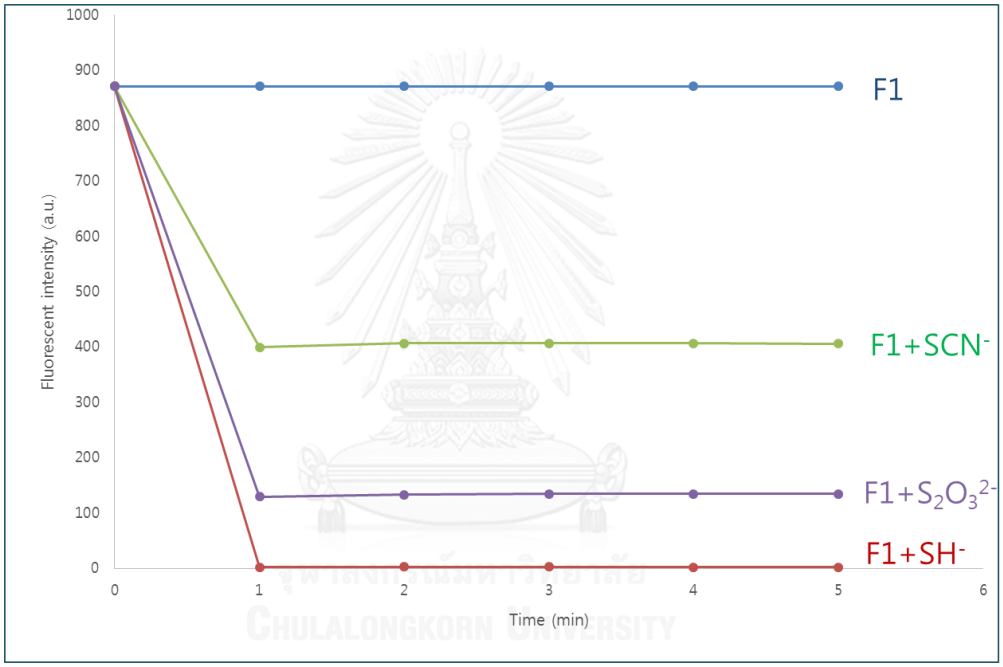

Figure 3.7 Time dependents changes in fluorescence intensity of **F1** (5μM) upon addition of SH^-, SCN^- and $S_2O_3^{2-}$ 50 equivalent in 10 mM HEPPES buffer pH 7.0.

3.2.3 Effect of water contents on SH^- sensing properties of F1

The effect of water contents on sensing properties was studied by varying the ratio between HEPES buffer (10 mM, pH 7.0) and DMSO from 10 to 100%, as show in Figure 3.8. The results showed that **F1** exhibited weaker emission intensity in solvent with higher water content. This behavior may cause by the poorer solubility as the triethynyltriphenylamine group is hydrophobic and tend to form **π–π** stacking. The lower water content can dissolve **F1** more efficiently, thus the starting emission intensity was much higher. Upon the addition of SH^-, there might be Coulombic

interactions between SH^- and the imidazolium groups that lead to a poorer solubility of such ion-pair, and lowering of the emission intensity.

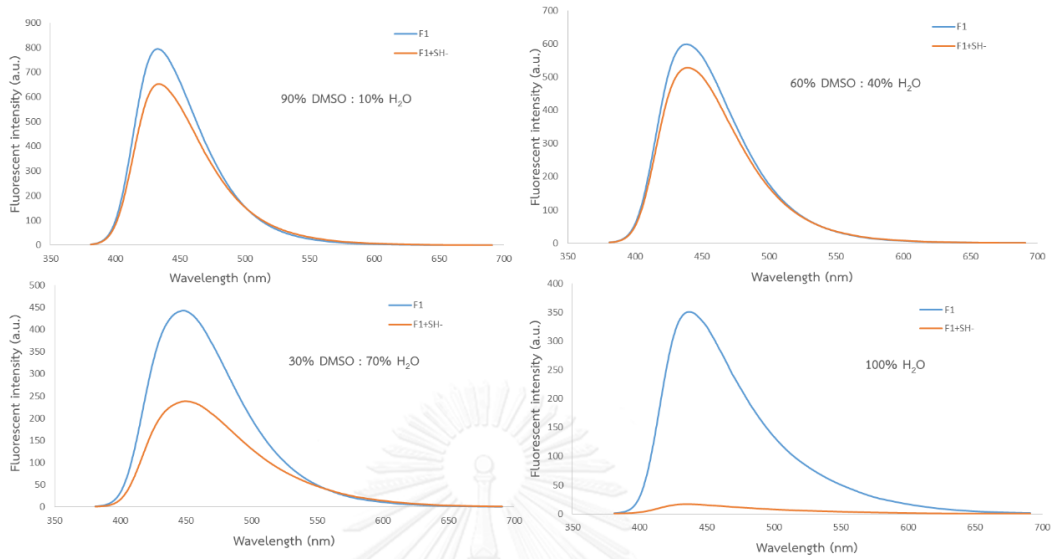

Figure 3.8 Fluorescent spectra of **F1** before and after addition of SH^- in various water contents.

3.2.4 Effect of interfering ions on selectivity of F1 towards SH^-

The interference studies for the SH^- sensing by **F1** were performed by addition of SH^- (250 μM) into a solution of **F1** (5 μM) in 10 mM HEPES buffer pH 7.0, followed by addition of each foreign anion (1,250 μM, 5-fold of SH^-) (Figure 3.9). The effect of foreign anions on quenching with SH^- from other anion, the solution of, in presence of was used as a blank. The quenching ratio in the presence of additional anions Therefore, quenching fluorescence signal of this sensor is a good indication for the predominant presence of SH^-. In quantitative determination of SH^-, samples however should be free from these interfering anions.

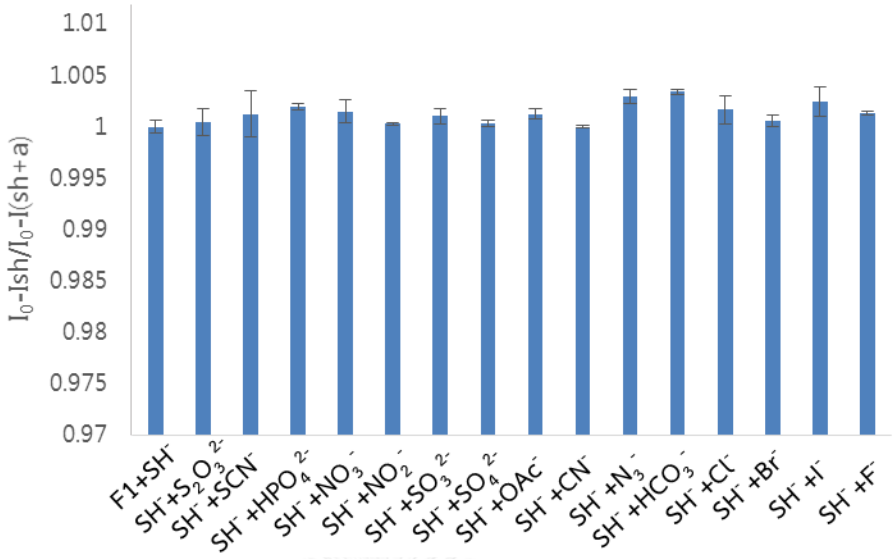

Figure 3.9 Competitive experiments of **F1** (5 μM) and SH^- (250 μM) with 15 interfering anion ions (1250 μM).

3.2.5 Sensitivity of F1 toward hydrogen sulfide

The relationship between the fluorescent intensity of **F1** and the concentration of SH^- was investigated upon addition of 0-50 equivalent of sodium sulfide. Spectra in Figure 3.10 indicated that the fluorescent intensity decreased gradually when the ratio between **F1** and sodium sulfide is less than 1:50. At the higher concentrations of sodium sulfide, there is no significant change in quenched fluorescent signal. The mechanism of fluorescent quenching may involve the electrostatic interaction between the imidazolium groups and the hydrogen sulfide ion to produce a stable ion-pair, which may aggregates under the experiment conditions. This hypothesis was partly supported by the decrease in absorbance upon addition of SH^- (Figure 3.10, inset).

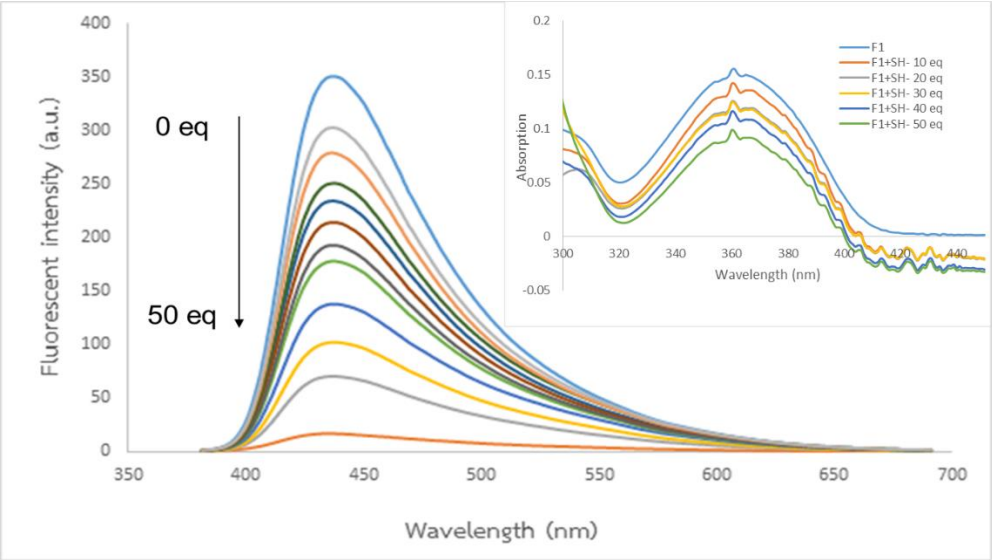

Figure 3.10 The fluorescence intensity of compound **F1** (5 μM) with SH^- titration (0-250 μM) in 10 mM HEPES buffer pH 7.0. Inset: The absorption spectra of **F1**, **F1**+SH^- and SH^-.

3.2.6 The Stern-Volmer plot for fluorescent quenching of F1 by SH^-

In order to determine the quenching efficiency of **F1** by SH^-, a plot between various concentrations of SH^- and (I_0/I) of **F1** was constructed (Figure 3.11). A Stern-Volmer constant (K_{sv}) of 0.45 x 10^6 M^{-1} was determined from the slope of that plot, which was later used to estimate the detection limit for SH^- at three-times-noise of 0.11 μM

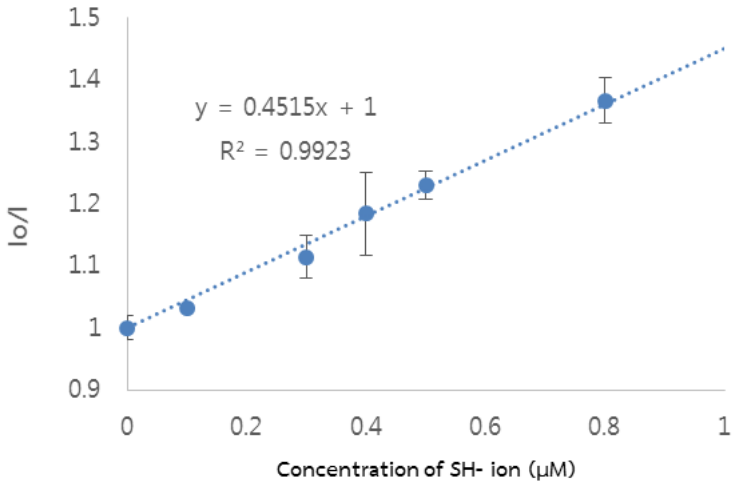

Figure 3.11 The Stern-Volmer plot for fluorescent quenching of **F1** by SH^-.

3.2.7 Thiol sensing

As **F1** exhibited selectivity towards sulfur-containing anions, it might be interesting to expand the application of **F1** for the detection of thiol derivatives. To prove this assumption, 4-chlorothiophenol was used a representative thiol analyses. The fluorescence responses of **F1** in the presence of various concentration of 4-chlorothiophenol (2-50 μM) is shown in Figure 3.12. The Stern-Volmer constant (K_{sv}) was determined to be 1.04 x 10^6 M^{-1}, which corresponds to a detection limit at three-times-noise of 0.11 μM.

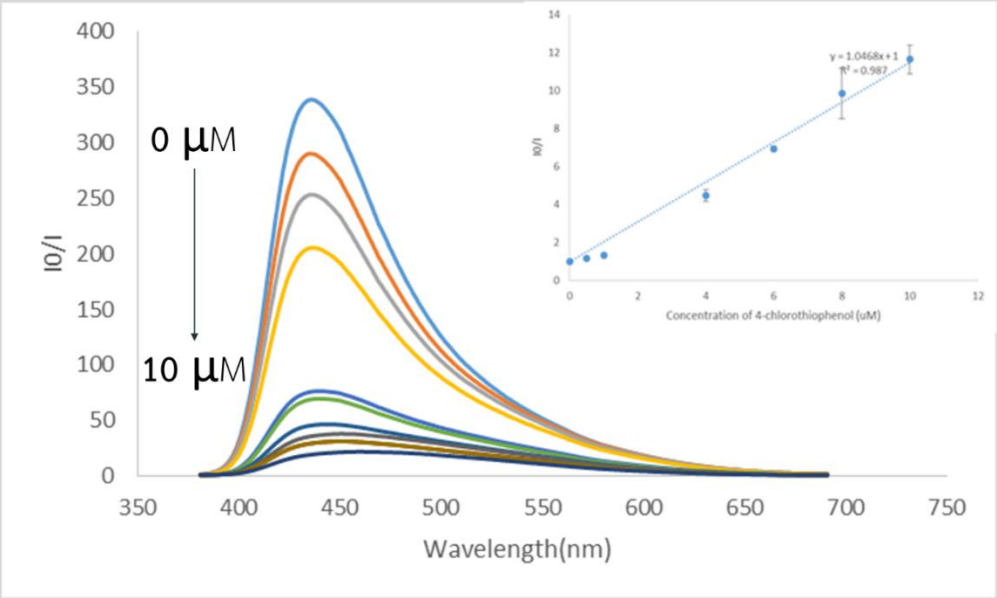

Figure 3.12 The fluorescence intensity of **F1** (5 μM) with 4-chlorothiophenol (0-50 μM) in 0.03% MeOH/10 mM HEPES buffer pH 7.0. Inset: The Stern-Volmer plot for fluorescent quenching of **F1** by 4-chlorothiophenol.

3.3 Synthesis and characterization of F3, a comparative analog for F1

From the previous result, it was found that **F1** showed selective fluorescent quenching towards three sulfur-containing anions. For better understanding on the sensing mechanism of **F1** and comparison to its analog with one imidazolium pendant, we chose to synthesize **F3** (Figure 3.13) and study its sensing properties.

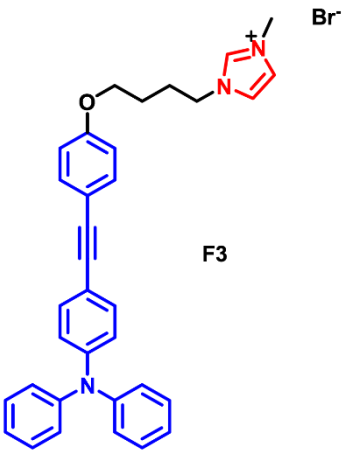

Figure 3.13 Structure of **F3**.

F3 was synthesized in four steps as outlined in Scheme 3.3. Beginning with the bromomination of triphenylamine, Sonogashira coupling with trimethylsilyl acetylene, and desilylation, compound **14** was produced in excellent yield. Another Sonogashira coupling between **14** and **2** afford **15** in 72% yield. The final step which involved nucleophilic replacement of the bromo groups on **15** with *N*-methylimidazole to afford the **F3** in 86% yield.

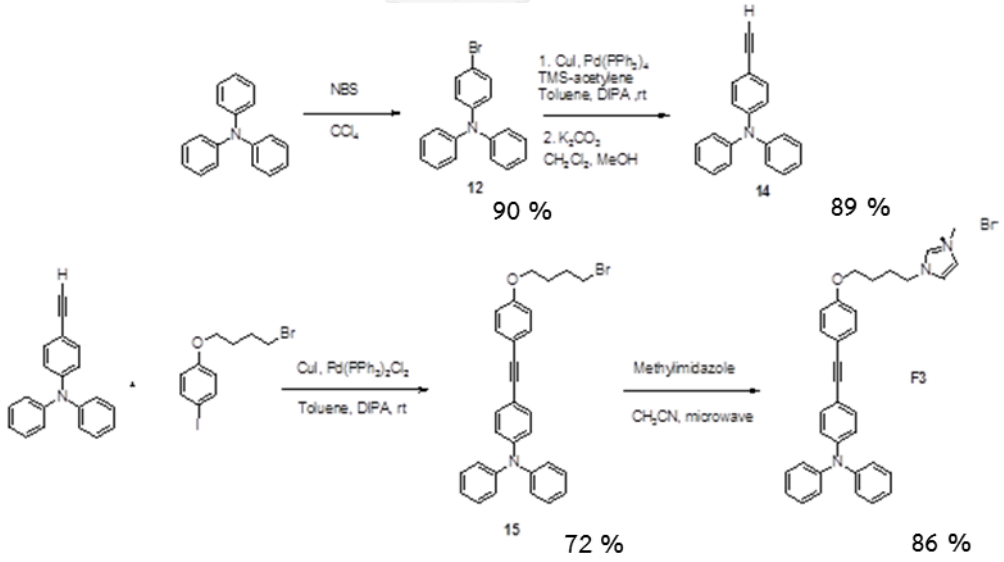

Scheme 3.3 Synthesis of **F3**.

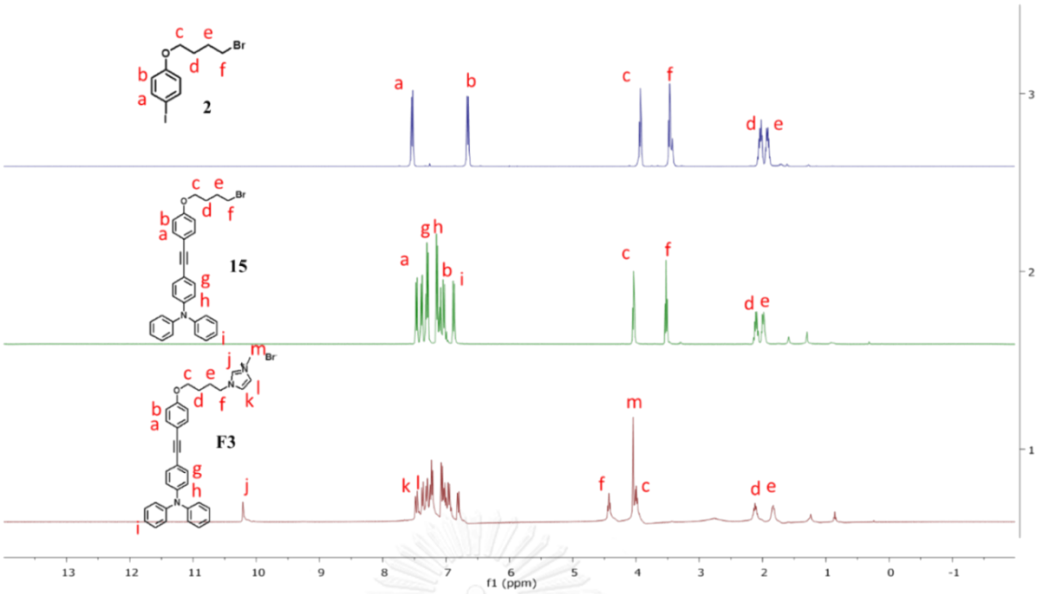

Figure 3.14 ^{1}H-NMR (400 MHz) of **2**, **15** and **F3** in $CDCl_3$.

The ^{1}H-NMR spectra of **2**, **15** and **F3** in $CDCl_3$ are shown in Figure 3.14. The presence of all signals from **2** and **15**, and a singlet peak at 3.99 ppm in the spectrum of **F3** indicated a successful transformation. Moreover, the analysis by mass spectrometry confirmed the structural composition of **F3** as a mass of 577.1728 was found for the compound whose calculated exact mass is 577.1674.

3.3.1 Photophysical properties of F3

The absorption and emission properties of **F3** in 0.017% DMSO/10 mM HEPES buffer, pH 7.0 were compared with those of **F1** in Table 3.2. Compound **F3** exhibited absorption maxima at 352 nm and emission maxima at 437 nm (Figure 3.15). The shorter maximum absorption wavelength and lower molar extinction coefficient in **F3** may result from the shorter conjugated system.

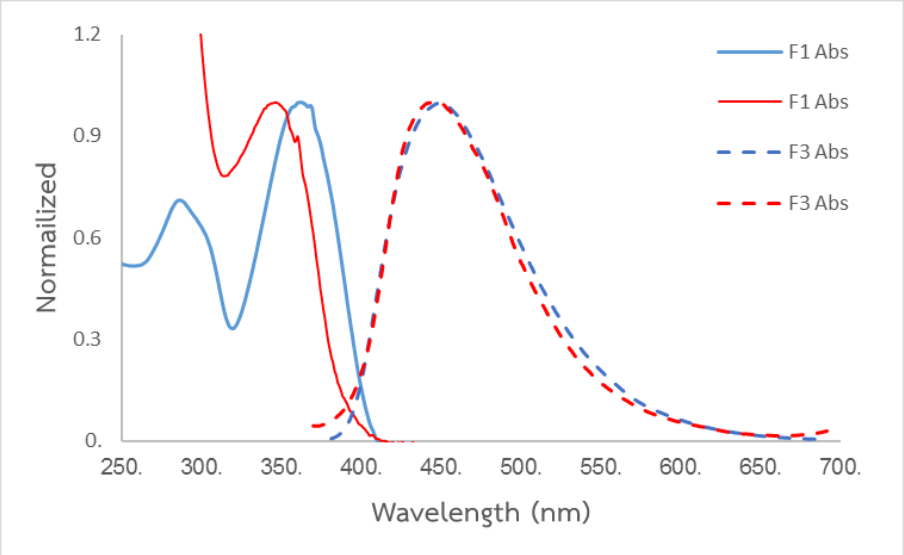

Figure 3.15 Normalized absorption and emission spectra of **F1** in 10 mM HEPES buffer pH 7.0 and **F3** in 0.017% DMSO/10 mM HEPES buffer, pH 7.0.

The quantum efficiency of **F3** was also determined using quinine sulfate (0.1 M H_2SO_4 (Φ = 54%)) as a reference standard. As expected, **F1** which has three imidazolium groups has high quantum yield than **F3** because of better solubility in aqueous media.

Table 3.2 Photophysical properties of **F1** and **F3** in aqueous solution.

Sensor	Absorption		Emission	
	λ_{ab} (nm)	Epsilon	λ_{em} (nm)	Φ (%)[a]
F1	362	42,200	450	17.97
F3	352	14,200	437	3.16

[a]Quinine sulfate in 0.1 M H_2SO_4 (Φ = 54%) was used as the standard.

3.3.3 Sensing property of F3

Upon addition of various anions (250 μM) to the solution of **F3** (5 μM) in 0.017% DMSO/10 mM HEPES buffer pH 7.0, it was found that the fluorescent signal of **F3** could be slightly quenched by $S_2O_3^{2-}$ and SH^-, with a preference toward $S_2O_3^{2-}$ (Figure 3.16). However, the I_0/I for SH^- of nearly 3.5 suggested that **F3** is less sensitive towards SH^-

compared to **F1**, which showed the I_0/I for SH^- of almost 28. This result signifies the essential of three imidazolium groups in **F1**.

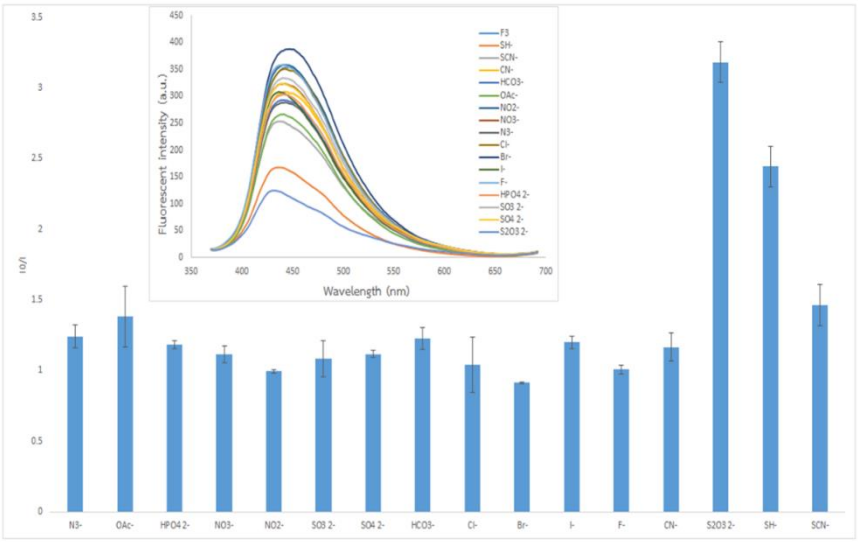

Figure 3.16 Fluorescence quenching of **F3** (5 μM) by various anions (250 μM) in 0.017% DMSO/10 mM HEPES buffer pH 7.0. Inset: Fluorescence spectra of **F3** (5 μM) in the presence of 16 anion (250 μM) in 0.017% DMSO/10 mM HEPES buffer pH 7.0.

Since the fluorescent quenching of **F1** or **F3** was postulated to result from the formation of ion-pair between the SH^- and the imidazolium groups, the investigation of such mechanism was carried out by several NMR experiments. When a solution of **F1** in CD_3OD was added a solution of Na_2S in D_2O (4 eq), no significant signal shift was observed except for the gradual disappearing of the singlet peak at 8.99 ppm which corresponded to the imidazolium C-H proton (i-position). The similar experiment with compound **F3** also result in the same spectral change. We thus opted to use N-butyl-N'-methylimidazolium bromide (**20**) as a model compound for the NMR experiment. To our surprise, when the solution of **20** in D_2O was treated with Na_2S in D_2O (excess), the signal for C-H proton on the imidazolium ring disappeared (Figure 3.18). There are a number of reports on the fast deuterium exchange at the 2-position of the imidazolium rings ([36, 37]). However, the special hydrogen-bonding between imidazolium C-H and anions such as Cl^-, Br^-, and phosphate are well known in the literatures ([12-14, 38-42]). With the limited solubility of Na_2S in organic solvents, we therefore chose to probe this hydrogen-bonding between the model compound (**20**)

and 1-octanethiol instead (Figure 3.19). From the data, it is apparent that the addition of 1-octanethiol result in a downfield shift of the imidazolium proton (C-2) as a result of hydrogen-bonding. This interaction could result in the formation of ion-pair between **F1** and sulfur-containing anion, which further aggregate and lead to fluorescent signal quenching.

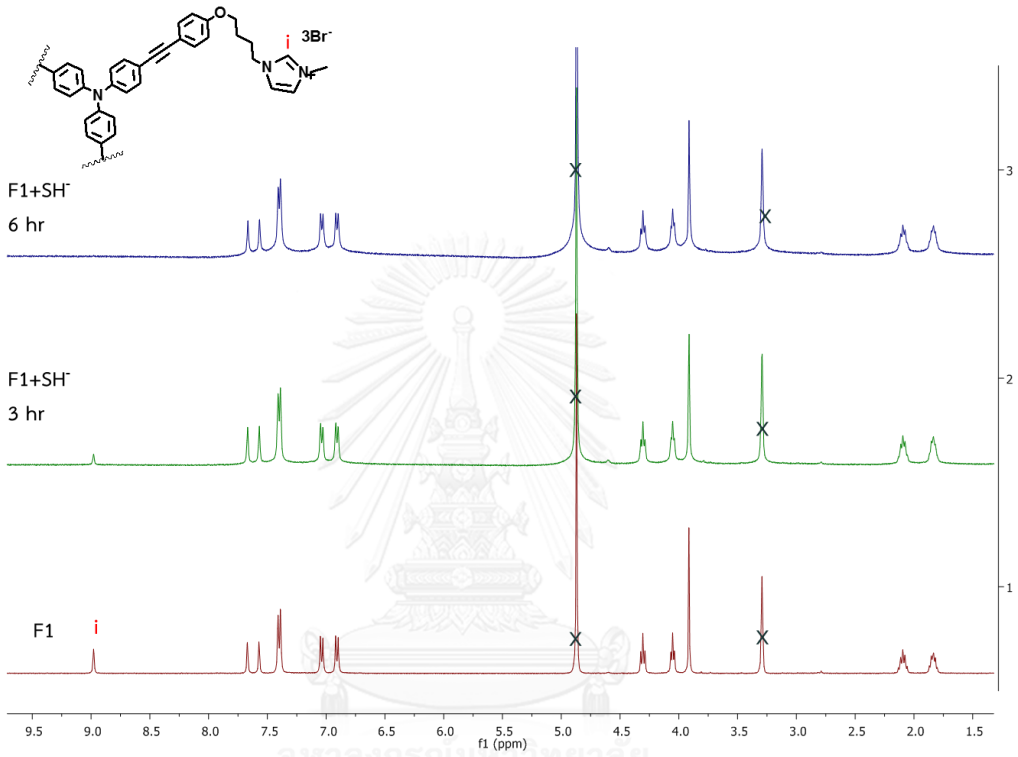

Figure 3.17 ^{1}H NMR of **F1** adding hydrogen sulfide ion in CD_3OD.

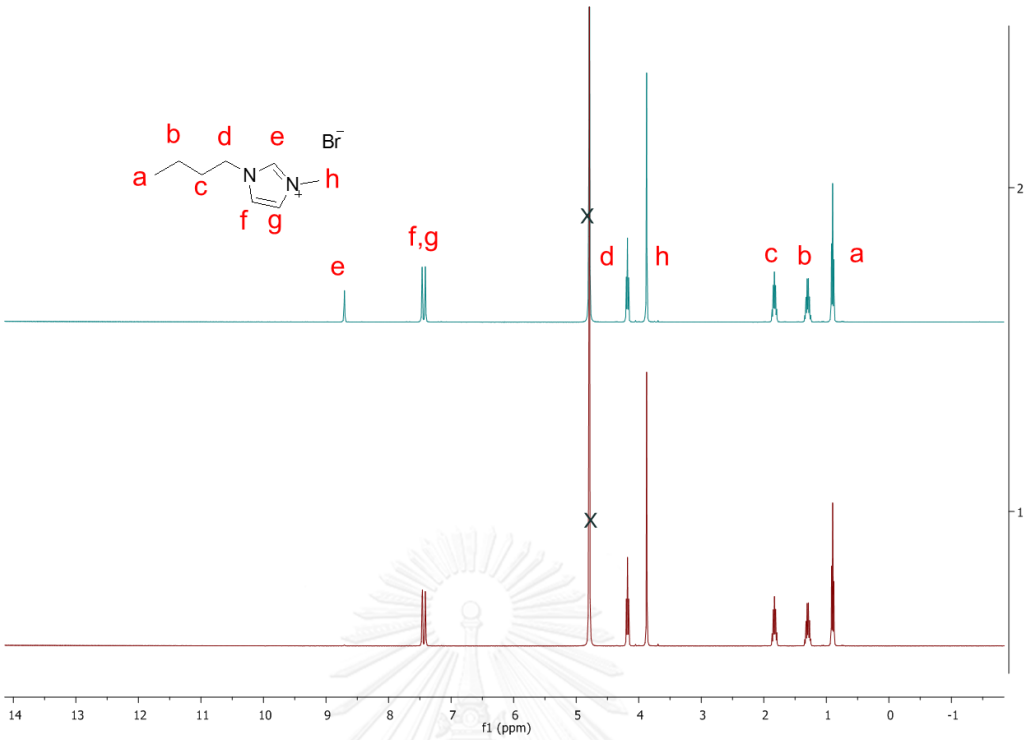

Figure 3.18 ^{1}H NMR of **20** adding hydrogen sulfide ion in D_2O

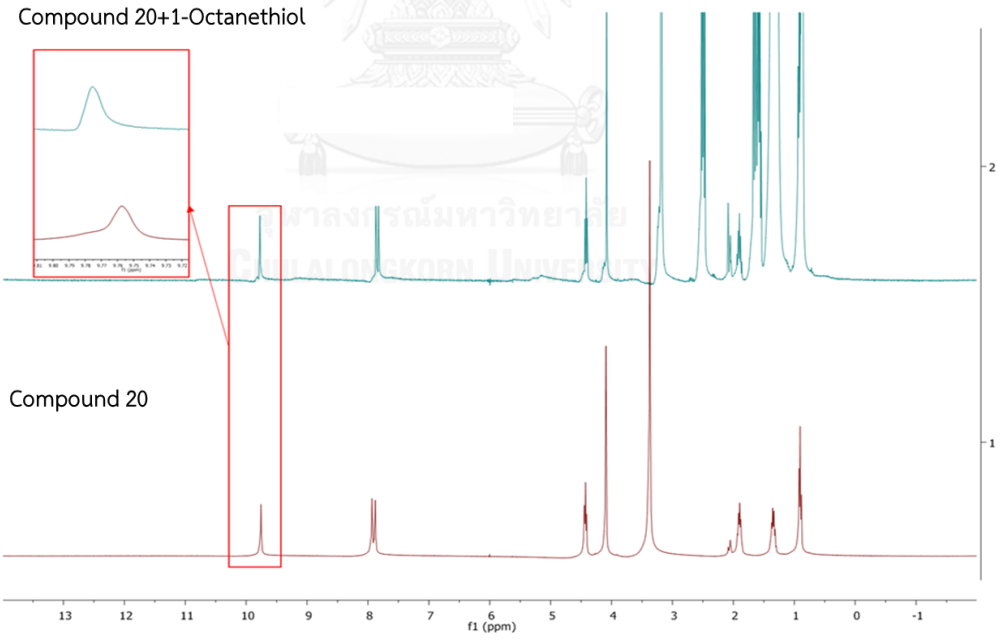

Figure 3.19 ^{1}H NMR of **20** upon the addition of 1-octanethiol in acetone-d_6.

3.4 Sensing property of F2

The sensing ability of **F2** was screened using its solution in 0.017% DMSO/10mM HEPES buffer pH 7.0 against sixteen different anions such as N_3^-, AcO^-, HPO_4^{2-}, NO_3^-, NO_2^-

SO_3^{2-}, SO_4^{2-}, HCO_3^-, Cl^-, Br^-, I^-, F^-, CN^-, $S_2O_3^{2-}$, SCN^- and SH^- at 250 uM. The results which are summarized in Figure 3.20 showed that the fluorescent signal of **F2** can be selectively quenched by $S_2O_3^{2-}$.

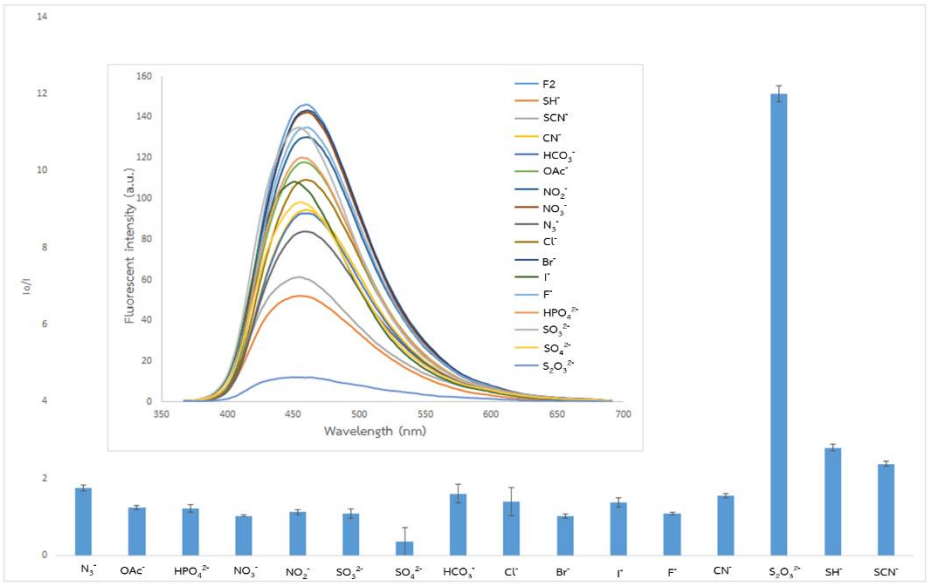

Figure 3.20 Fluorescence quenching of **F2** (5 μM) by various anions (250 μM) in 10 mM HEPES buffer pH 7.0. Inset: Fluorescence spectra of **F2** (5 μM) in the presence of 16 anion (250 μM) in 10 mM HEPES buffer pH 7.0.

3.4.1 Competitive experiments of F2

The interfering effect of other anions on detection of $S_2O_3^{2-}$ by **F2** was investigated as the solutions of **F2** (5 μM) in 0.017% DMSO/10 mM HEPES buffer pH 7.0 and $S_2O_3^{2-}$ (250 μM) were added the foreign anion (1,250 μM) (Figure 3.21). The data indicated that some anions such as NO_2^-, Cl^-, I^- and F^- can interfere the detection of $S_2O_3^{2-}$.

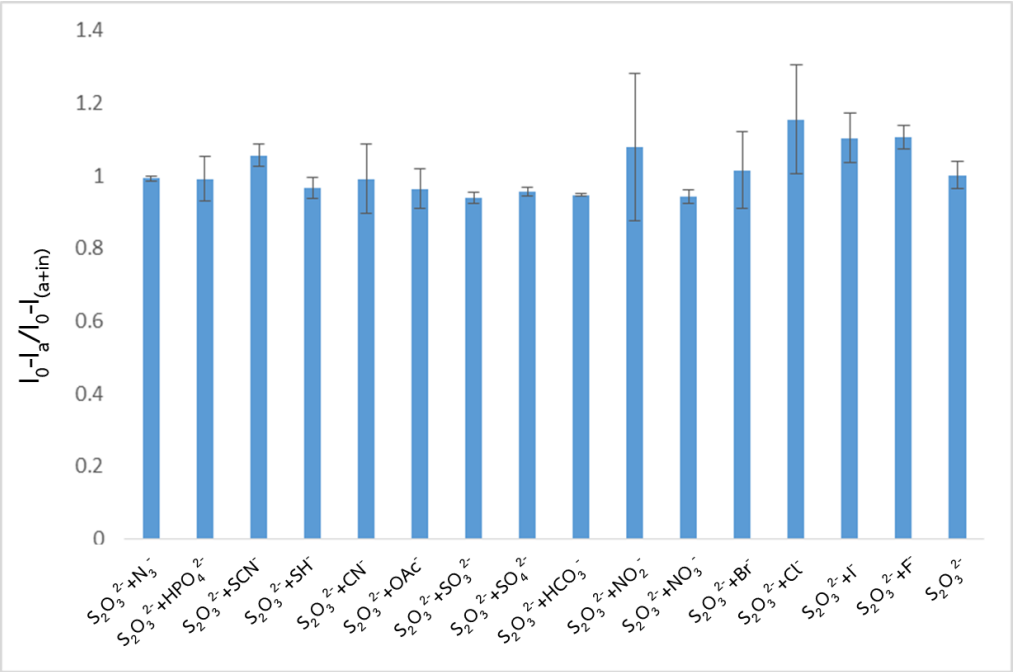

Figure 3.21 Competitive experiments of **F2** (5 μM) and $S_2O_3^{2-}$ (250 μM) with 15 interfering anion ions (1250 μM).

3.4.2 The Stern-Volmer plot for fluorescent quenching of F2 by $S_2O_3^{2-}$

The Stern-Volmer constant (K_{sv}) of 0.10x10^6 $M^{-1}$was determined from slope of the plot between the (I_0/I) and the concentration of $S_2O_3^{2-}$. The detection limit at three-times-noise was then estimated to be 1.30 μM Figure 3.22.

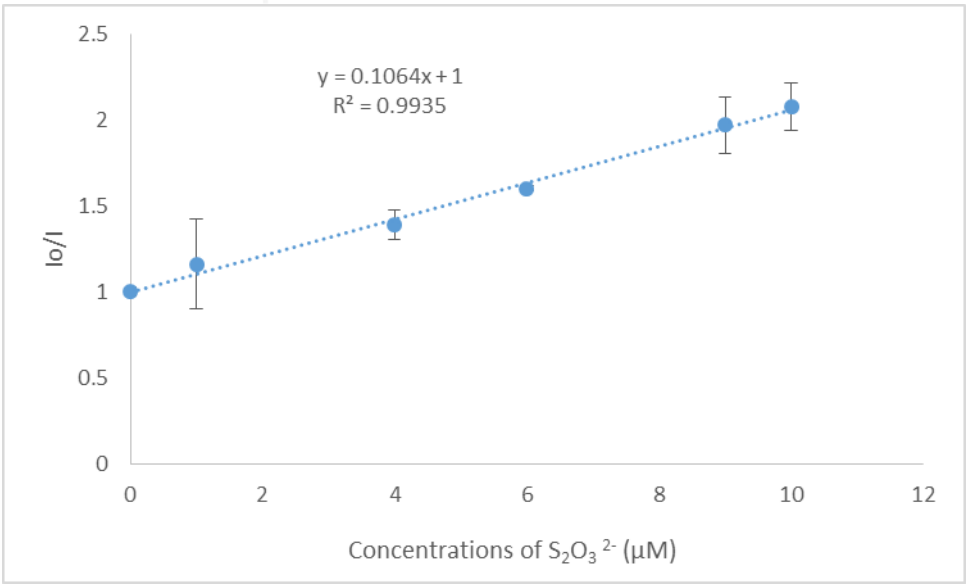

Figure 3.22 The Stern-Volmer plot for fluorescent quenching of **F2** by $S_2O_3^{2-}$.

Several attempts were carried out in order to deprotect the guanidine group in **F2** (Scheme 3.4). However, the presence of alkyne functional groups may lead to undesired side-reaction when **F2** was treated with acidic reagents. In fact, all of the reactions in Scheme 3.4 gave rise to inseparable complex mixtures. As a result, we redesigned and synthesized compound **F4** with an aim to study the effect of guanidinium group on sensing properties in this class of compounds.

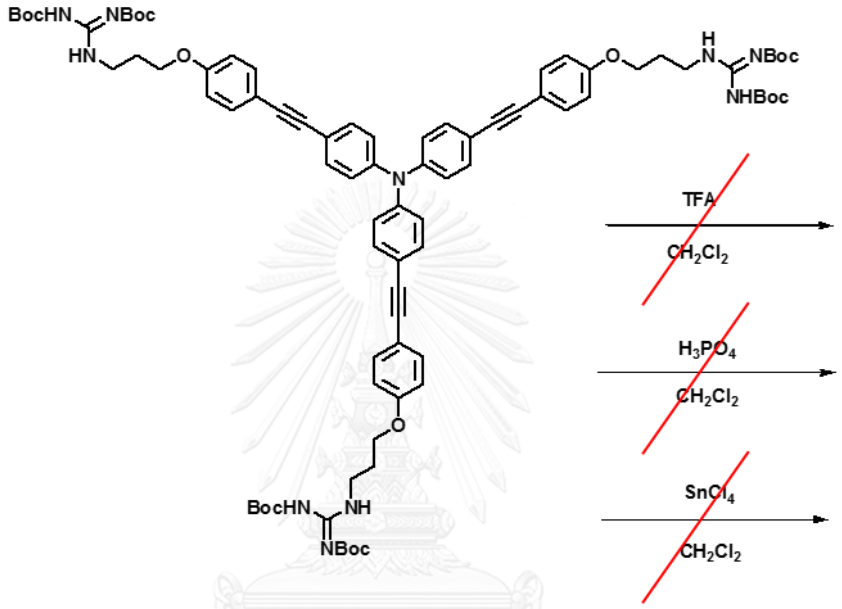

Scheme 3.4 Synthesis part deprotect diBoc.

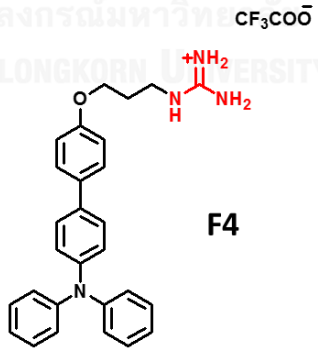

F4

Figure 3.23 Structure of **F4**.

3.5 Synthesis and characterization of F4

The synthesis of **F4** began with a Suzuki coupling on the iodo group of 4-iodophenol with the commercially available 4-(diphenylamino)phenylboronic acid to afford **16** in 52% yield. The alkylation of *N*-(tert-Butoxycarbonyl)-3-bromopropylamine

providing **17**, then deprotection of the Boc group by TFA cleanly gave **18** in 62% yield. Compound **18** reacted with 1-*H*-pyrazole-1-(*N*,*N*'-bis(*tert*-butyloxycarbonyl)) carboxamidine to provide **19** in 46% yield. In the final step, **19** was deprotected by TFA to providing guanidinium **F4** in 47% yield.

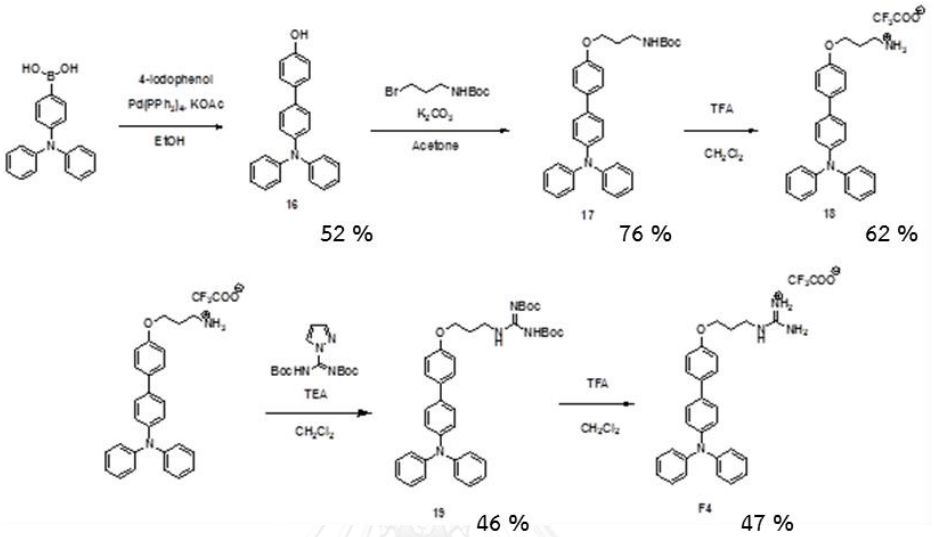

Scheme 3.5 Synthesis of **F4**.

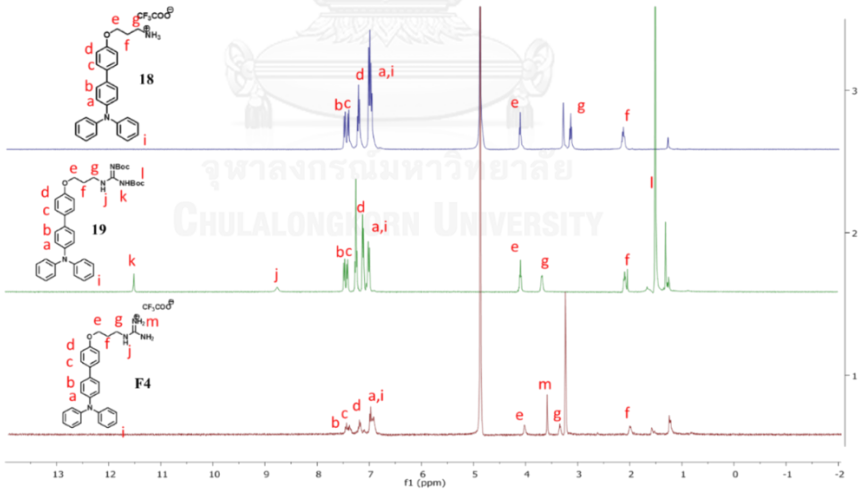

Figure 3.24 ^{1}H-NMR (400 MHz) of **19** in $CDCl_3$ and **18** and **F4** in CD_3OD.

The ^{1}H-NMR spectra of **19** in $CDCl_3$ and **18** and **F4** in CD_3OD were shown in Figure 3.24. The successful synthesis of **F4** was evidenced by the existing of all signals of **19** and **18** with the disappearing of the signal for the Boc groups and exchangeable N-H protons.

3.5.1 Photophysical properties of F4

The absorption and emission properties of **F4** were studied in 0.017% DMSO/10 mM HEPES buffer, pH 7.0. The fluorophore **F4** exhibited absorption maxima at 319 nm and emission maxima at 428 nm (Figure 3.25). From the data, the absorption wavelength of **F4** was shorter than **F2** as resulted from the shorter conjugated system in **F4**. Other photophysical properties of **F4** were compared to **F2** and summarized in Table 3.3.

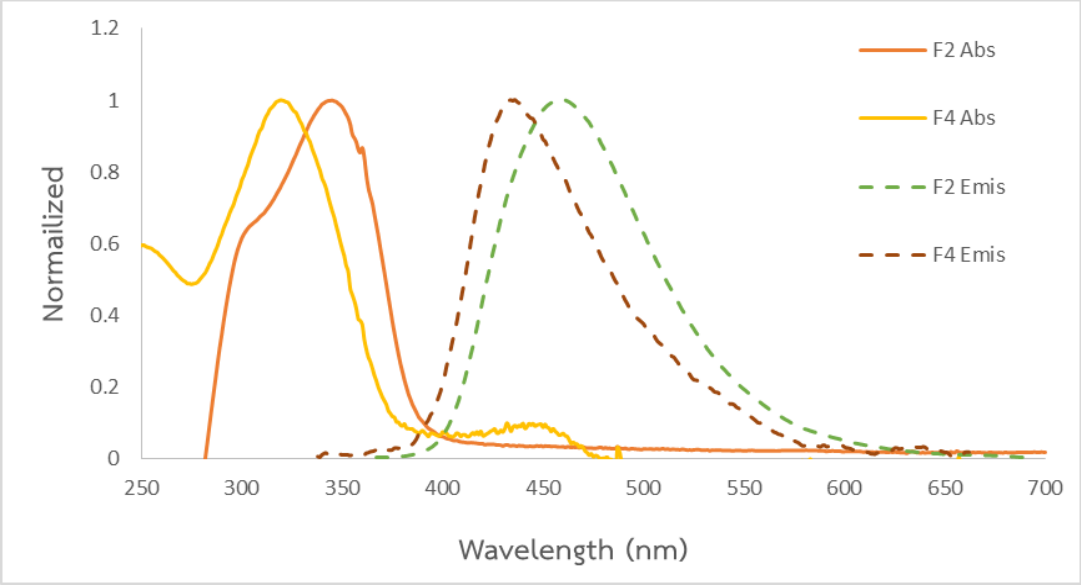

Figure 3.25 Normalized absorption and emission spectra of **F2** and **F4** in 0.017% DMSO/10 mM HEPES buffer, pH 7.0.

Table 3.3 Photophysical properties of sensor **F2** and **F4** in aqueous solution.

Sensor	Absorption		Emission	
	λ_{ab} (nm)	Epsilon	λ_{em} (nm)	Φ (%)[a]
F2	353	43,600	456	7.40
F4	319	6,500	428	2.39

[a]Quinine sulfate in 0.1 M H_2SO_4 (Φ = 54%) was used as the standard.

3.5.2 Sensing property of F4

The selectivity of **F4** was then screened against various anions as shown in Figure 3.26. Unfortunately, this compound did not show selectivity towards any analytes, as its fluorescent signal decreased without any distinguishable trend.

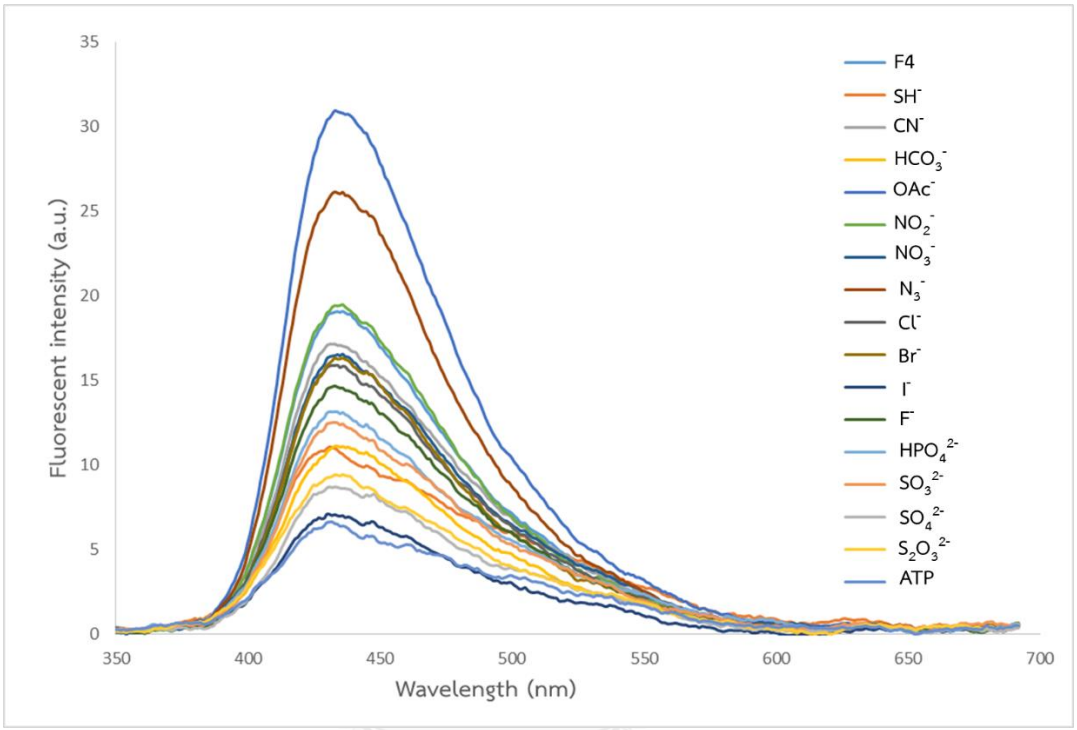

Figure 3.26 Fluorescent spectra of **F4** (5 μM) in the presence of 15 anion (250 μM) in 10 mM HEPES buffer pH 7.0.

CHAPTER IV
CONCLUSION

In summary, four new fluorophores **F1**-**F4** were successfully synthesized by Sonogashira and Suzuki coupling reactions. These compounds were characterized by ^{1}H NMR spectroscopy, mass spectrometry, UV-Vis and fluorescent spectrophotometry. The comparison of photophysical properties of **F1**-**F4** in 10 mM HEPES buffer pH 7.0 solution, wavelengths the maximum absorption of **F1**-**F4** were around 319-362 nm and the maximum emission wavelengths showed around 437-456 nm. The quantum efficiency of **F1** was highest because the solubility in water of **F1** was better than **F2**-**F4** resulting in **F2**-**F4** were lower quantum efficiency. The screening results of **F1**-**F4** with different anions showed that **F1** was selective for hydrogen sulfide ion, **F2** was selective for thiosulfate ion via a fluorescent quenching process, while **F3** and **F4** were low selectivity. The selectively quenching effect was probably associated with binding between the proton at the 2-position of the imidazolium rings of **F1** with hydrogen sulfide ion. For **F2** is selectively quenching by thiosulfate ion. The sensor exhibited a great specificity of hydrogen sulfide ion in **F1** and thiosulfate ion in **F2** were good detection limit.

REFERENCES

[1] Fan, L.-J., et al. Fluorescent Conjugated Polymer Molecular Wire Chemosensors for Transition Metal Ion Recognition and Signaling. Coordination Chemistry Reviews 253(3–4) (2009): 410-422.

[2] Callan, J.F., de Silva, A.P., and Magri, D.C. Luminescent Sensors and Switches in the Early 21st Century. Tetrahedron 61(36) (2005): 8551-8588.

[3] de Silva, A.P., et al. Signaling Recognition Events with Fluorescent Sensors and Switches. Chemical Reviews 97(5) (1997): 1515-1566.

[4] Martínez-Máñez, R. and Sancenón, F. Fluorogenic and Chromogenic Chemosensors and Reagents for Anions. Chemical Reviews 103(11) (2003): 4419-4476.

[5] Gunnlaugsson, T., et al. Fluorescent Photoinduced Electron Transfer (PET) Sensors for Anions; From Design to Potential Application. Journal of Fluorescence 15(3): 287-299.

[6] Carlson, H.J. and Campbell, R.E. Genetically Encoded FRET-Based Biosensors for Multiparameter Fluorescence Imaging. Current Opinion in Biotechnology 20(1) (2009): 19-27.

[7] Sapsford, K.E., Berti, L., and Medintz, I.L. Materials for Fluorescence Resonance Energy Transfer Analysis: Beyond Traditional Donor–Acceptor Combinations. Angewandte Chemie International Edition 45(28) (2006): 4562-4589.

[8] Ma, X., et al. Fluorescence Aggregation-Caused Quenching Versus Aggregation-Induced Emission: A Visual Teaching Technology for Undergraduate Chemistry Students. Journal of Chemical Education 93(2) (2016): 345-350.

[9] Lodeiro, C. and Pina, F. Luminescent and Chromogenic Molecular Probes Based on Polyamines and Related Compounds. Coordination Chemistry Reviews 253(9–10) (2009): 1353-1383.

[10] Introduction to Fluorescence. in Lakowicz, J.R. (ed.) Principles of Fluorescence Spectroscopy, pp. 1-26. Boston, MA: Springer US, 2006.

[11] Vendrell, M., Zhai, D., Er, J.C., and Chang, Y.-T. Combinatorial Strategies in Fluorescent Probe Development. Chemical Reviews 112(8) (2012): 4391-4420.

[12] Shirinfar, B., et al. Selective Fluorescent Detection of RNA in Living Cells by Using Imidazolium-Based Cyclophane. Journal of the American Chemical Society 135(1) (2013): 90-93.

[13] Ahmed, N., Shirinfar, B., Geronimo, I., and Kim, K.S. Fluorescent Imidazolium-Based Cyclophane for Detection of Guanosine-5′-triphosphate and I^- in Aqueous Solution of Physiological pH. Organic Letters 13(20) (2011): 5476-5479.

[14] Kim, H.N., et al. Unique X-ray Sheet Structure of 1,8-Bis(imidazolium) Anthracene and Its Application as a Fluorescent Probe for DNA and DNase. Organic Letters 13(6) (2011): 1314-1317.

[15] Sun, Y., Zhong, C., Gong, R., Mu, H., and Fu, E. A Ratiometric Fluorescent Chemodosimeter with Selective Recognition for Sulfite in Aqueous Solution. The Journal of Organic Chemistry 74(20) (2009): 7943-7946.

[16] Noguchi, T., et al. Nonlinear Fluorescence Response Driven by Atp-Induced Self-Assembly of Guanidinium-Tethered Tetraphenylethene. Chemical Communications 48(65) (2012): 8090-8092.

[17] Niamnont, N., Siripornnoppakhun, W., Rashatasakhon, P., and Sukwattanasinitt, M. A Polyanionic Dendritic Fluorophore for Selective Detection of Hg^{2+} in Triton X-100 Aqueous Media. Organic Letters 11(13) (2009): 2768-2771.

[18] Niamnont, N., Kimpitak, N., Tumcharern, G., Rashatasakhon, P., and Sukwattanasinitt, M. Highly Sensitive Salicylic Fluorophore for Visual Detection of Picomole Amounts of Cu^{2+}. RSC Advances 3(47) (2013): 25215-25220.

[19] Cao, X., Lin, W., and He, L. A Near-Infrared Fluorescence Turn-On Sensor for Sulfide Anions. Organic Letters 13(17) (2011): 4716-4719.

[20] Wang, M.-Q., Li, K., Hou, J.-T., Wu, M.-Y., Huang, Z., and Yu, X.-Q. BINOL-Based Fluorescent Sensor for Recognition of Cu(II) and Sulfide Anion in Water. The Journal of Organic Chemistry 77(18) (2012): 8350-8354.

[21] Zhang, W., Kang, J., Li, P., Wang, H., and Tang, B. Dual Signaling Molecule Sensor for Rapid Detection of Hydrogen Sulfide Based on Modified Tetraphenylethylene. Analytical Chemistry 87(17) (2015): 8964-8969.

[22] Liu, Y. and Feng, G. A Visible Light Excitable Colorimetric and Fluorescent ESIPT Probe for Rapid and Selective Detection of Hydrogen Sulfide. Organic & Biomolecular Chemistry 12(3) (2014): 438-445.

[23] Lippert, A.R., New, E.J., and Chang, C.J. Reaction-Based Fluorescent Probes for Selective Imaging of Hydrogen Sulfide in Living Cells. Journal of the American Chemical Society 133(26) (2011): 10078-10080.

[24] Zhang, H., et al. An Iminocoumarin Benzothiazole-Based Fluorescent Probe for Imaging Hydrogen Sulfide in Living Cells. Talanta 135 (2015): 149-154.

[25] Lewis, T.A., et al. 5-Lipoxygenase inhibition by N-hydroxycarbamates in Dual-Function Compounds. Bioorganic & Medicinal Chemistry Letters 15(4) (2005): 1083-1085.

[26] Jin, Z., et al. Clicking Fluoroionophores onto Mesoporous Silicas: A Universal Strategy toward Efficient Fluorescent Surface Sensors for Metal Ions. Analytical Chemistry 82(15) (2010): 6343-6346.

[27] Georgiades, S.N. and Clardy, J. Preparation of a Psammaplysene-Based Library. Organic Letters 8(19) (2006): 4251-4254.

[28] Onitsuka, K., Ohara, N., Takei, F., and Takahashi, S. Synthesis and Redox Properties of Trinuclear Ruthenium-Acetylide Complexes with Tri(Ethynylphenyl)amine Bridge. Dalton Transactions (30) (2006): 3693-3698.

[29] Le Floch, F., Simonato, J.-P., and Bidan, G. Electrochemical Signature of the Grafting of Diazonium Salts: A Probing Parameter for Monitoring the Electro-Addressed Functionalization of Devices. Electrochimica Acta 54(11) (2009): 3078-3085.

[30] Dong, L., Zheng, Z., Wang, Y., Li, X., Hua, J., and Hu, A. Co-Sensitization of N719 with Polyphenylenes from The Bergman Cyclization of Maleimide-Based Enediynes for Dye-Sensitized Solar Cells. Journal of Materials Chemistry A 3(21) (2015): 11607-11614.

[31] Quinton, C., Alain-Rizzo, V., Dumas-Verdes, C., Clavier, G., Vignau, L., and Audebert, P. Triphenylamine/Tetrazine Based [small pi]-Conjugated Systems as Molecular Donors for Organic Solar Cells. New Journal of Chemistry 39(12) (2015): 9700-9713.

[32] Medina, A., et al. Accelerating Charge Transfer in a Triphenylamine-Subphthalocyanine Donor-Acceptor System. Chemical Communications (15) (2008): 1759-1761.

[33] Gruzdev, M.S., Ramenskaya, L.M., Chervonova, U.V., and Kumeev, R.S. Preparation of 1-butyl-3-methylimidazolium Salts and Study of Their Phase Behavior and Intramolecular Intractions. Russian Journal of General Chemistry 79(8) (2009): 1720-1727.

[34] Du, H., Fuh, R.-C.A., Li, J., Corkan, L.A., and Lindsey, J.S. PhotochemCAD‡: A Computer-Aided Design and Research Tool in Photochemistry. Photochemistry and Photobiology 68(2) (1998): 141-142.

[35] Zangmeister, C.D., et al. Fermi Level Alignment in Self-Assembled Molecular Layers: The Effect of Coupling Chemistry. The Journal of Physical Chemistry B 110(34) (2006): 17138-17144.

[36] Giernoth, R. and Bankmann, D. Transition-Metal-Free Synthesis of Perdeuterated Imidazolium Ionic Liquids by Alkylation and H/D Exchange. European Journal of Organic Chemistry 2008(17) (2008): 2881-2886.

[37] Fahlbusch, T., Frank, M., Schatz, J., and Schühle, D.T. Kinetic Acidity of Supramolecular Imidazolium SaltsEffects of Substituent, Preorientation, and Counterions on H/D Exchange Rates. The Journal of Organic Chemistry 71(4) (2006): 1688-1691.

[38] Singh, N.J., et al. Quinoxaline–Imidazolium Receptors for Unique Sensing of Pyrophosphate and Acetate by Charge Transfer. Organic Letters 9(3) (2007): 485-488.

[39] Ihm, H., Yun, S., Kim, H.G., Kim, J.K., and Kim, K.S. Tripodal Nitro-Imidazolium Receptor for Anion Binding Driven by $(C–H)^{+}$---X^{-} Hydrogen Bonds. Organic Letters 4(17) (2002): 2897-2900.

[40] Kwon, J.Y., Singh, N.J., Kim, H.N., Kim, S.K., Kim, K.S., and Yoon, J. Fluorescent GTP-Sensing in Aqueous Solution of Physiological pH. Journal of the American Chemical Society 126(29) (2004): 8892-8893.

[41] Ahmed, N., Shirinfar, B., Youn, I.S., Bist, A., Suresh, V., and Kim, K.S. A Highly Selective Fluorescent Chemosensor for Guanosine-5[prime or minute]-

Triphosphatevia Excimer Formation in Aqueous Solution of Physiological pH. Chemical Communications 48(21) (2012): 2662-2664.

[42] Kim, H.N., et al. A Pyrene-Imidazolium Derivative that Selectively Recognizes G-Quadruplex DNA. Biomaterials 33(7) (2012): 2282-2288.

APPENDIX

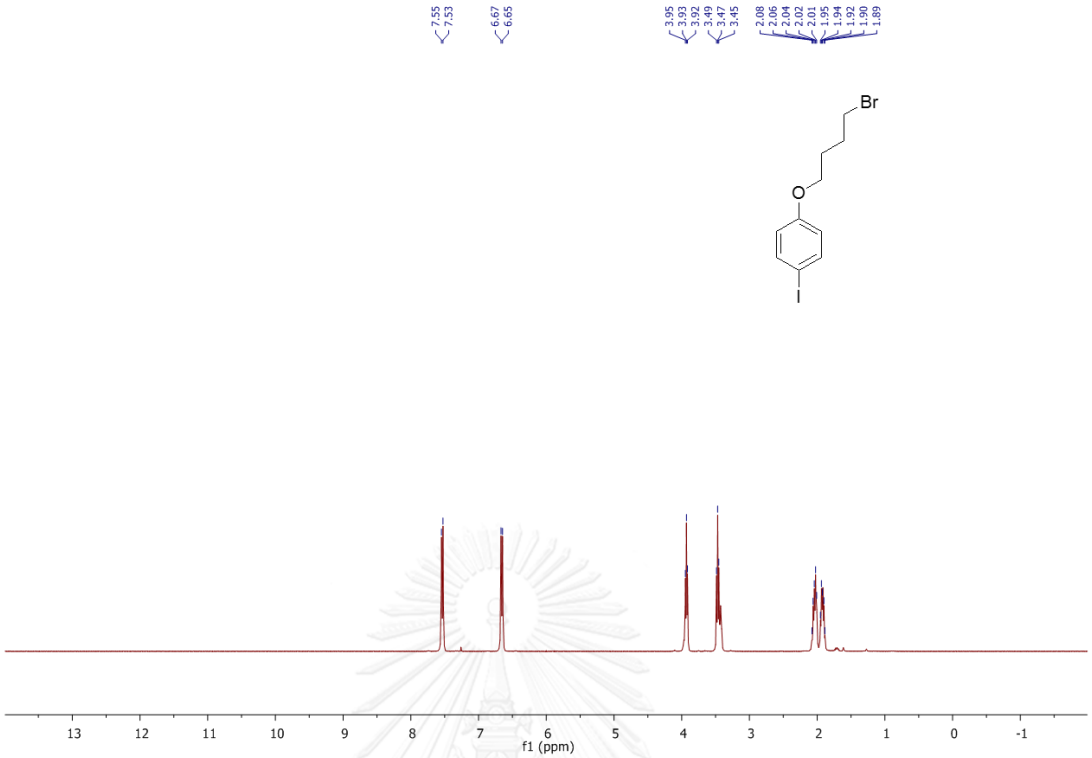

Figure A.1 ^{1}H-NMR of 1-(4-Bromobutoxy)-4-iodobenzene (**2**) in $CDCl_3$.

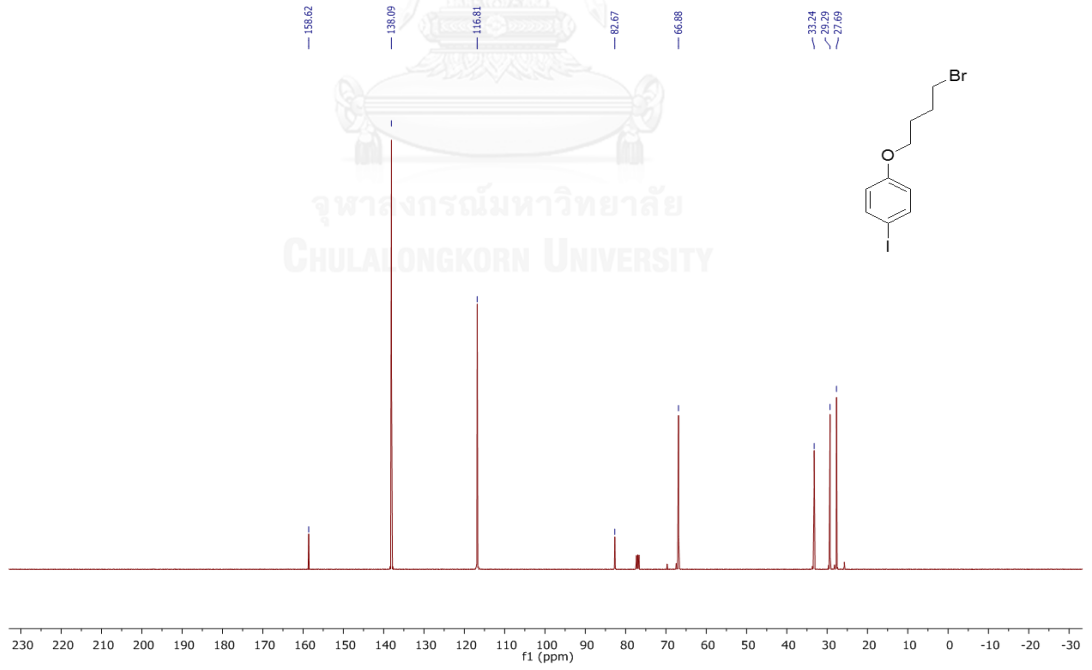

Figure A.2 ^{13}C-NMR of of 1-(4-Bromobutoxy)-4-iodobenzene (**2**) in $CDCl_3$.

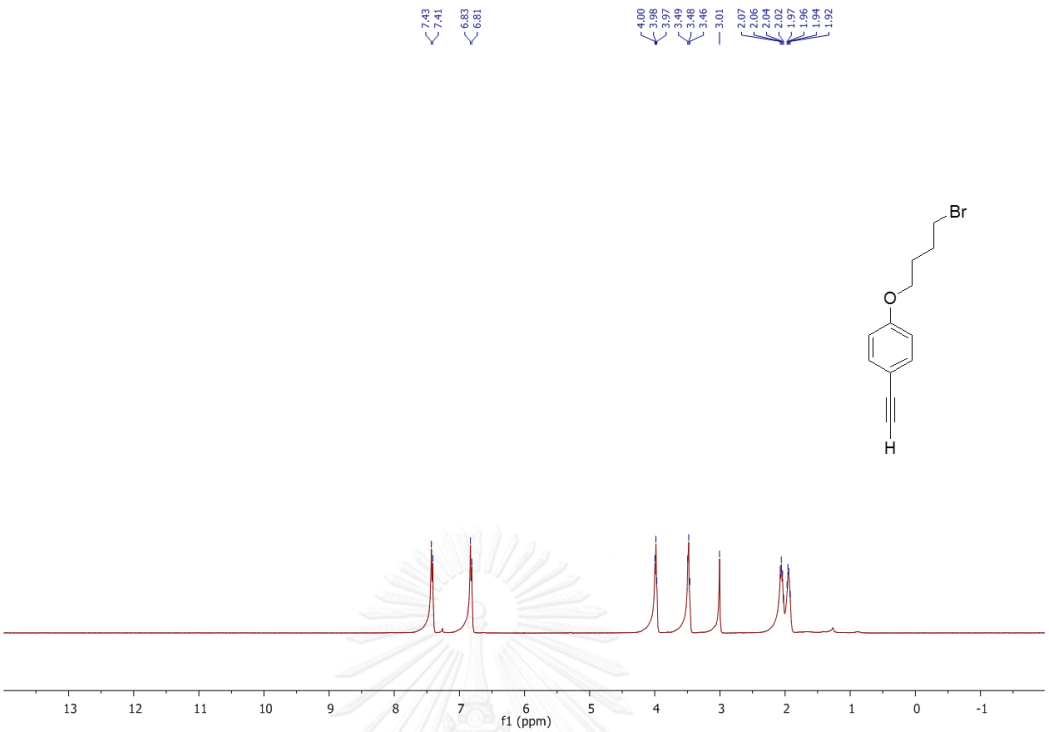

Figure A.3 ^{1}H-NMR of 1-(4-Bromobutoxy)-4-ethynylbenzene (**4**) in $CDCl_3$.

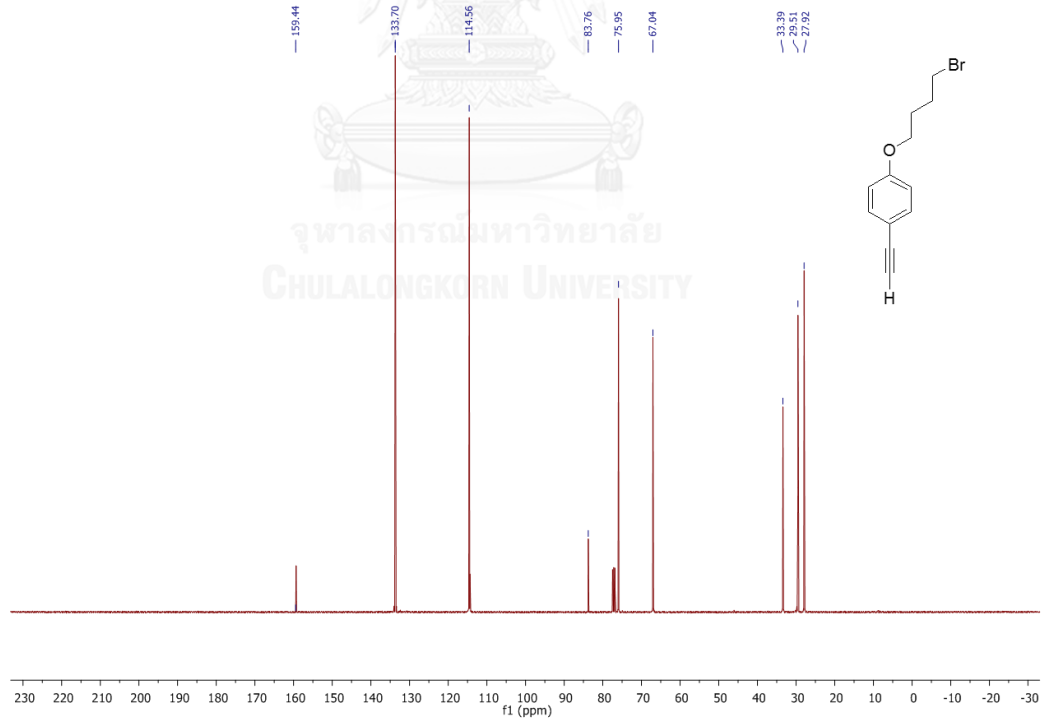

Figure A.4 ^{13}C-NMR of 1-(4-Bromobutoxy)-4-ethynylbenzene (**4**) in $CDCl_3$.

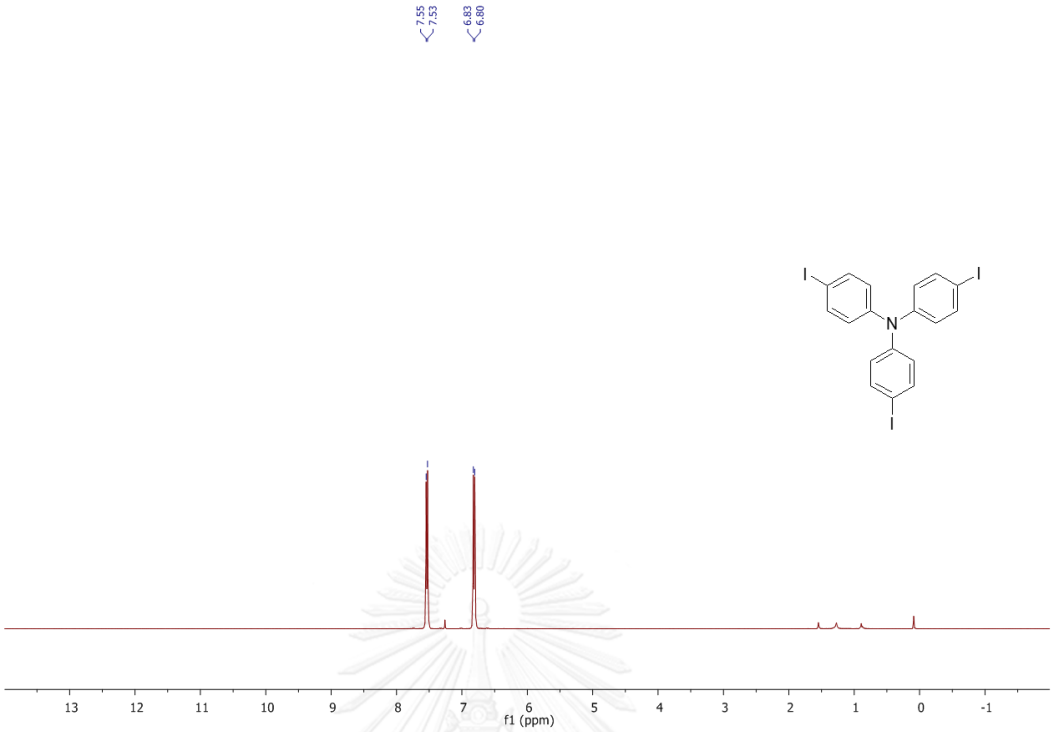

Figure A.5 ^{1}H-NMR of 4, 4', 4''-Triiodotriphenylamine (**1**) in $CDCl_3$.

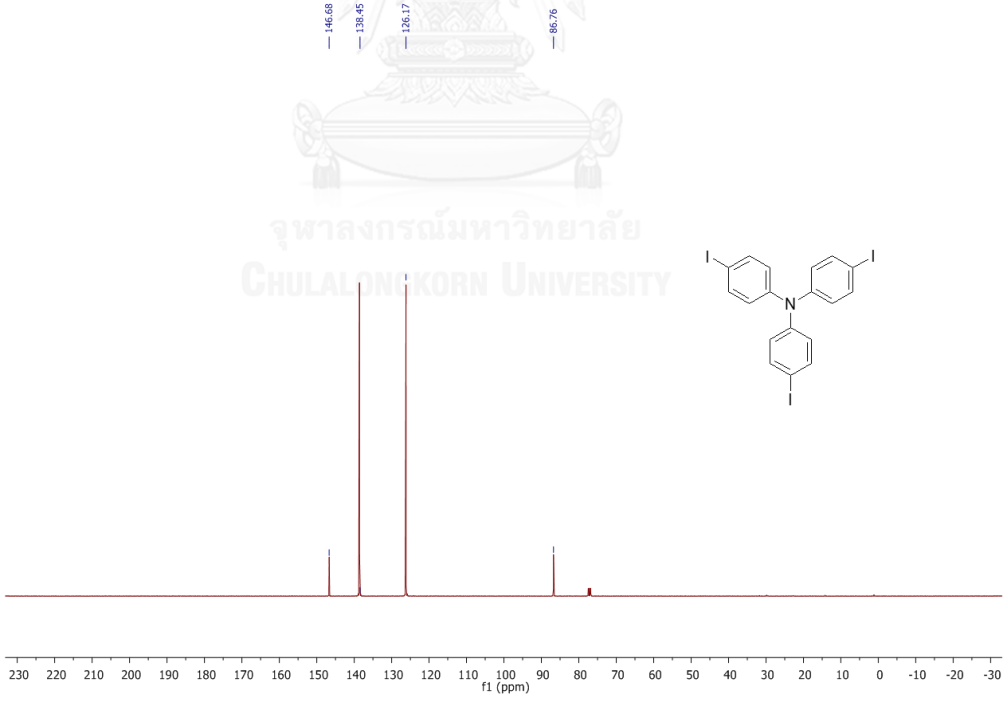

Figure A.6 ^{13}C-NMR of 4, 4', 4''-Triiodotriphenylamine (**1**) in $CDCl_3$.

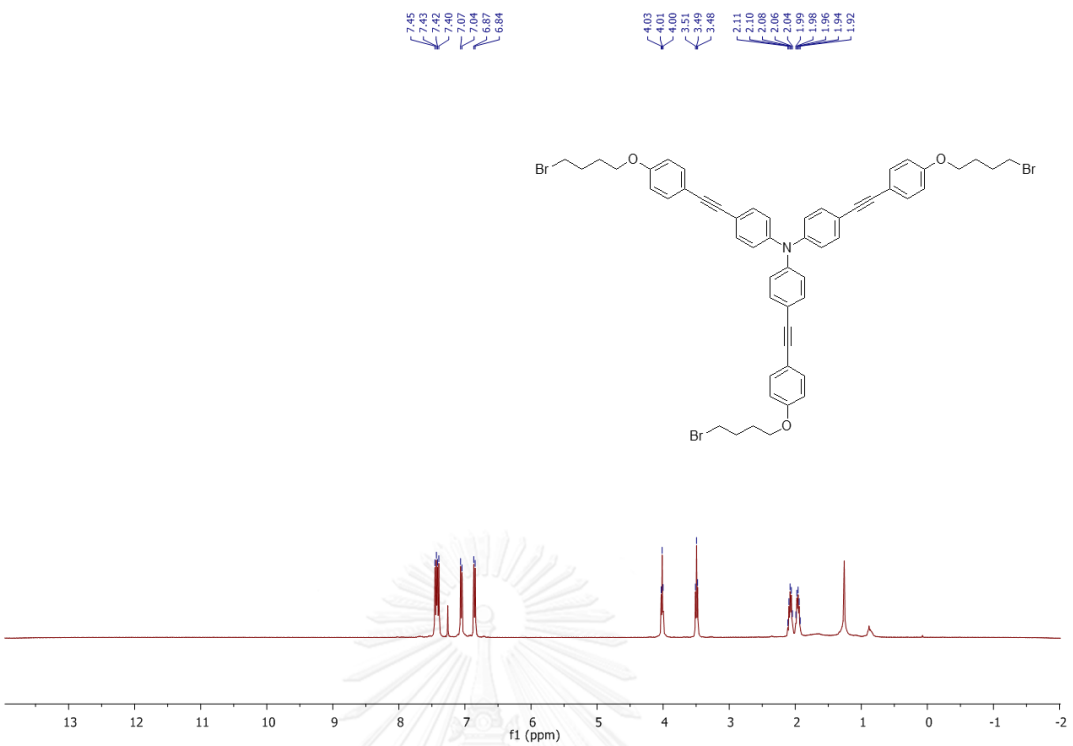

Figure A.7 ^{1}H-NMR of Tribromo (**5**) in $CDCl_3$.

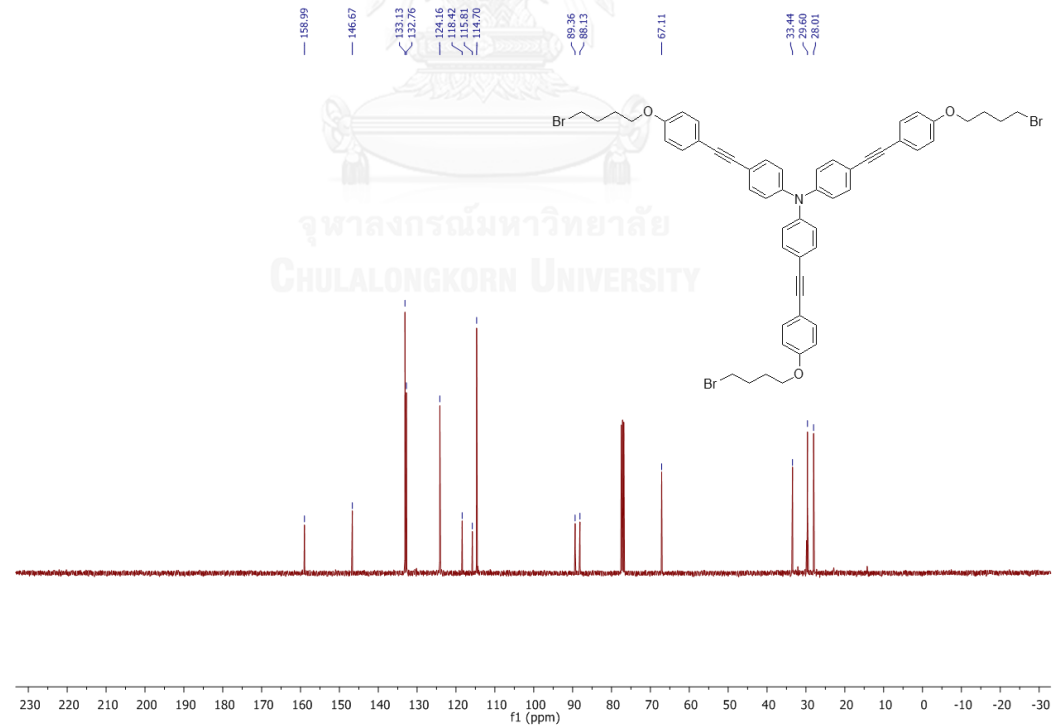

Figure A.8 ^{13}C-NMR of Tribromo (**5**) in $CDCl_3$.

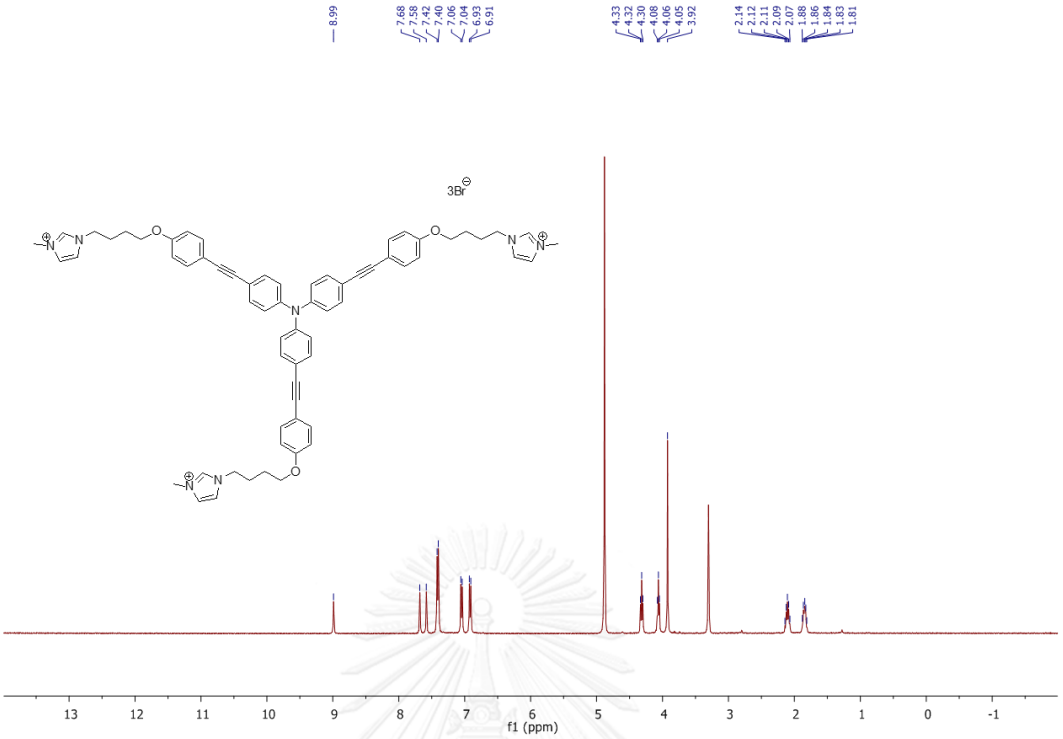

Figure A.9 ^{1}H-NMR of **F1** in CD_3OD.

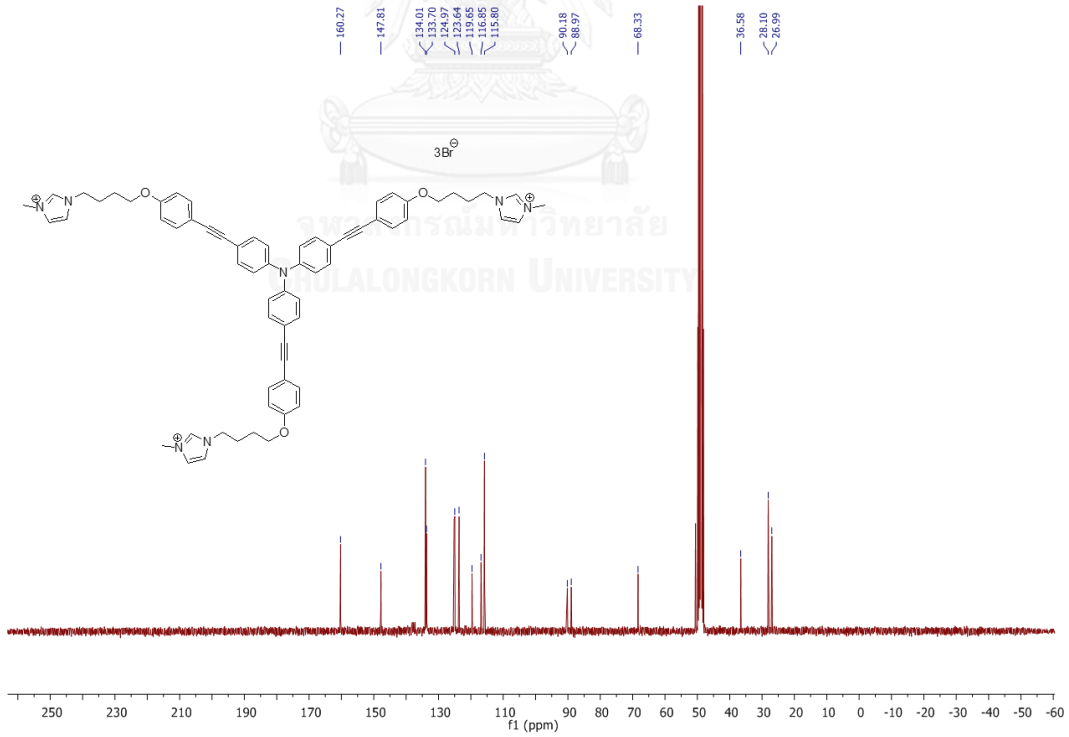

Figure A.10 ^{13}C-NMR of **F1** in CD_3OD.

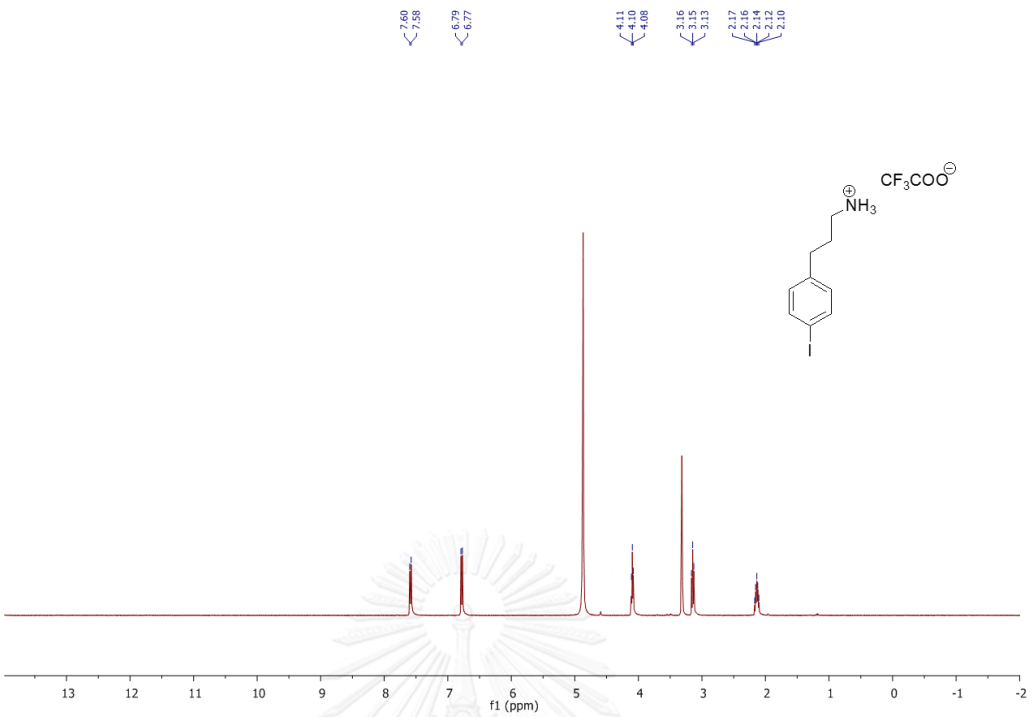

Figure A.11 ^{1}H-NMR of **8** CD_3OD.

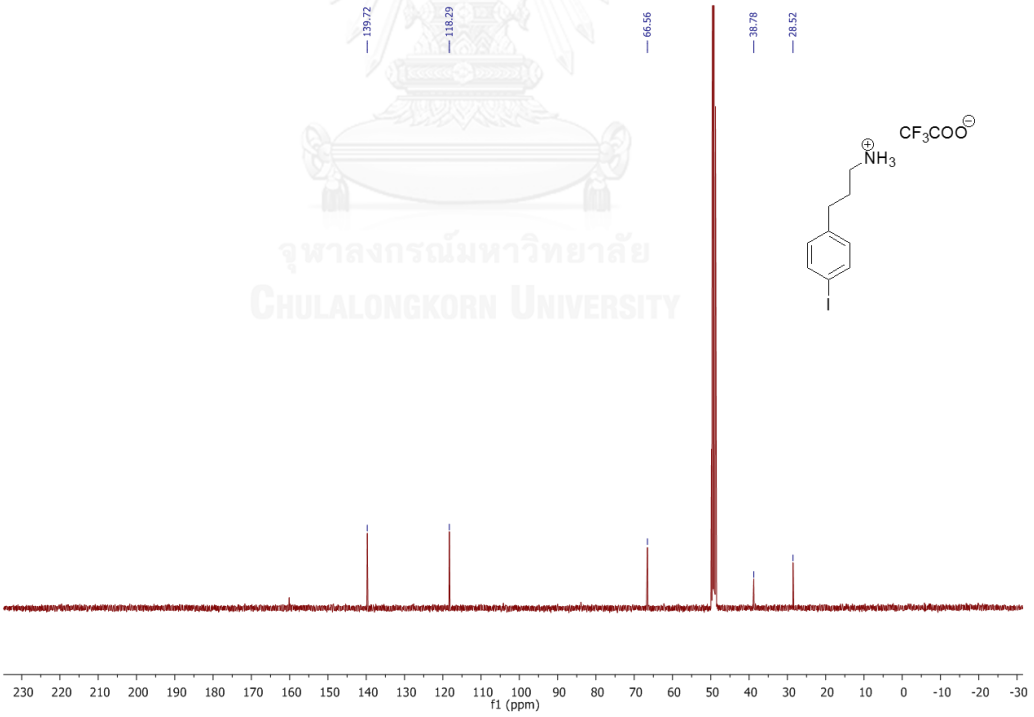

Figure A.12 ^{13}C-NMR of **8** CD_3OD.

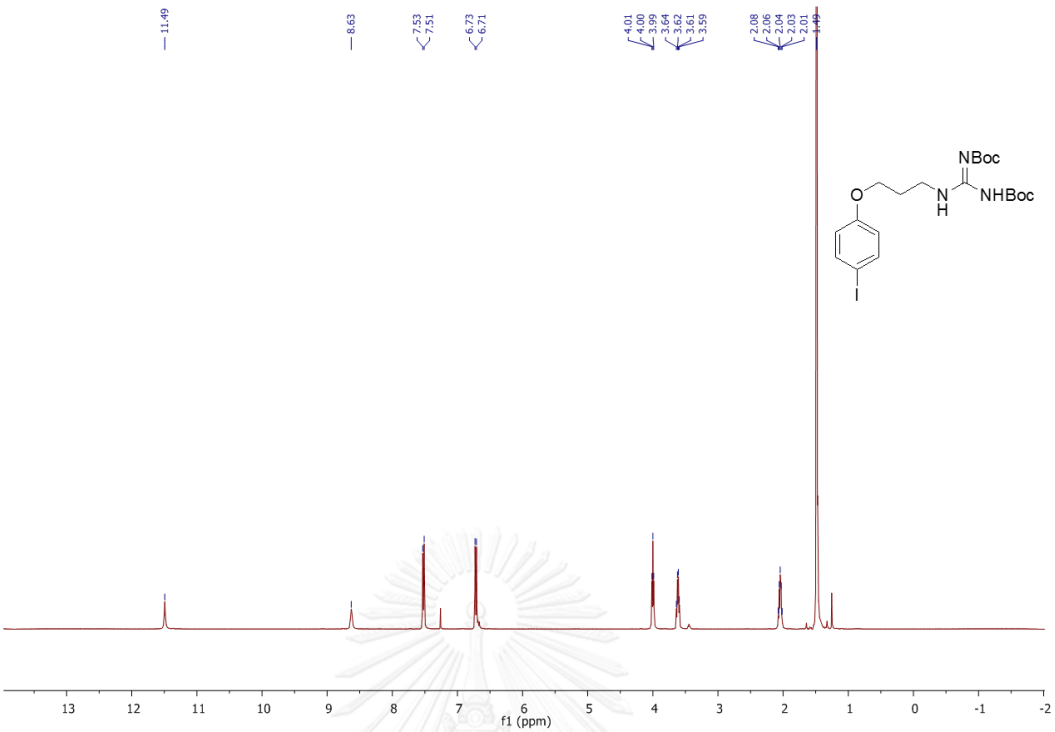

Figure A.13 ^{1}H-NMR of **9** $CDCl_3$.

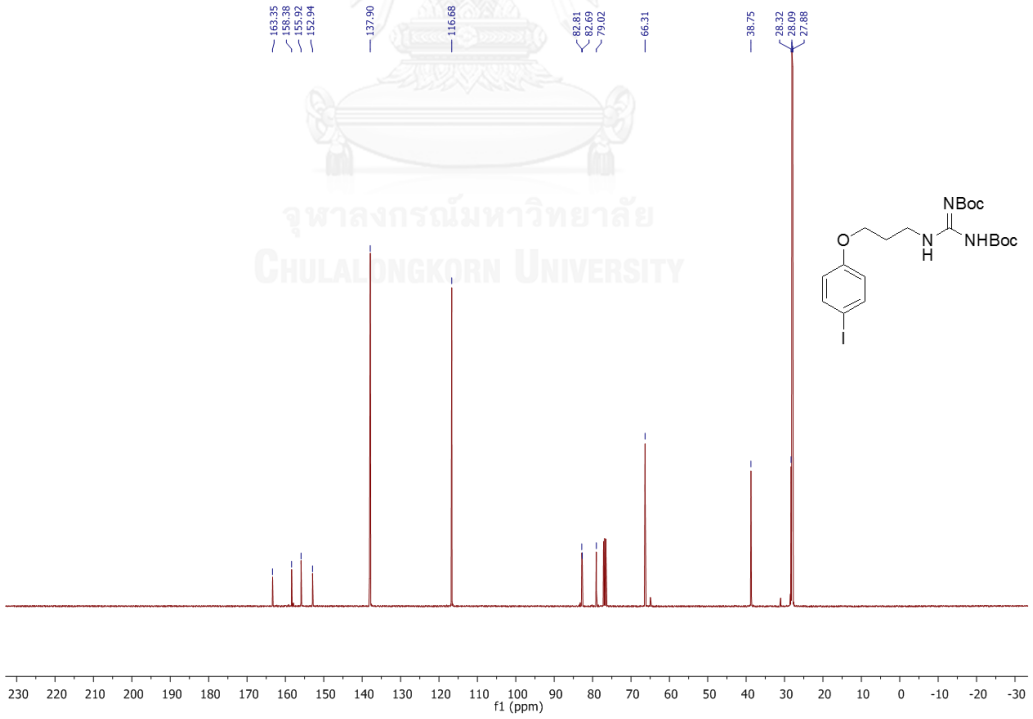

Figure A.14 ^{13}C-NMR of **9** $CDCl_3$.

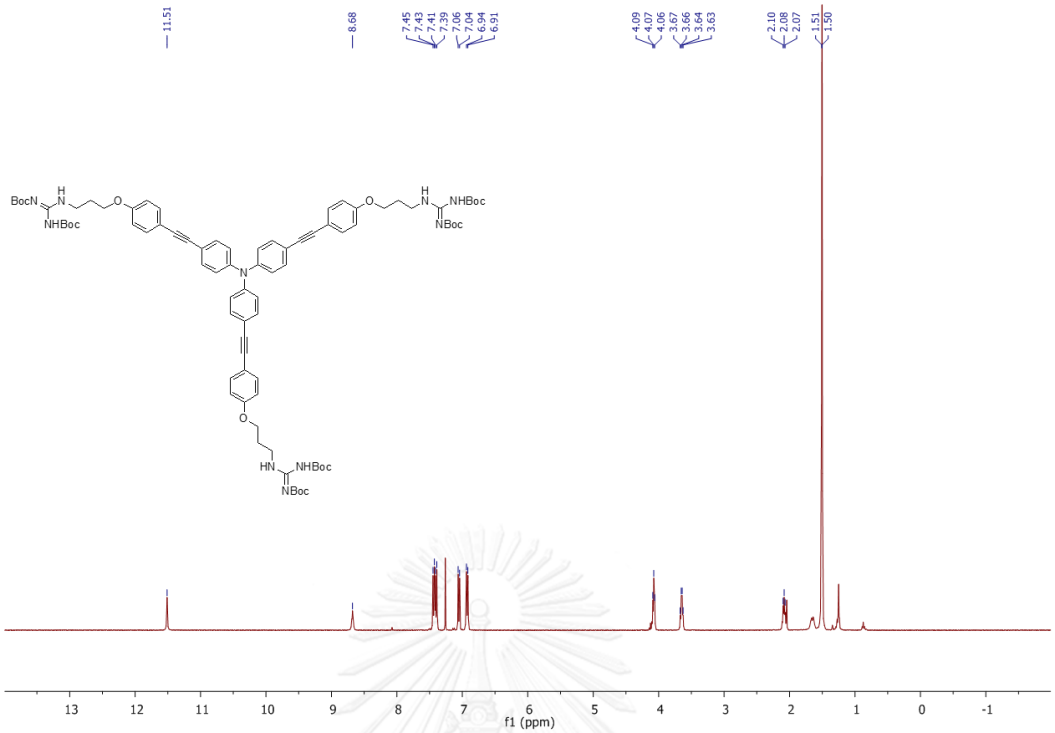

Figure A.15 ^{1}H-NMR of **F2** in $CDCl_3$.

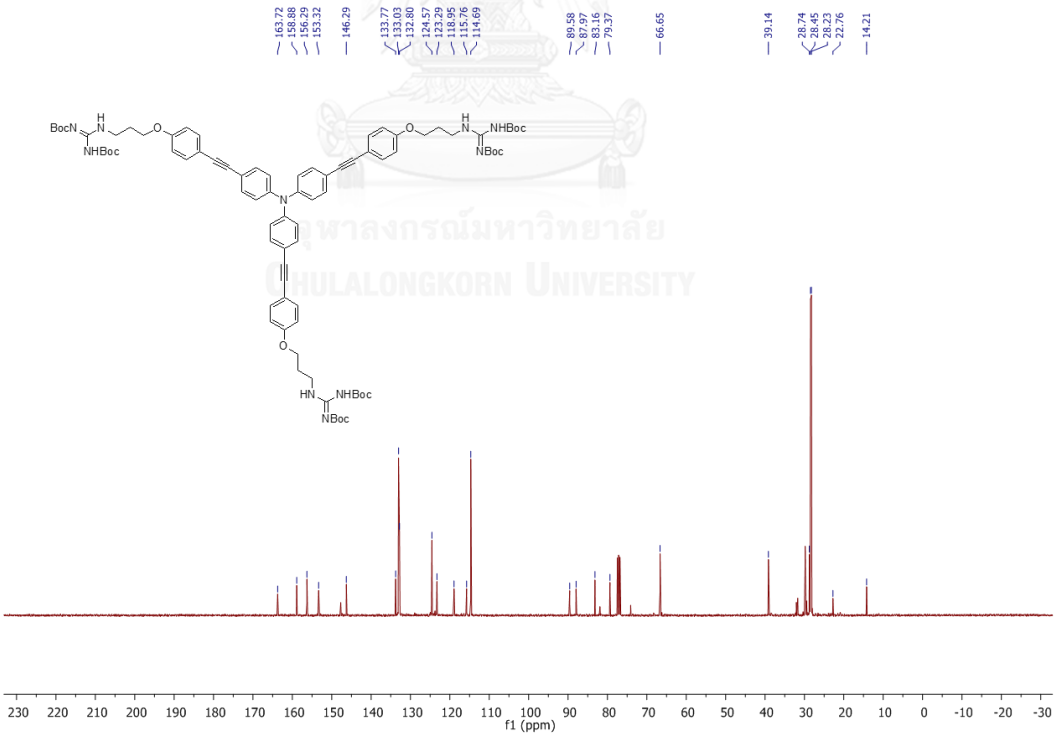

Figure A.16 ^{13}C-NMR of **F2** in $CDCl_3$.

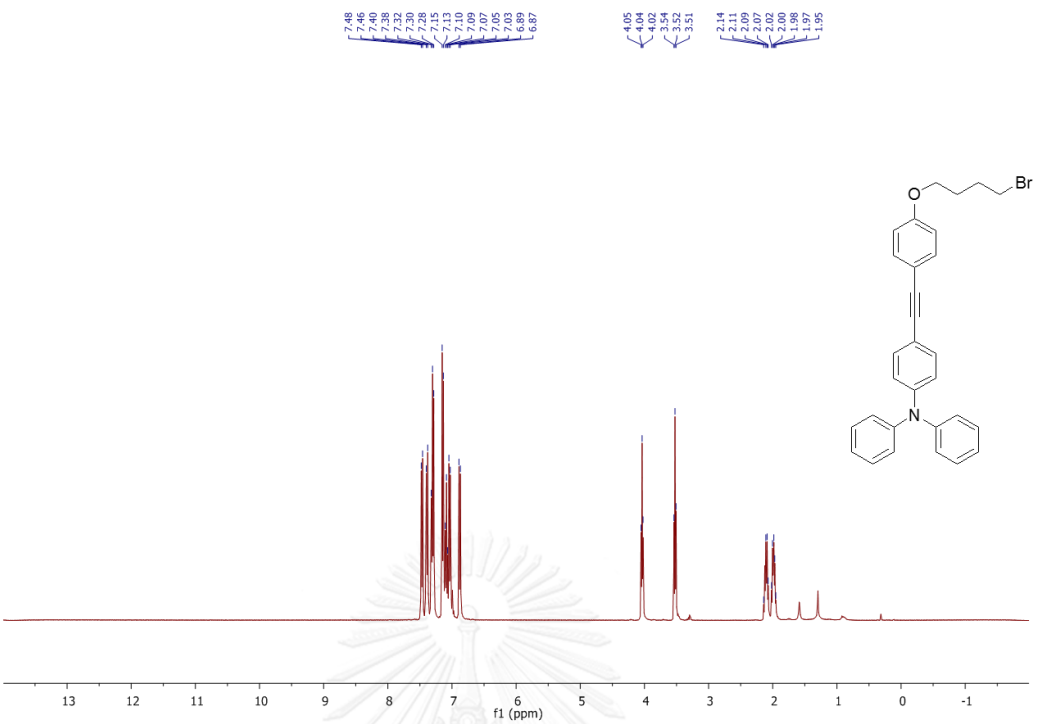

Figure A.17 ^{1}H-NMR of **15** in $CDCl_3$.

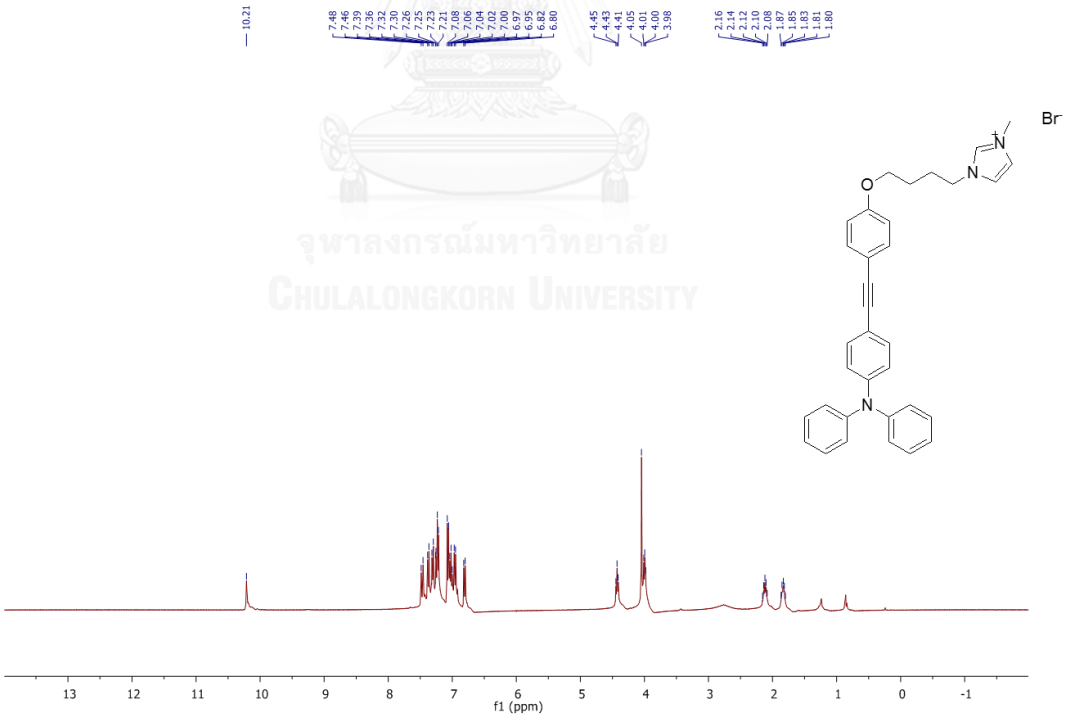

Figure A.18 ^{1}H-NMR of **F3** in $CDCl_3$.

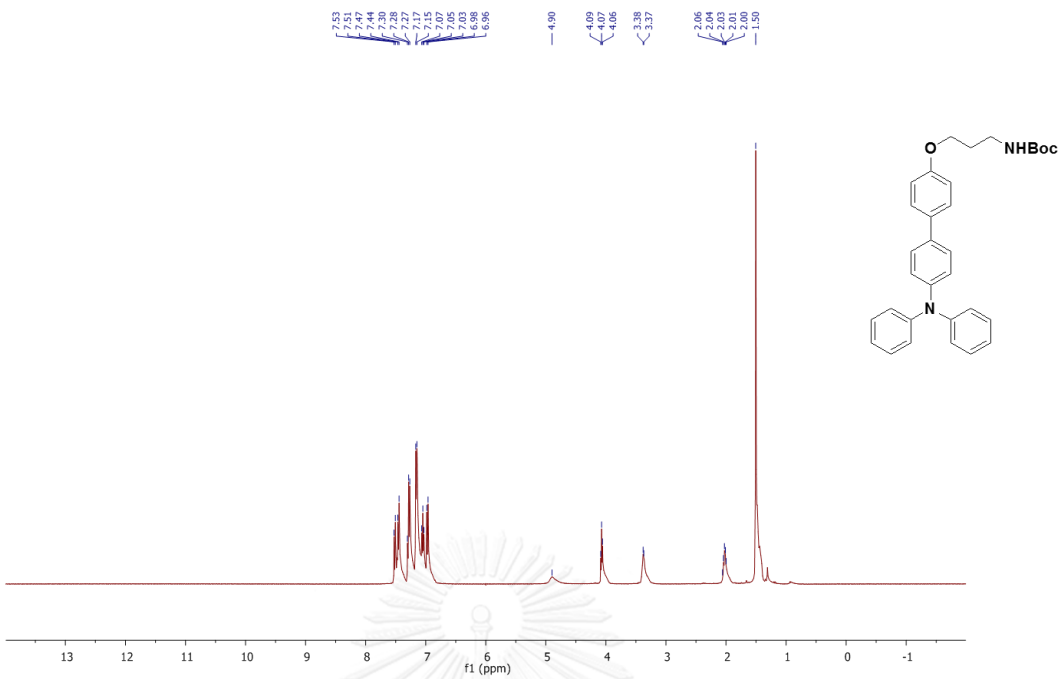

Figure A.19 ^{1}H-NMR of **17** in $CDCl_3$.

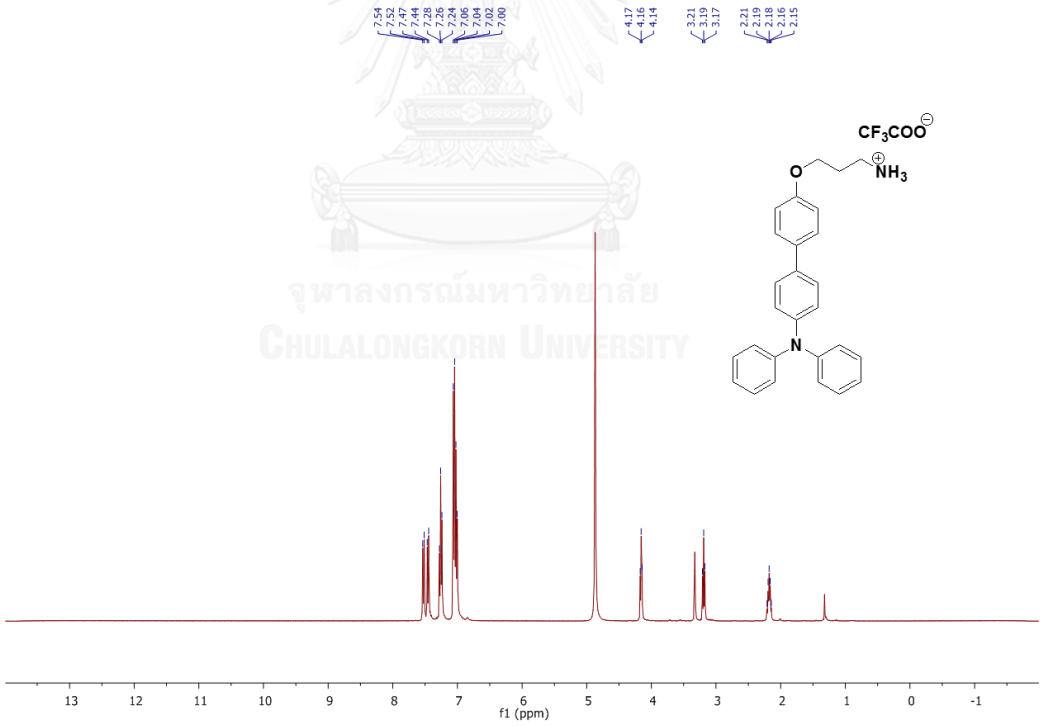

Figure A.20 ^{1}H-NMR of **18** in CD_3OD.

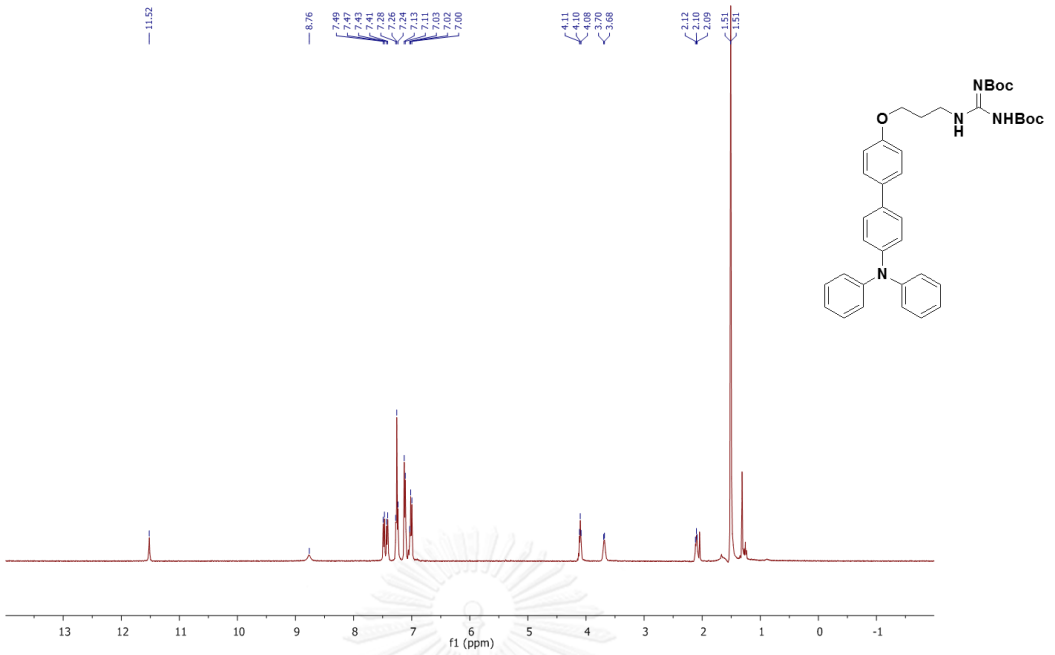

Figure A.21 ^{1}H-NMR of **19** in $CDCl_3$.

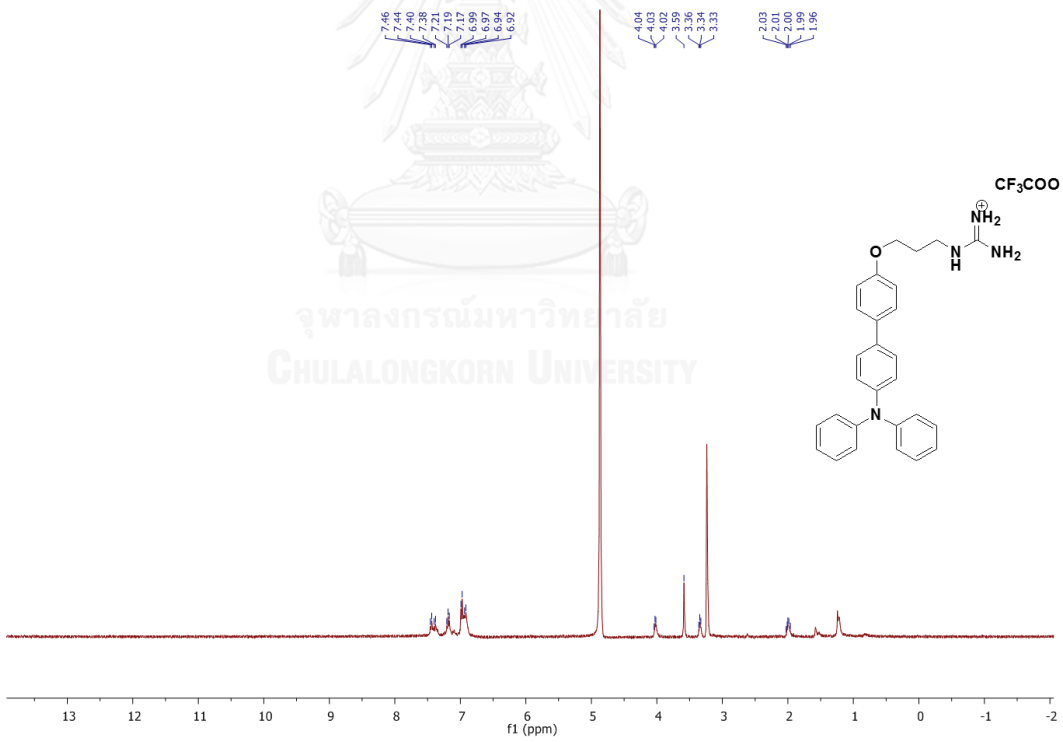

Figure A.22 ^{1}H-NMR of **F4** in CD_3OD.

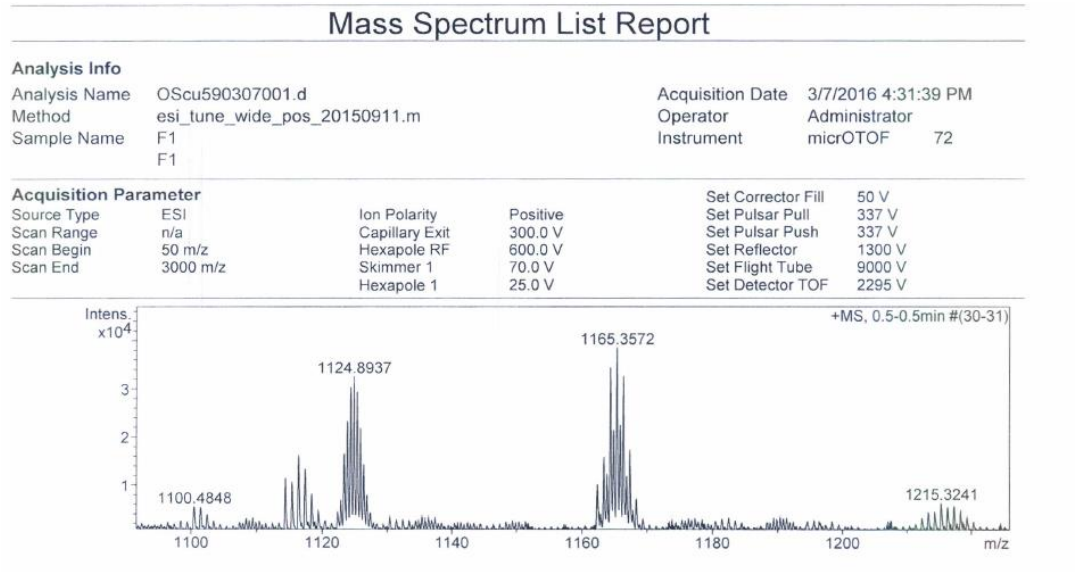

Figure A.23 HRMS of **F1**.

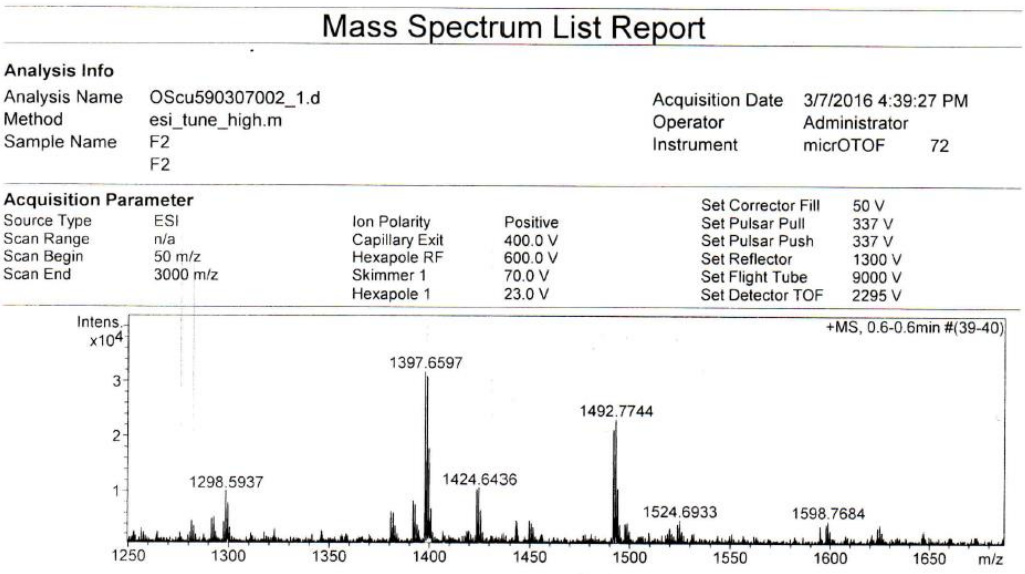

Figure A.24 HRMS of **F2**.

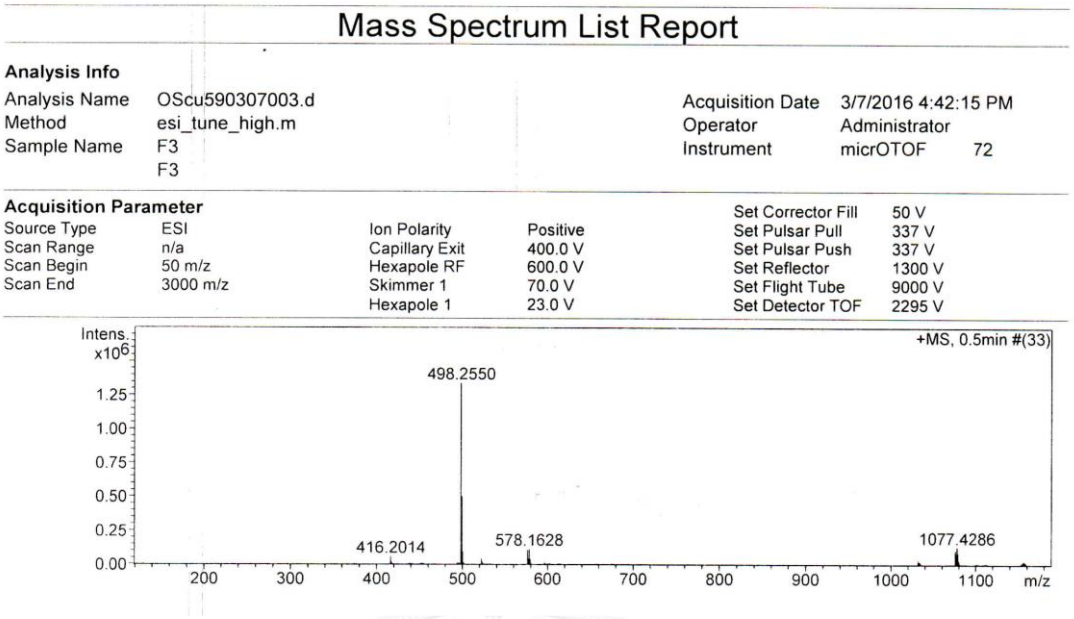

Figure A.25 HRMS of **F3**

VITA

Mr. Sattawat dueansawang was born on April, 1991 in Phitsanulok, Thailand. He graduated with high school degree from Phichitpittayakom School, Phichit. He graduated with bachelor drgree of Science, major of chemistry from Nareasuan University, in 2013. He has been a graduate student in Petrochemistry and Polymer Science and become a member of Material Advancement via Proficient Synthesis Group. Under supervision of Assoc. Prof. Dr. Paitoon Rashatasakhon and he further received a Master Degree in Petrochemistry and Polymer Science from Chulalongkorn University. His present address is 26/4 Moo 2 Nai Mueang, Mueang, Phichit, Thailand 66000